AD-A047 124 AIR FORCE INST OF TECH WRIGHT-PATTERSON AFB OHIO F/G 17/7
COMPENSATION FOR PROPAGATION UNCERTAINTIES IN THE OMEGA NAVIGAT--ETC(U)
1976 R L VANALLEN
UNCLASSIFIED AFIT-CI-77-13 NL

1 OF 2
ADA047 124

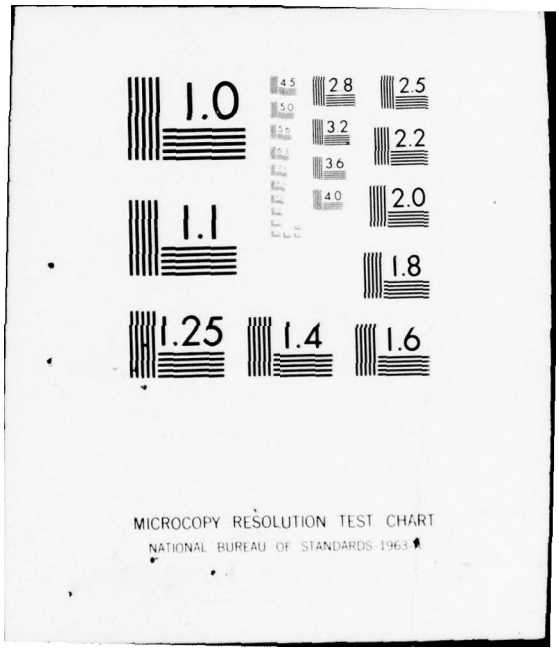
1.0
1.1
1.25
1.4
1.6
1.8
2.0
2.2
2.5
2.8
3.2
3.6
4.0
4.5
5.0
5.6
6.3
MICROCOPY RESOLUTION TEST CHART
NATIONAL BUREAU OF STANDARDS 1963

77-13

(1)

B.S.

Compensation for propagation uncertainties in the OMEGA navigation system

by

Robert Lee VanAllen

A Dissertation Submitted to the
Graduate Faculty in Partial Fulfillment of
The Requirements for the Degree of
DOCTOR OF PHILOSOPHY

Major: Electrical Engineering

Approved:

F. E. Brown
In Charge of Major Work

For the Major Department

For the Graduate College

Iowa State University
Ames, Iowa

1976

UNCLASSIFIED

SECURITY CLASSIFICATION OF THIS PAGE *(When Data Entered)*

REPORT DOCUMENTATION PAGE

READ INSTRUCTIONS BEFORE COMPLETING FORM

1. REPORT NUMBER: AFIT-CI-77-13	2. GOVT ACCESSION NO. (9) Doctoral thesis,
3. RECIPIENT'S CATALOG NUMBER	
4. TITLE *(and Subtitle)*: (6) Compensation for Propagation Uncertainties in the OMEGA Navigation System,	5. TYPE OF REPORT & PERIOD COVERED: Dissertation
	6. PERFORMING ORG. REPORT NUMBER
7. AUTHOR(s): (19) ROBERT L. VANALLEN, CAPTAIN, USAF	8. CONTRACT OR GRANT NUMBER(s)
9. PERFORMING ORGANIZATION NAME AND ADDRESS: AFIT Student at Iowa State University, Ames, Iowa	10. PROGRAM ELEMENT, PROJECT, TASK AREA & WORK UNIT NUMBERS
11. CONTROLLING OFFICE NAME AND ADDRESS: AFIT/CI, Wright-Patterson AFB Ohio 45433	12. REPORT DATE: (10) 1976
	13. NUMBER OF PAGES: ~~163~~ pages (12) 114p.
14. MONITORING AGENCY NAME & ADDRESS *(if different from Controlling Office)*	15. SECURITY CLASS. *(of this report)*: Unclassified
	15a. DECLASSIFICATION/DOWNGRADING SCHEDULE

16. DISTRIBUTION STATEMENT *(of this Report)*

Approved for Public Release; Distribution Unlimited

17. DISTRIBUTION STATEMENT *(of the abstract entered in Block 20, if different from Report)*

18. SUPPLEMENTARY NOTES

JERRAL F. GUESS, Captain, USAF
Director of Information, AFIT

APPROVED FOR PUBLIC RELEASE AFR 190-17.

19. KEY WORDS *(Continue on reverse side if necessary and identify by block number)*

20. ABSTRACT *(Continue on reverse side if necessary and identify by block number)*

Attached

012200

DD FORM 1 JAN 73 1473 EDITION OF 1 NOV 65 IS OBSOLETE

UNCLASSIFIED

SECURITY CLASSIFICATION OF THIS PAGE *(When Data Entered)*

TABLE OF CONTENTS

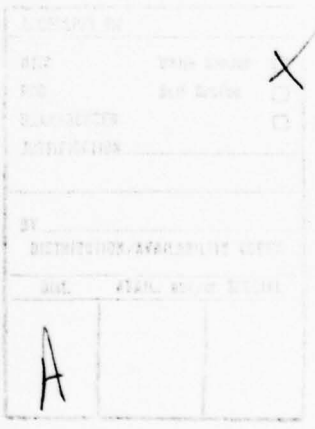

I. INTRODUCTION

During the past decade, an increased demand for long-range navigation aides has been exhibited by commercial and military interests. Fishing fleets, oil exploration companies, and global airlines are among the host of potential users for which very accurate, remotely available navigation information is imperative. OMEGA is a long range radio navigation system that has shown considerable promise in such applications and in fact has demonstrated a world-wide capability with accuracies on the order of 1 to 2 nautical miles.

Although OMEGA has gained modest acceptance within the navigation community (particularly in marine applications), it is a propagation limited system and several problems persist. Certain changes in the daytime and nighttime characteristics of the transmission medium cause day to night changes in the received navigation signals, inducing what is known as diurnal shift. In addition to this repeatable (and somewhat predictable) phenomenon, unusual solar activity can cause severe and rapid changes in the medium which also affects the received signal. Large volumes of predicted diurnal shift values have been published which reduce errors caused by diurnal shift, but their useage is cumbersome at best and, of course, they cannot account for errors induced by high solar activity or other anomalous propagation conditions.

This dissertation presents two new techniques which may be used to compensate for propagation-induced errors in the OMEGA navigation system. Chapter II includes a description of OMEGA and appropriate navigation

schemes and is entirely tutorial in nature. Certain kinds of unusual propagation conditions and the data collecting scheme for this study are also described. Chapter III introduces a methodology which enables one to compensate for diurnal shift effects. This technique resulted from the combined efforts of Dr. R. G. Brown, Iowa State University, and the author over the past year. Chapter IV presents an additional compensation method developed entirely by the author, which enables the OMEGA user to detect and compensate for anomalous propagation conditions entirely on an on-line basis. Both the methods of Chapters III and IV are deduced from physical interpretations of VLF (Very Low Frequency) wave propagation, and offer improved accuracies in current OMEGA techniques and increased insight into the VLF navigation problem.

II. THE OMEGA NAVIGATION SYSTEM

A. System Description

OMEGA is a very-long-range, VLF radio navigation system which transmits at several assigned frequencies in the 10 to 14 kHz frequency band. Global coverage is provided by eight transmitting stations located at various points around the world. Due to its very low transmitting frequency, OMEGA provides adequate navigation signals at longer ranges than other systems and is generally insensitive to prevailing weather conditions. The system is normally used in a single frequency hyperbolic mode although three frequencies are available and it can be used in a ranging mode (see Section II.B).

The primary navigational signal (10.2 kHz) and the remaining two signals ($11\frac{1}{3}$ kHz and 13.6 kHz) are transmitted sequentially as coherent time-synchronized continuous wave bursts. Note that the transmitted frequencies are in the exact ratio 9:10:12. Each burst is of about one-second duration and is repeated at ten-second intervals. The transmitting format is unambiguous and allows each station to be identified by a decoding of the received sequence of bursts. Transmissions are derived from a bank of cesium frequency standards and each station is controlled as a source of standard signals. An expanded discussion of OMEGA system operation can be found in (1) - (4), and the interested reader is referred to these documents for additional details.

B. Navigation Using OMEGA

A convenient model for describing VLF radio propagation is that of wave propagation in a waveguide (4). In this case the boundaries of the waveguide are the lower D region of the ionosphere and the surface of the earth. One of the immediate consequences of such a model is that if one resonance "mode" is dominant, then phase and amplitude should vary regularly as a function of distance from the transmitter without fluctuations due to interference between various modes. In our case, this condition occurs at frequencies near 10 kHz and at distances greater than 1000 km and, in fact, measurements have shown that outside a 1000 km "near-field" zone, each transmitter radiates a stable signal pattern which is repeated in a radial direction at approximately 30 km segments from the station (Figure 1). These repeated segments are proportional

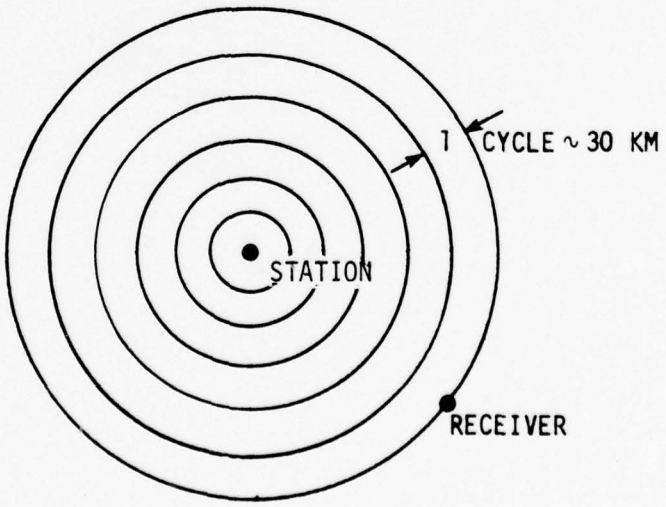

Figure 1. Phase - distance relationship at 10.2 kHz.

to distance and, therefore, also to the cumulative phase (or phase delay as it is more commonly known) between the transmitting station and a receiver. The above phase delay/distance relationship plays a key role in using OMEGA as a navigational tool, since the phases of the OMEGA signals can be measured using VLF receivers. Of course distance is proportional to the total phase delay while the user is only able to measure phase difference modulo 2π, i.e., if $\phi_c = 2\pi(n + a)$ is the cumulative phase difference (n = integer), then $2\pi a$ is the phase difference measured by the receiver. We therefore tacitly assume that the user has resolved any lane ambiguities via some external position fix. Thus distance is obtained from the relation

$$\text{distance} = \text{time delay} \cdot \text{velocity of phase propagation}$$

$$= T_1 \cdot v_1$$

$$= \frac{\phi_1}{f_1} \cdot v_1$$

where T_1 is the time required for the phase front at some frequency f_1 to travel from a transmitting station to the receiver, v_1 is the presumed known phase velocity at f_1, and ϕ_1 is the measured phase delay in cycles. Note that the accuracy in obtaining a measure of distance is limited not only by the ability to measure the signal phase but also by the validity of the presumed known phase velocity v_1.

It was mentioned previously that OMEGA can be employed in either a hyperbolic or ranging mode. In the ranging mode the user measures the

phase of a transmitted OMEGA signal with a receiver which is equipped with a very accurate internal oscillator. This oscillator has been previously synchronized with the master oscillators at the OMEGA sites and the difference in phase between it and the received OMEGA signal represents a measure of range from the transmitting station. Range determinations from two or three transmitters are used to compute position.

OMEGA is also used in a hyperbolic mode. In this mode, the phases of signals from pairs of stations are differenced and used to establish position along a line-of-position (LOP). LOP's (shown in Figure 2) are lines of constant phase difference between a signal received from station A and a signal received from station B, and therefore also are a measure

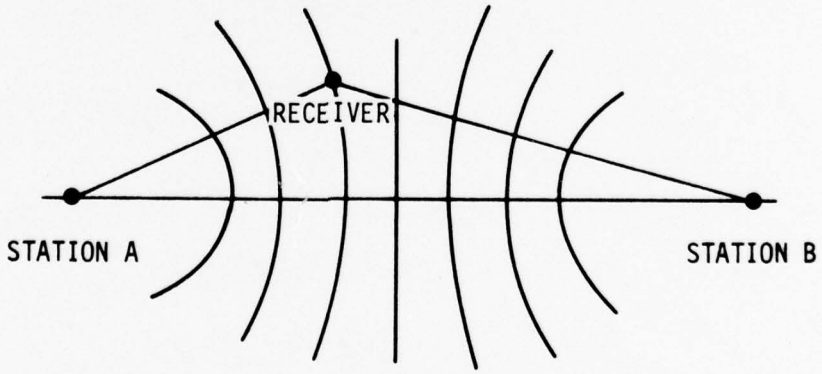

Figure 2. Hyperbolic geometry.

of constant range difference from stations A and B. When referenced to the surface of the earth these lines are described by sets of spherical

hyperbolas unique to each pair of stations. By selecting different pairs of stations the navigator generates several LOP's, the intersection of which is his position on the earth. To facilitate the construction of LOP lattices necessary for navigation, the U. S. Defense Mapping Agency has published standard charts and tables for this purpose. The popularity of the hyperbolic configuration lies in the simplicity and low-cost of the receiver hardware. Since any absolute radio-frequency phase shifts are common to all the OMEGA stations, it follows that these shifts are removed in the differencing operation. This eliminates the need for the user to have an extremely precise reference oscillator and allows a considerable cost-saving.

C. Propagation Uncertainties

In the previous section we noted that we could estimate the distance from an OMEGA transmitter to a receiver by multiplying the measured time delay at an appropriate frequency (10.2 kHz in this case) by an assumed nominal phase velocity. Obviously as the true velocity varies from the nominal, errors in position occur. One error of this type is what is known as diurnal shift. Diurnal shift is caused by a change in the effective reflecting height of the ionosphere between night and day, thereby changing the phase velocity. If not corrected for diurnal shift causes errors on the order of 10 nautical miles over typical propagation paths. Fortunately the velocity variations are somewhat predictable and large sets of phase correction tables (or PPC's as they are known) are available for compensation of varying propagation parameters. The PPC's

list corrections as a function of user location, hour, day, month, and selected transmitting station, and allow navigation with accuracies of about 1 to 2 nautical miles.

Along with the logistics problem associated with the use of the tables, the PPC's are "open-loop" corrections. Any anomalous atmospheric conditions which affect the signal phase velocity, cause navigational errors which can neither be detected nor corrected by use of the tables. The most important of these, Sudden Ionospheric Disturbances (SID's) and Polar Cap Absorptions (PCA's), mainly occur during periods of high solar activity and are characterized by a lowering of the reflecting height of the ionosphere (5). The resultant increase in phase velocity can cause navigational errors on the order of 5-10 n.m. Since recovery from these events is slow (tens of minutes to several hours for SID's, several days for PCA's), single-frequency OMEGA performance suffers in comparison with other navigation schemes during these unusual conditions (6).

D. Phase Monitoring and Recording

The U. S. Coast Guard's OMEGA Navigation System Operations Detail (ONSOD) maintains monitoring stations throughout the world and collects phase measurement data on all the OMEGA frequencies. This is done primarily to verify the accuracy of the PPC's but also serves as a check on the operation of the transmitting stations. The phase measurements are recorded via plot printers and then read at the rate of one measurement per hour by site personnel. The entire receiver/recorder system has an rms accuracy of roughly 2 centicycles (cec).

Strip-charts from two monitoring sites (North Dakota - station D, and Hawaii - station C) were obtained from the Coast Guard for the month of March 1975 and comprise the bulk of the data base used in the present study. Phase measurements (at all three OMEGA frequencies) were read from the charts at the rate of one per hour, corrected for gross lane count, and transferred to punched computer cards. Propagation paths for which the data was read include B-D (Trinidad - North Dakota), C-D (Hawaii - North Dakota), D-C (North Dakota - Hawaii), A-D (Norway - North Dakota), and H-C (Japan - Hawaii). The notation B-D indicates that the signal was transmitted at station B (Trinidad) and recorded at station D (North Dakota); thus the recorded phase measurement represents the total phase delay over the path B-D. The data used for each path is 10-31 March for B-D and C-D, 10-22 March for D-C, and 1-31 March for A-D.

In addition to the 2 cec measurement accuracy limitation mentioned earlier, other errors appear to be present in the data. For the March 1975 data analyzed, errors apparently occur in the C-D data due to a dead zone in the recording equipment at the monitoring site. The strip-chart paper used at the site has a recording width of 100 cec (1 cycle). Thus when the phase of a signal "crosses over" from one cycle to the next, the pen plotter resets itself from 100 cec to 0 cec and continues on. When this happens on the C-D recording, the plotter continues to track the 100 cec value for some time before switching over to zero. The error induced by this equipment delay ranges from .5 to 3 cec and was not corrected for in this study. This is mentioned merely to point out that errors of a certain magnitude may be expected in the data base. It is not a reflec-

tion on the quality of the recording scheme which, after all, is only designed to meet a 2 cec rms accuracy specification.

The paths selected in this study afford a variety of propagation conditions. Path B-D is predominantly South - North while D-C and C-D are East - West and West - East respectively. Path A-D was included since it traverses the Greenland ice cap and causes some unusual propagation problems. H-C (Japan - Hawaii) was originally chosen as an additional West - East path but, because of frequency synchronization problems at the transmitting station, it was not used in the final analysis.

The information recorded on data cards included:

a. hour of day in Greenwich Mean Time (GMT)

b. day

c. month

d. path

e. phase measurements at 10.2, $11\frac{1}{3}$, and 13.6 kHz.

f. strip chart error associated with each phase measurement

g. "unusual" data flag

h. day/night/transition flag

The day/night/transition flag indicated whether the total path was in light (day), darkness (night), or a combination of both (transition). These definitions of day and night are standard and are used in this context throughout this paper.

III. COMPENSATING FOR DIURNAL SHIFT

A. Overview

Diurnal shift in the measured phase of the OMEGA transmissions is the most common cause of error in the OMEGA system. The use of PPC tables effectively minimizes this problem but the procedure is awkward and slow. In addition, with the recent advances in microprocessor technology, there has been increased interest in developing on-line, real-time OMEGA navigation schemes which do not depend on PPC tables. One approach is to implement, on-line, a simplified version of the prediction algorithms used to generate the published tables. Beavers and others (7) have recently suggested that such a technique is now feasible. The other approach is to compute a fictitious propagation time from on-line phase measurements made at more than one frequency, and Papousek and Reder (8) and Pierce (9) have proposed navigation schemes based on this concept. The present chapter expands on this latter approach and offers an algorithm for computing a propagation time that is based on all three phase measurements. The concepts of group velocity and associated group delay play an important role in the development that follows, so a few remarks about wave propagation in a waveguide are appropriate at this point.

B. Relation of Group and Phase Velocity

For simple parallel-plane waveguide modes, the phase and group velocities vary with frequency as shown in Figure 3. These velocities have the physical interpretation as the velocities at which the wave's fine structure (phase) and envelope (group) propagate (10). The height

of the guide determines the cut-off frequency, so the height will also affect the phase and group velocities. For example, increasing the waveguide height in a simple parallel-plane waveguide lowers the cutoff frequency at the dominant mode. For a wave at a frequency above cutoff, the group velocity is then increased and the phase velocity decreased. Furthermore, for simple modes the geometric mean of the phase and group velocities, v_p and v_g, is invariant and equal to the free velocity, i.e.,

$$\sqrt{v_p v_g} = v_0$$

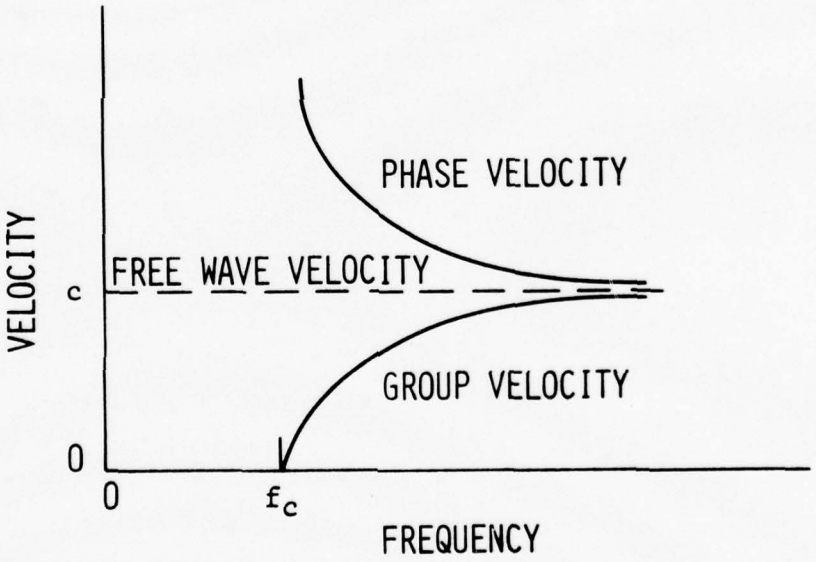

Figure 3. Phase and group velocities for parallel-plane waveguide.

To get a better feel for the physical meaning of group velocity consider the example of transmitting information with a carrier, $E_0 \cos\omega t$, amplitude modulated by a signal whose frequency is $\Delta f = \Delta\omega/2\pi$.

Such a signal would be represented by

$$E = E_0(1 + m\cos\Delta\omega t)\cos\omega t$$

where ω is the angular frequency and m the modulation factor. This can be expanded to show the presence of the carrier and side-band frequencies (11)

$$E = E_0\cos\omega t + \frac{mE_0}{2}[\cos(\omega + \Delta\omega)t + \cos(\omega - \Delta\omega)t]$$

When such a signal is propagated in the z direction under conditions where the phase velocity varies with frequency, i.e., in a <u>dispersive</u> medium, the resultant wave is written as

$$E = E_0\cos(\omega t - \beta z) + \frac{mE_0}{2}\{\cos[(\omega + \Delta\omega)t - (\beta + \Delta\beta)z]$$

$$+ [\cos(\omega - \Delta\omega)t - (\beta - \Delta\beta)z]\}$$

where β is phase lag per unit length and z is the distance traveled. Using well-known trigonometric identities E can also be written as

$$E = E_0[1 + m\cos(\Delta\omega t - \Delta\beta z)]\cos(\omega t - \beta z)$$

The bracketed part of the expression represents the envelope of the wave and we see that the envelope travels in the z direction with a velocity

$$v_g = \frac{\Delta\omega}{\Delta\beta} \qquad (1)$$

If the frequency spread is small, this may be written as the limit

$$v_g = \frac{d\omega}{d\beta} \tag{2}$$

The idea of group and phase velocities is sometimes visualized in terms of Figure 4. A person "running alongside" the wave packet as it progresses through space would see the envelope slipping backward with respect to the component waves. This is because it is moving forward with the group velocity v_g, which is less than the phase velocity of the component waves. If β is plotted as a function of ω, the phase and group velocity may be interpreted geometrically. Figure 5 shows such a plot for wave-guide propagation. We see that the slope of $\beta/\omega = 1/v_p$ is always less than that of $\frac{d\beta}{d\omega} = 1/v_g$ so that v_p is always greater than v_g but both approach the free velocity of the guide, v_0, as ω approaches

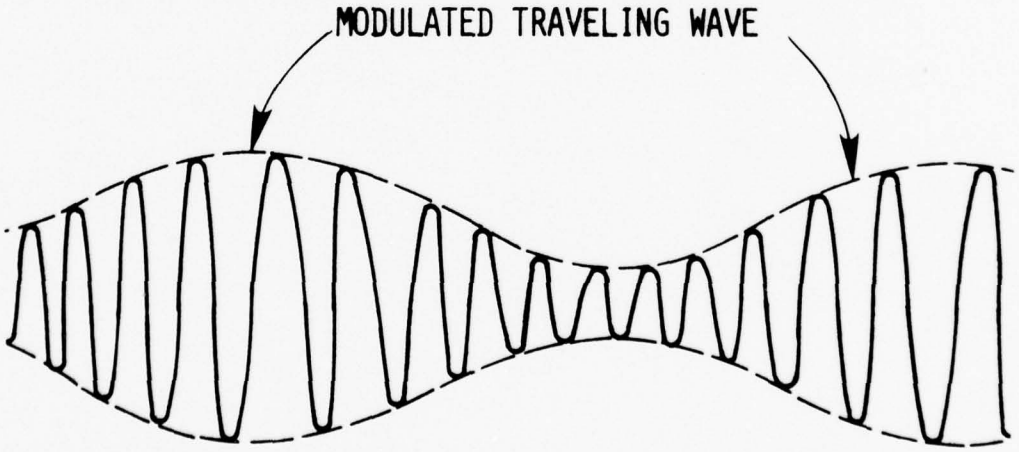

Figure 4. Modulated traveling wave.

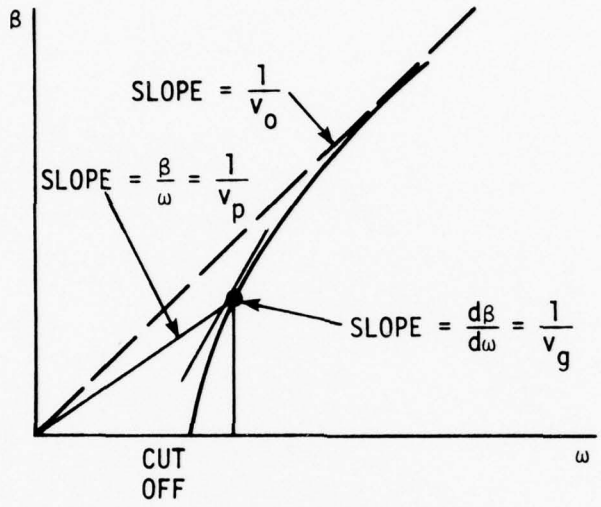

Figure 5. Phase shift versus frequency.

infinity (11).

C. Composite and Difference OMEGA

The theoretical existence of an invariant free velocity throughout the OMEGA frequency range led J. A. Pierce in 1968 to suggest a navigational scheme called composite OMEGA (9). Consider a flat-earth propagation model as shown in Figure 6. At the OMEGA frequencies, the phase and group velocities are nearly equal, one being slightly greater than the free velocity and the other slightly less (see for example, (1), (5), or (12)). Thus the geometric mean is approximately equal to the arithmetic mean, i.e.,

$$\sqrt{v_p v_g} \approx \frac{v_p + v_g}{2} \approx v_0$$

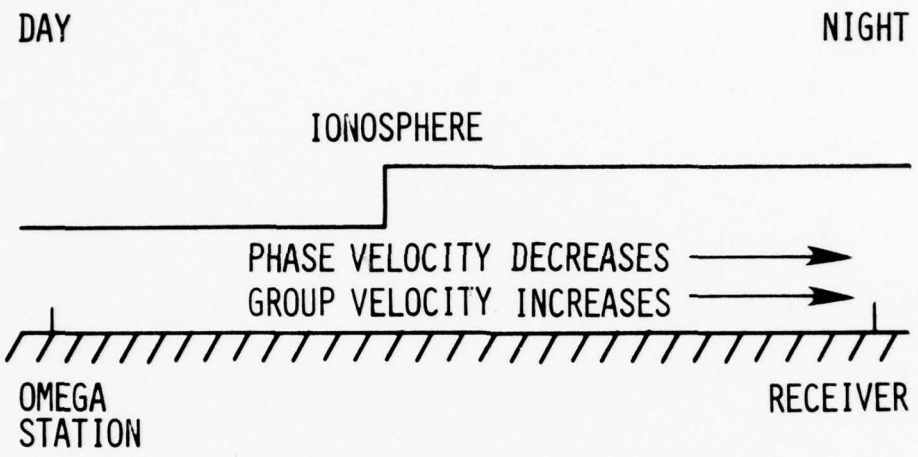

Figure 6. Flat-earth model.

The phase and group delays are similarly related and this leads to an analytic free-wave delay T_c (which Pierce called composite time) where

$$T_c \simeq \frac{T_g + T_p}{2} \tag{3}$$

In actually computing this composite time, the user cannot directly measure the group delay T_g. However as noted above,

$$v_g \simeq \frac{\Delta\omega}{\Delta\beta}$$

Thus for a fixed distance d,

$$T_g = \frac{d}{v_g} \simeq \frac{d}{\Delta\omega/\Delta\beta}$$

or since β is phase shift per unit distance

$$T_g = \frac{\Delta\phi}{\Delta\omega} = \frac{\phi_2 - \phi_1}{\omega_2 - \omega_1}$$

where ϕ_1 and ϕ_2 are the total phase shifts in radians over the propagation path at angular frequencies ω_1 and ω_2 respectively, and T_g is the group delay referred to the mid-frequency $\frac{\omega_1 + \omega_2}{2}$.

For composite OMEGA, Pierce used as the group delay

$$T_g \simeq \frac{\phi_3 - \phi_1}{f_3 - f_1} \tag{4}$$

where f_1 = 10.2 kHz and f_3 = 13.6 kHz, and ϕ_3 and ϕ_1 are the total phase shifts in cycles. The group delay is then referred to the mid-frequency

$$\frac{f_3 + f_1}{2} = 11.9 \text{ kHz}.$$

The phase delay can also be referred to 11.9 kHz through the approximation

$$T_p \simeq \frac{T_{p_3} + T_{p_1}}{2} = \frac{\phi_3/f_3 + \phi_1/f_1}{2} \tag{5}$$

where T_{p_3} and T_{p_1} represent the phase delays at f_3 and f_1 respectively. Substituting Equations 4 and 5 into Equation 3 then yields (after some algebraic manipulations), Pierce's composite time which should be relatively insensitive to changes in the ionospheric height. Note that T_c is a linear combination of the phase delay times at the upper and lower OMEGA frequencies.

$$T_c = \frac{\phi_1}{f_1} + 2.25\left\{\frac{\phi_3}{f_3} - \frac{\phi_1}{f_1}\right\}$$

$$= T_{p_1} + 2.25(T_{p_3} - T_{p_1}) \qquad (6)$$

The way in which the composite time is formed can also be viewed from another perspective. In the discussion above we developed the idea of a composite time by giving equal weight to the phase and group delays. If instead we view T_c as a weighted sum of the phase and group delays referred to 11.9 kHz, i.e.,

$$T_c = kT_g + (1 - k)T_p$$

it works out that T_c can again be written as a linear combination of the phase delay times at the upper and lower OMEGA frequencies

$$T_c = T_{p_1} + m(T_{p_3} - T_{p_1}) \qquad (7)$$

where $m = \frac{1}{2}\left[\frac{k(f_3 + f_1)}{(f_3 - f_1)} + 1\right]$. We see that changing the "blending" (k factor) of the phase and group delays results in different values of m and, in fact, both extremes in blending and all variations in between can be obtained by varying m from 0.5 to 4.0 (Figure 7).

The concept of viewing propagation delay as a blending of group and phase delays can also be applied to other navigation schemes. In difference OMEGA the propagation delay is obtained by subtracting the phase delays at the upper and lower frequencies and dividing by the difference

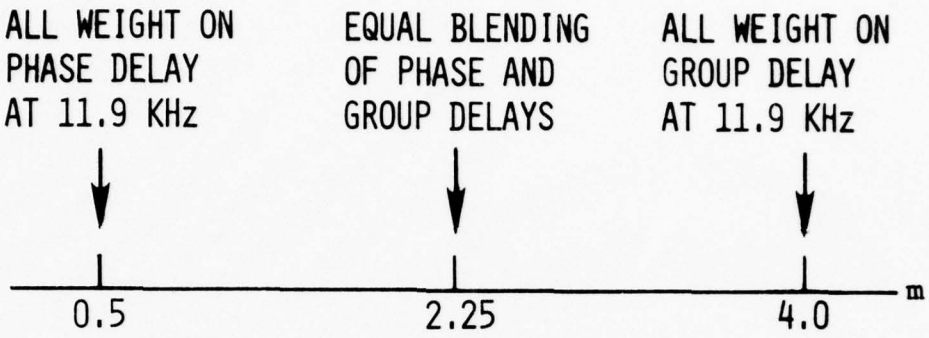

Figure 7. Interpretation of Pierce's m factor in terms of blending mid-frequency phase and group delays.

frequency. That is,

$$T_d = \frac{\phi_3 - \phi_1}{f_3 - f_1}$$

But this can be shown to be precisely the composite time with m=4, that is with all the weight on the group delay. So the difference OMEGA delay can be thought of as a finite-difference approximation to the true group delay at 11.9 kHz. In the OMEGA case, the error in using the approximation is less than .01 per cent (13). Furthermore, this "error" is not one of substance, it simply means that the envelope velocity obtained from the finite-difference form corresponds exactly to a group velocity evaluated at a frequency near to, but not exactly at, the mid-frequency. This is assured by the mean-value theorem of calculus.

In summary, we see that difference OMEGA is dependent entirely on group delay at the mid-frequency of 11.9 kHz, whereas composite OMEGA

employs a blend of both phase and group delays at the same mid-frequency. Of course, the mid-frequency phase and group delays are analytic in both cases, because they are formed as linear combinations of measured phase delays at the end frequencies. Nevertheless, this mid-frequency phase and group delay viewpoint is useful in assessing variations in delay times due to changes in the transmission medium.

The result of implementing composite OMEGA with equal weighting of phase and group delay is shown in Figure 8. Propagation time is plotted against time of day (GMT) for the path B-D (Trinidad to North Dakota). Each solid line represents a time span of one day so the entire graph contains 22 days of superimposed data.

In viewing Figure 8, we see that a difference in the day/night levels of about 25 μsec is quite evident. The reason for this diurnal shift lies in the fact that the invariance of the average of the phase and group delays is only valid at the mean height of energy flow in the waveguide (9). In a curved waveguide such as the earth-ionosphere guide, this mean height is located somewhere between the earth's surface and the lower ionosphere (Figure 9). Thus from purely geometrical considerations we see that, for some fixed distance along the ground, the path at a height h' increases from day to night. Therefore although the free velocity is invariant at h', the composite time as seen from the ground changes from day to night because the mean path length at h' changes.

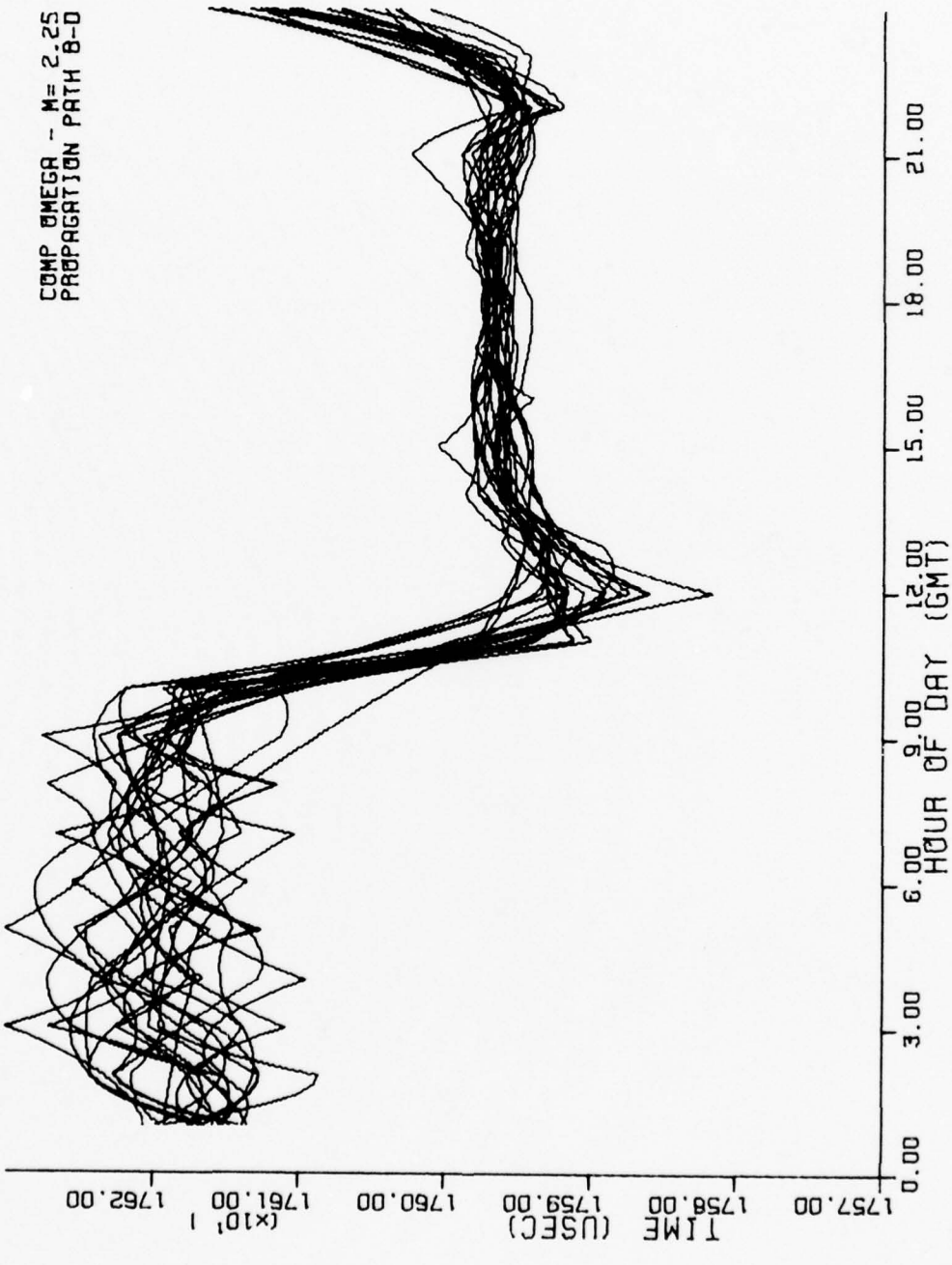

Figure 8. Composite time (m=2.25) versus time of day (GMT). Trinidad - North Dakota (B-D). 10-31 March 1975.

D. Three-Frequency Difference OMEGA

Although some researchers have suggested increasing m to compensate for the diurnal shift in composite OMEGA (8), (14), a reexamination of Figure 9 suggests another approach. Earlier we mentioned that group velocity increases as we go from the day to the night portion of the waveguide. One might speculate, then, whether or not there is a frequency at which the diurnal increase in path length at h' is exactly offset by a corresponding increase in group velocity, thereby resulting in an invariant group delay.

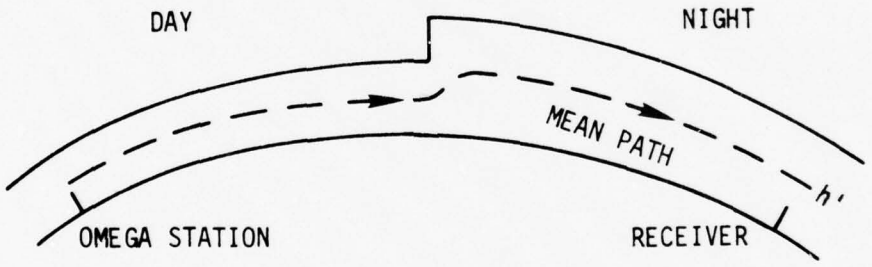

Figure 9. Curved-earth model.

Theory indicates that such a frequency does exist. In Figure 10, v_g/c is plotted as a function of frequency for several values of ionospheric height (13). We see that the curves for the nominal day (h=70 km) and nominal night (h=90 km) conditions cross over in the frequency range 12.0 to 12.5 kHz. That is, the group velocity during the day and the group velocity at night should be equal at some particular frequency. Not only is the existence of such a frequency of interest but also

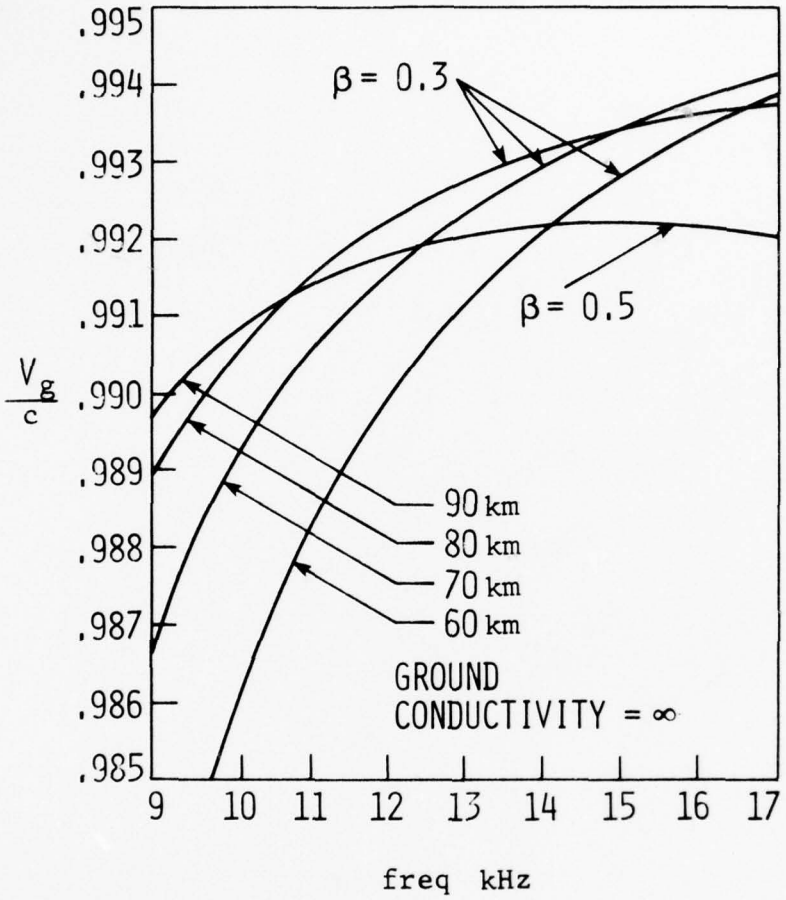

Figure 10. Theoretical group velocities for different ionospheric heights.

whether it is invariant under a variation of transmission parameters, e.g., direction of propagation, ground conductivity, etc.

To compute a group delay that can be referred to any frequency, we utilize all three OMEGA frequencies. Assume we have three time delay measurements T_1, T_2, T_3 corresponding to the three OMEGA frequencies ω_1, ω_2, ω_3. Each of these time delays represents a ratio of total phase

shift to frequency, i.e.,

$$T_i = \frac{\phi_i}{\omega_i} = \frac{\beta_i d}{\omega_i} \qquad i = 1, 2, 3$$

It is tacitly assumed that lane ambiguities for all three frequencies have been resolved. In effect, the three phase measurements give us three points on the βd versus ω curve as shown in Figure 11. Now assume

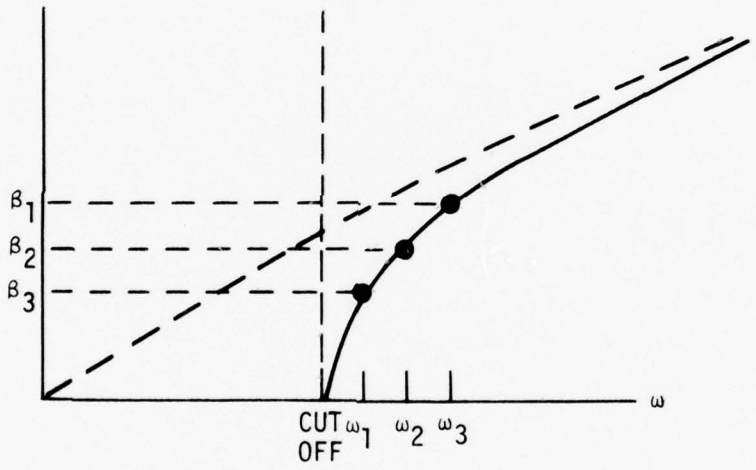

Figure 11. Phase shift versus frequency.

that βd can be approximated as a quadratic function of ω over a reasonable range of ω; i.e., let

$$\beta d = C_2\omega^2 + C_1\omega + C_0 \tag{8}$$

We can then choose the coefficients C_0, C_1, C_2 such that βd goes through the measured ϕ_1, ϕ_2, ϕ_3 points as shown by solving the equations

$$C_0 + C_1\omega_1 + C_2{\omega_1}^2 = \phi_1$$

$$C_0 + C_1\omega_2 + C_2{\omega_2}^2 = \phi_2$$

$$C_0 + C_1\omega_3 + C_2{\omega_3}^2 = \phi_3$$

Returning to Equation 8 we note that

$$T_g = \frac{d}{v_g} = \frac{d}{\frac{d\omega}{d\beta}} = \frac{d(\beta d)}{d\omega} = 2C_2\omega + C_1 \qquad (9)$$

Substituting the solutions for C_1 and C_2 into Equation 9 and recognizing that the ratios ω_1, ω_2, and ω_3 occur in the exact ratio 9:10:12, the following equation results (15),

$$T_g = (60\frac{\omega}{\omega_2} - 66)T_1 + (-100\frac{\omega}{\omega_2} + 105)T_2 + (40\frac{\omega}{\omega_2} - 38)T_3$$

$$= K_1T_1 + K_2T_2 + K_3T_3 \qquad (10)$$

Equation 10 enables one to compute a group time delay referred to <u>any</u> arbitrary frequency ω, in terms of the three measured phase delays T_1, T_2, and T_3. Note that T_g is a <u>linear</u> function of T_1, T_2, and T_3 and that the sum of the coefficients (weight factors) is unity.

In Equation 10 it is of interest to look at variations in the coefficients of T_1, T_2, and T_3 with frequency. These variations are plotted in Figure 12 and we note that in the 12.0-12.5 kHz range none of

the coefficients exceeds 6. Purely random errors in the phase delay measurements do, of course, get "amplified" by the coefficients, so large values are undesirable. How undesirable, though, is a matter of

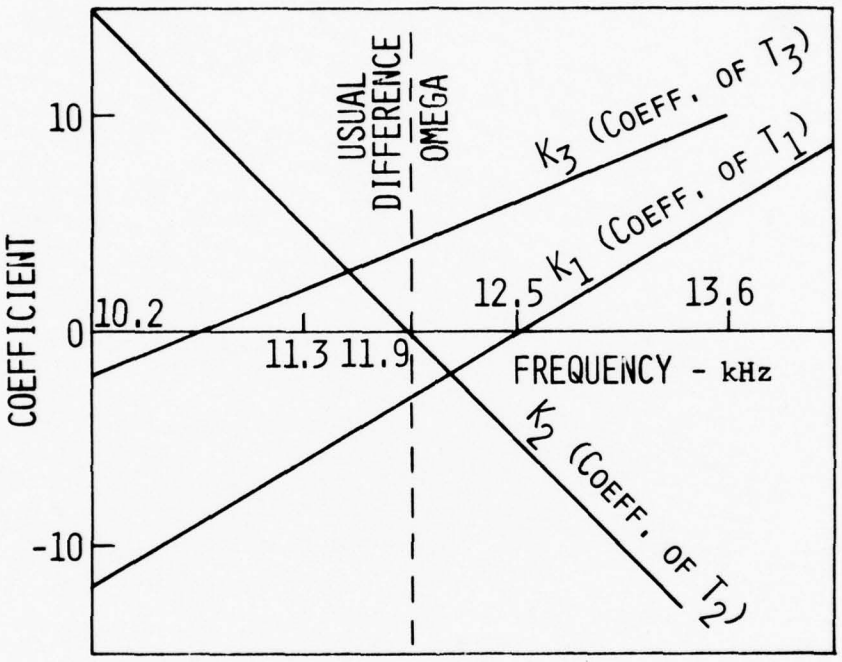

Figure 12. Variation of K_1, K_2, K_3 coefficients with frequency.

degree and depends on equipment accuracy and the application. For example, if one assumes the three measurement errors associated with T_1, T_2, and T_3 to be independent and each having unity variance, the resultant rms error in T_g would be as shown in Figure 13. It should be apparent that the best choice of reference frequency involves a compromise between the noise error shown in Figure 13 and the diurnal shift error. Note particularly that the total amplification factor ranges from 5 to 8 in the 12.0 to 12.5 kHz range.

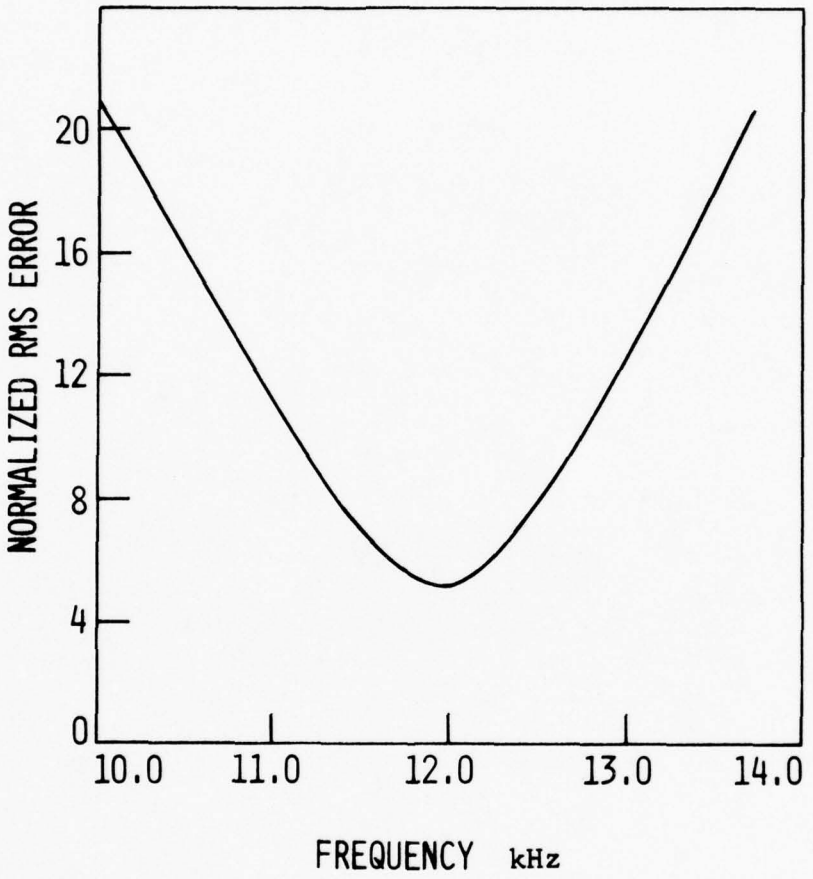

Figure 13. Normalized rms error due to measurement noise.

An example of applying the three-frequency algorithm to one path is illustrated in Figure 14. The propagation path is B-D; thus the computed group delays represent the group propagation time of the Trinidad signal (station B) as it is seen at North Dakota (station D). Each of the four figures in Figure 14 contains the group delays for 22 days computed at a particular frequency. Frequencies of 11.7, 11.9, 12.2, and 12.4 kHz were selected for comparison. In the graphs, the hours 0200-0900 corre-

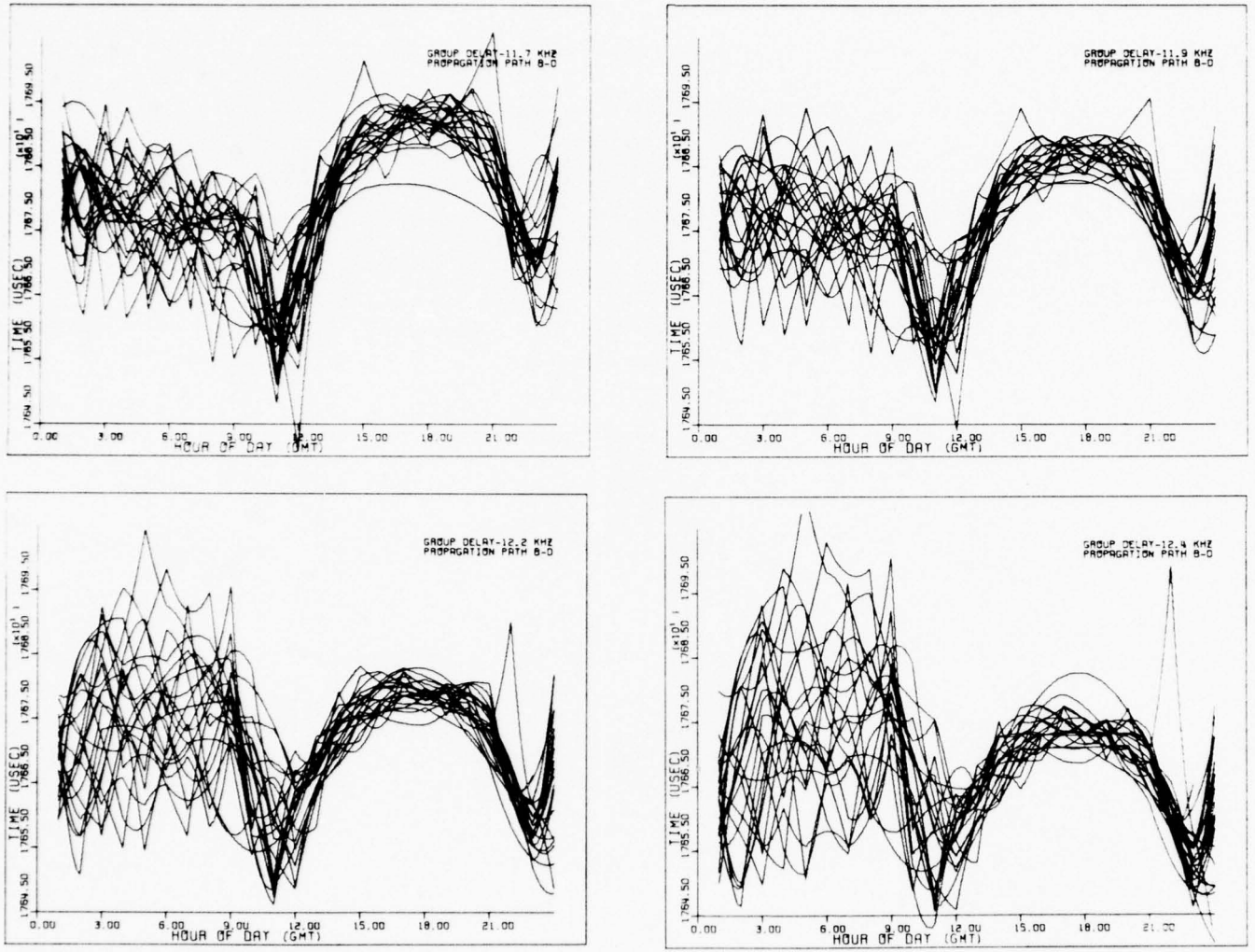

Figure 14. Group delay versus hour of day (GMT) for various values of reference frequency. Trinidad - North Dakota (B-D). 10-31 March 1975.

spond to "night" or the time in which the entire propagation path is in darkness; and 1400-2100 corresponds to "day" or that time in which the entire path is in sunlight.

In viewing Figure 14 several items are of interest.

(1) We note that a diurnal variation is quite noticeable at 11.7 kHz, decreases somewhat at 11.9 kHz, and is essentially zero at 12.2 kHz. The average group delays during the day and night periods are plotted as a function of frequency in Figure 15, and we see that the average diurnal shift is indeed minimized at the crossover fre-

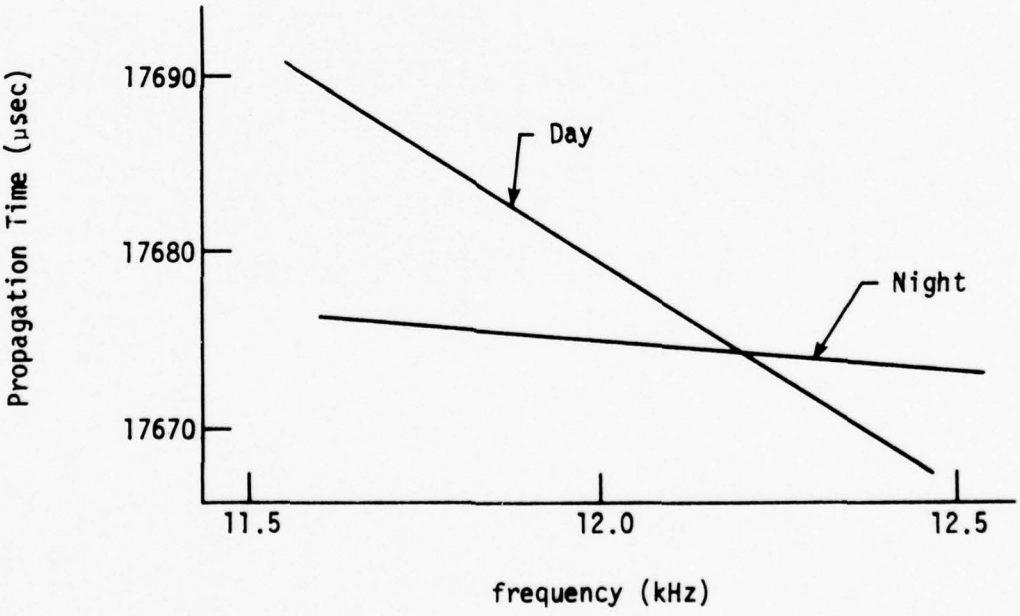

Figure 15. Average group delay versus frequency. Trinidad - North Dakota (B-D). 10-31 March 75.

quency of 12.2 kHz. This is consistent with the theoretical curves in Figure 10. Assuming a nighttime height of 90 km and a daytime

height of 70 km, the group velocity at frequencies below crossover is higher at night than during the day; therefore, the night group-delay times are lower than those during daytime.

(2) From Figure 14 we also note that during the transition periods between night and day, the group delay decreases sharply and then recovers. Again in terms of Figure 10, this indicates that the ionospheric height is at some level between 70 and 90 km. At the crossover frequency, for example, the group velocity, which is the same for night and day moves higher ("towards" 80 km) when entering the transition period and then returns to the crossover value.

(3) Finally, we see that the noise-like excursions at night (random or otherwise) become greater as the frequency increases above 11.9 kHz. In fact an examination of Figure 16 shows that the standard deviation of the group delay is minimized at 12.2 kHz during day conditions and at 11.8 kHz at night. This indicates two things:

(i) noise amplification which is of little consequence during day increases in importance at night, and

(ii) phase changes due to small fluctuations of ionosphere height are minimized at different frequencies during day and night. This is to be expected since from Figure 10 we note that the 90 (night) and 80 km curves intersect at a frequency much less than 11.9 kHz while the 70 (day) and 80 km curves approach each other as frequency increases. Thus the frequency at which the "noise" in the group delay is minimized is a compromise between 11.9 kHz,

where the instrument error amplification is least (from Figure 13), and the frequency associated with minimizing random fluctuations in the transmission medium.

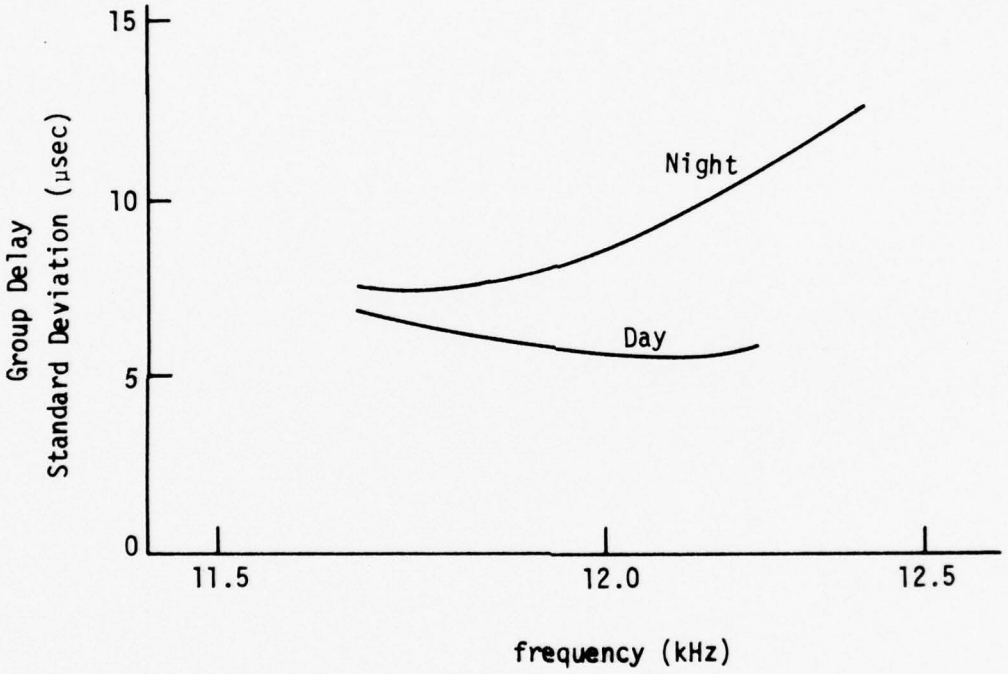

Figure 16. Group delay standard deviation versus frequency. Trinidad - North Dakota (B-D). 10-31 March 75.

For comparison purposes, propagation times computed from Pierce's composite OMEGA algorithm are shown for various m factors in Figure 17. Again propagation time is plotted against time of day (GMT) and it is quite apparent why increasing the m factor decreases the diurnal shift. For Pierce's original value of m=2.25, there is very little noise associated with the composite delay, but a diurnal shift of about 30 μsec is

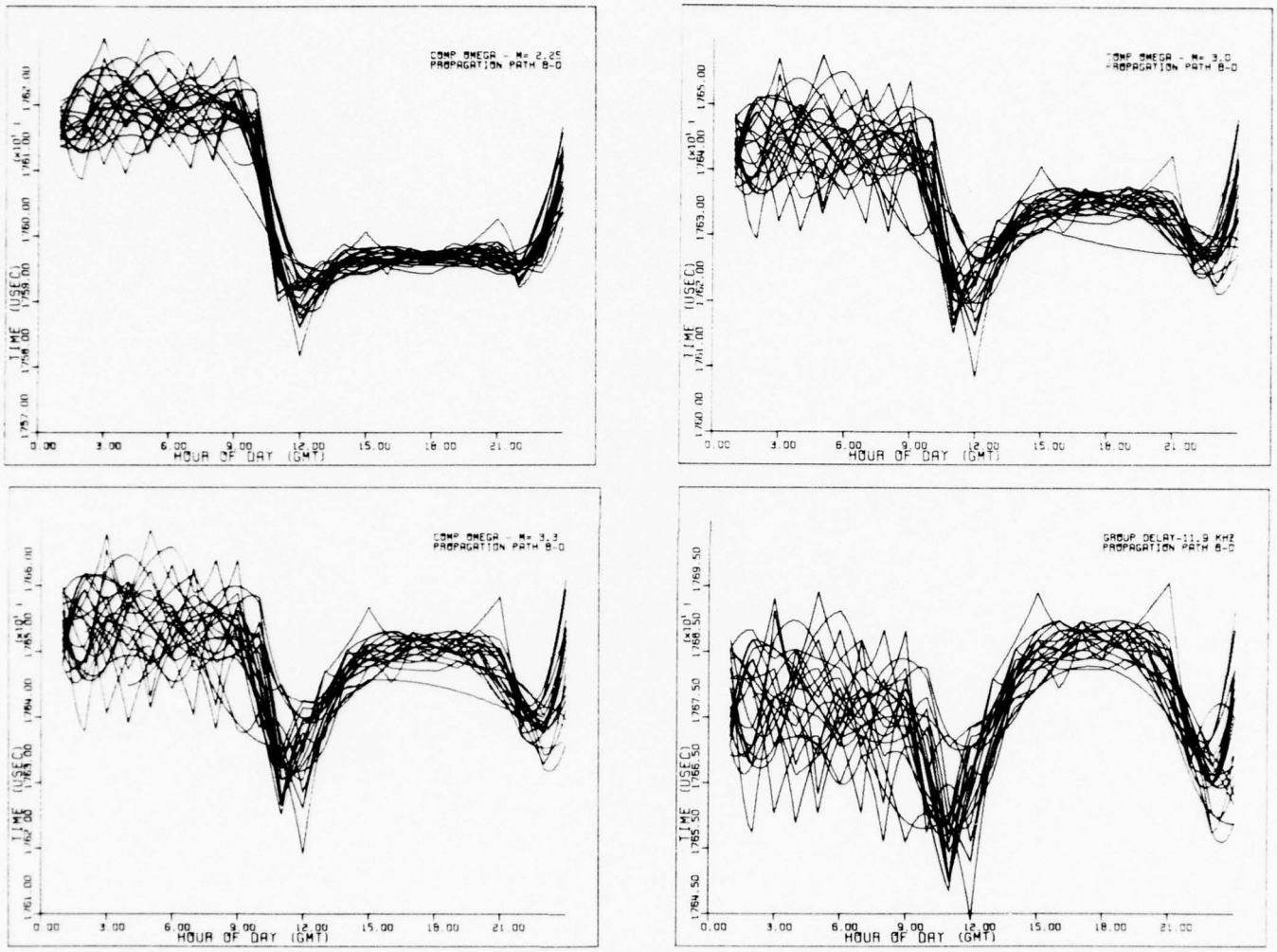

Figure 17. Composite time versus hour of day (GMT) for various m coefficients. Trinidad - North Dakota (B-D). 10-31 March 1975. Note: The figure labeled "Group Delay - 11.9 kHz" is the same as "Composite Time, m=4."

quite evident. As the value of m is increased from 2.25 to 4.0 (that is, as more weight is given to group delay and less to phase delay when forming the composite time), the average diurnal shift reverses itself. The result is, for this path, the diurnal shift is nullified at m=3.3. An increase in noise level is also seen as m increases. This is to be expected because m is a direct noise amplification factor, just as are the K_1, K_2, K_3 coefficients in the three-measurement group delay formula.

E. Application to Hyperbolic Navigation

In the three-frequency difference OMEGA development we tacitly assumed that we were using OMEGA in a ranging mode. That is, the group delays were computed as a linear combination of phase measurements of signals received from <u>one</u> transmitting site (say, for example, station A). Then

$$T_{g_A} = K_1 T_{1_A} + K_2 T_{2_A} + K_3 T_{3_A}$$

where K_1, K_2, K_3 are constants and T_{1_A}, T_{2_A}, T_{3_A} are the measured phase delays from station A. But the above algorithm can also be applied in a hyperbolic situation where we have access to the <u>differences</u> in phase between signals transmitted by a pair of stations. Then, applying the three-frequency scheme to the phase differences between stations A and B.

$$T_{g_{A-B}} = K_1(T_{1_A} - T_{1_B}) + K_2(T_{2_A} - T_{2_B}) + K_3(T_{3_A} - T_{3_B})$$

$$= (K_1T_{1_A} + K_2T_{2_A} + K_3T_{3_A}) - (K_1T_{1_B} + K_2T_{2_B} + K_3T_{3_B})$$

$$= T_{g_A} - T_{g_B}$$

So the group delay computed with phase differences from stations A and B is equivalent to the difference between group delays from A and B and, thus, can be used for hyperbolic navigation. Note that the propagation delay being a linear combination of the phase delays insures that the algorithm can be applied in a hyperbolic as well as ranging mode.

F. Summary of Results for the Three-Frequency Algorithm

A complete set of computer generated plots which reflect the results of applying the three-frequency algorithm to the test data is given in Appendix A. The results of implementing other OMEGA algorithms are also included for comparison. Propagation paths included are Trinidad - North Dakota (B-D), North Dakota - Hawaii (D-C), and Hawaii - North Dakota (C-D). The algorithms presented include three-frequency difference OMEGA referred to selected frequencies, composite OMEGA for three values of m, single-frequency OMEGA with PPC table corrections, and a "modified" composite technique, which utilizes nonlinear combinations of the phase measurements (8). Note that three-frequency difference OMEGA with f=11.9 kHz is equivalent to what is known as "difference OMEGA" and also to the composite OMEGA algorithm with m=4.0. Also note that path

B-D is predominantly South-North, D-C is East-West, and C-D is West-East.

The average group delays for night and day path conditions are plotted versus frequency in Figure 18. The day and night curves do

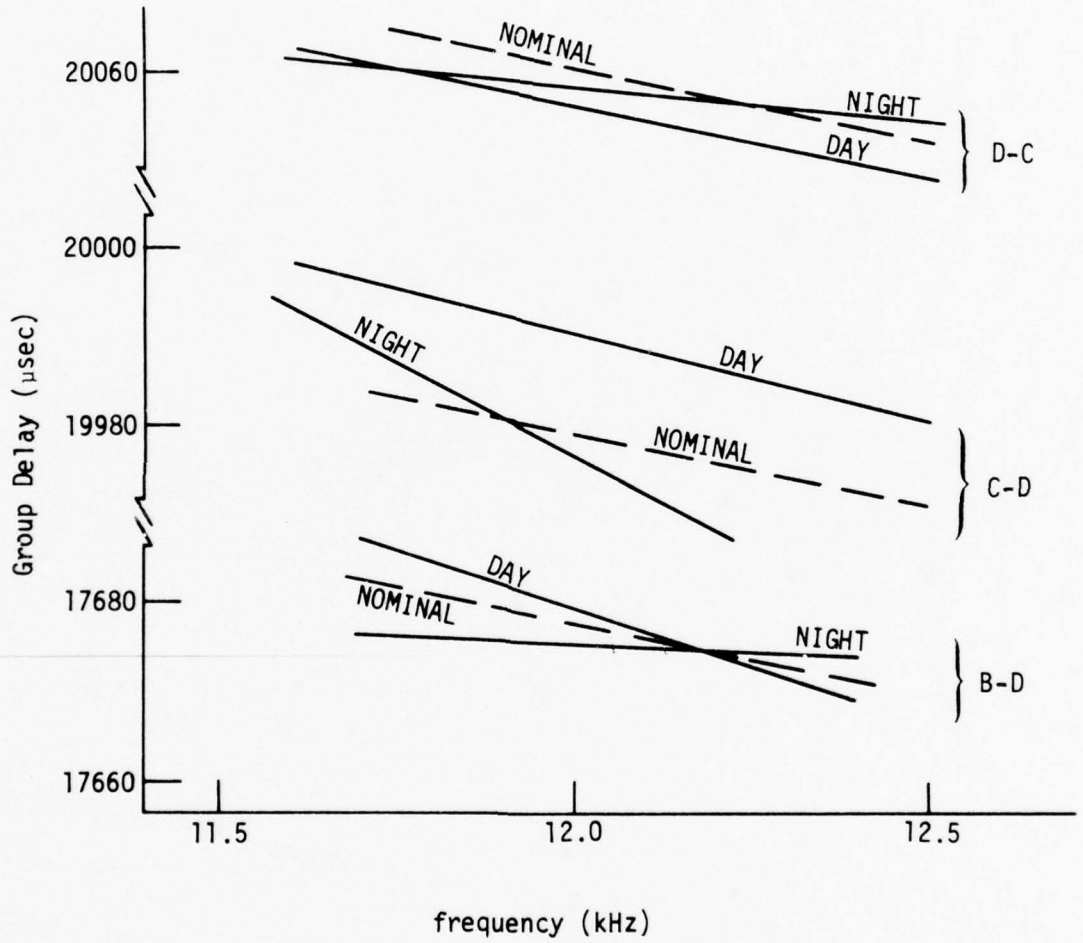

Figure 18. Average group delay versus frequency for several propagation paths. 10-31 March 75.

intersect in each case with the frequency of crossover ranging from about 11.5 to 12.2 kHz. It should be noted that the low crossover frequency for path C-D may be due to strip-chart errors in the 13.6 kHz signal (see

Chapter II). Non-reciprocal path effects caused by the earth's magnetic field are also in evidence. "Nominal" propagation times are plotted using the average B-D values for reference and we see that the D-C group delays are a little low while those for C-D are somewhat high. This can be predicted from theory (12) in that the phase velocities for East-West paths (D-C) are slightly higher, and for West-East paths (C-D) slightly lower than that for North-South paths (B-D).

In terms of selecting an appropriate reference frequency let us examine Figure 19. For each of the three paths under investigation the rms error is minimized in the region 12.0-12.2 kHz. Factors which influence the minimum-error frequency include diurnal shift, instrument-error amplification, and direction of propagation. In the present case the amplification factor plays the dominant role. For the D-C and C-D paths, it interacts with the directional considerations to yield a "best" frequency of 12.1-12.2 kHz. For the B-D path there are no directional type errors and the trade-off between minimizing noise amplification and diurnal shift results in a "best" frequency of 12.0 kHz.

A summary of rms errors for various OMEGA algorithms is given in Table I. In addition to the difference OMEGA and composite algorithms previously discussed, a difference OMEGA scheme compensated with PPC tables (16) is included for completeness. As might be expected, the algorithms utilizing PPC corrections were the most accurate followed by composite OMEGA and the various forms of three-frequency difference

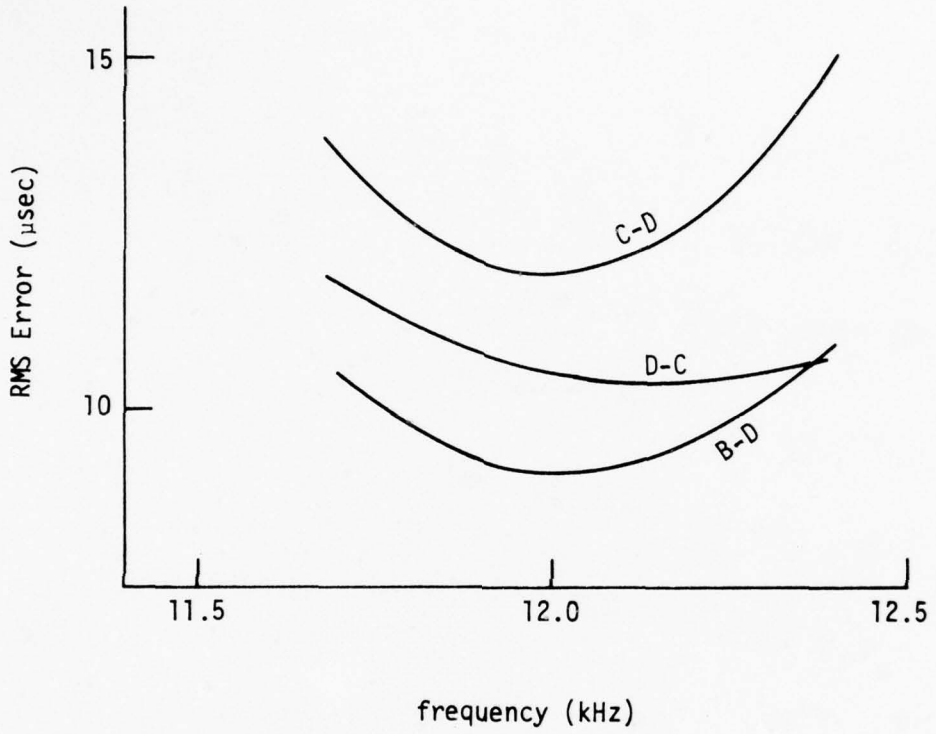

Figure 19. RMS error versus frequency for paths B-D, D-C, and C-D. 10-31 March 75.

OMEGA. In perspective, Table I illustrates that for the limited data analyzed, composite and difference OMEGA attain similar accuracies; and while neither is as good as single-frequency OMEGA with PPC corrections, the errors are quite acceptable and, hopefully, not as subject to gross peak errors in the event of SID's.

G. Observations

1. It has been shown that it is possible to compute a group delay

Table I. Summary of RMS Errors for Several OMEGA Navigation Algorithms. 10-31 March 1975.

Navigation Algorithm	RMS Errors Path B-D	Path D-C	Path C-D	Average RMS Errors for All Three Paths
Three-frequency difference OMEGA (Note that f=11.9 kHz coincides with usual difference OMEGA.)				
f=11.7 kHz	1.68 n.m.	1.89 n.m.	2.20 n.m.	1.92 n.m.
=11.9 kHz	1.49 n.m.	1.73 n.m.	1.96 n.m.	1.73 n.m.
=12.0 kHz	1.46 n.m.	1.70 n.m.	1.91 n.m.	1.69 n.m.
=12.2 kHz	1.52 n.m.	1.67 n.m.	2.04 n.m.	1.74 n.m.
=12.4 kHz	1.75 n.m.	1.73 n.m.	2.38 n.m.	1.95 n.m.
Composite OMEGA				
m=2.25	1.88 n.m.	2.30 n.m.	1.82 n.m.	2.00 n.m.
m=3.0	1.30 n.m.	1.77 n.m.	1.45 n.m.	1.51 n.m.
m=3.3	1.22 n.m.	1.69 n.m.	1.48 n.m.	1.46 n.m.
Modified composite OMEGA	1.36 n.m.	1.63 n.m.	1.89 n.m.	1.63 n.m.
Single-frequency OMEGA (Using PPC tables)	.73 n.m.	1.18 n.m.	1.12 n.m.	1.01 n.m.
Difference OMEGA (Using PPC tables)	1.10 n.m.	1.35 n.m.	2.06 n.m.	1.50 n.m.

at any arbitrary frequency. Insensitivity to diurnal phase variations, random noise amplification, and other factors influence the selection of a practical operating frequency.

2. For each propagation path examined, a frequency does exist for which the average day and night group delays are equal. Thus it appears that diurnal shift can be minimized by a judicious choice of reference frequency.

3. Navigational accuracies attained using three-frequency difference OMEGA are comparable to those associated with composite techniques.

4. The phase/group velocity viewpoint is satisfying from a theoretical standpoint and offers insight in developing techniques to compensate for other propagation phenomena, e.g., SID's, transition effects, etc.

IV. DETECTING AND COMPENSATING FOR UNUSUAL PROPAGATION CONDITIONS

A. Overview

One of the major limitations of OMEGA is that it is susceptible to anomalous propagation conditions (17) - (19). SID/PCA events can cause large errors in single-frequency OMEGA, and even composite techniques, which have reduced sensitivity to SID's, exhibit degraded accuracy over unusual paths, e.g., the Norway - North Dakota (A-D) path which traverses the Greenland ice mass (8). In this chapter a technique is presented for compensating computed signal propagation times by sensing changes in certain transmission parameters. We will see that the availability of phase measurements at three frequencies is crucial in the sense of providing information about propagation conditions along the path. It should be noted that in the development which follows, information obtained about propagation conditions can be utilized in any navigation scheme. Thus, when we talk about propagation delay, it is with respect to a delay time referred to the corresponding velocity (phase, group, or otherwise) with which we wish to navigate. We will also note here that the development assumes that the user is operating in a direct ranging mode. Extension to hyperbolic operation depends in part on certain geometric constraints and will not be considered below.

B. Using Phase Ratios to Sense Propagation Conditions

To begin let us again consider the navigation scenario where we assume that we are in a direct ranging mode. Using some navigation

algorithm, a user computes a propagation delay from the phase measurements at one or more of the OMEGA frequencies. Then, multiplying the time delay by some assumed nominal velocity of propagation, he obtains a measure of distance from the transmitting station. This measure of distance deviates from the actual distance depending on how the true velocity differs from the assumed nominal velocity. That is,

$$d_{comp} = T_{comp} v_{nom}$$

and

$$d_t = T_{comp} v_t = T_{comp} \left(\frac{v_t}{v_{nom}} \right) v_{nom}$$

so the propagation-induced error is

$$\text{error} = d_t - d_{comp} = T_{comp} v_{nom} \left(1 - \frac{v_t}{v_{nom}} \right) \qquad (11)$$

where d_t = true distance

d_{comp} = computed distance

v_t = true velocity

v_{nom} = nominal velocity (known)

T_{comp} = computed time delay

Note that the error is a function of the true velocity and it is apparent that any method which allows us to estimate this quantity is of interest. For example, if we could estimate v_t during a SID period then presumably we could compensate for its effects.

To see that the ratio of phase measurements at two frequencies can help us to estimate v_t, consider the case of propagation in a simple parallel-plane waveguide with perfectly conducting boundaries. The expression for phase velocity in this case is (5)

$$v_p = c\{1 - \left(\frac{c}{4hf}\right)^2\}^{-\frac{1}{2}} \tag{12}$$

where h is the ionospheric height, f the frequency, and c the velocity of light. In Equation 12, h is the only unknown parameter but we cannot estimate it from a phase measurement at one frequency because the total phase delay also depends upon distance, an additional unknown; i.e.,

$$T_1 = \frac{d}{v_1(h)} \tag{13}$$

However, if a phase measurement at another frequency were also available, then presumably we could "solve" Equation 13 for h and then obtain an explicit expression for v_1. Another approach, however, is to look at the ratio of phase measurements at two frequencies, i.e.,

$$\frac{\phi_2}{\phi_1} = \frac{f_2}{f_1}\frac{T_2}{T_1} = \frac{f_2}{f_1}\frac{dv_1}{dv_2} = g(h) \tag{14}$$

Distance cancels out and we are left with an expression in which h is the only variable. Assuming that an inverse exists we can write

$$h = g'\left(\frac{\phi_2}{\phi_1}\right) \tag{15}$$

or equivalently, since v is a function of h,

$$v_1 = g''\left(\frac{\phi_2}{\phi_1}\right) \tag{16}$$

This approach is useful from a practical standpoint in that the precise functional relationship between velocity and height need not be known. We need only to know that height is the lone variable and then take sufficient data to establish an empirical model.

Of course, in the case of OMEGA, there are considerably more variables at play than just ionospheric height. Height is the primary factor but earth conductivity, direction of propagation, ionospheric conductivity gradient, and other parameters also affect the propagation velocity to more or lesser degrees. Fortunately, as we shall see, it is possible to "lump" many of these parameters into generalized variables which then can be viewed as functions of the OMEGA phase ratios. Let us first consider the approximate model for phase velocity in the spherical earth-ionosphere waveguide as developed by Watt (see (5), page 277). Phase velocity can be approximated by

$$v_p \simeq v_0\{1 - h'/a + (1 - h/a)^2[(2\pi n + \phi_g + \phi_i)v_0/4\pi fh]^2/2\} \tag{17}$$

where n = mode number (1 in our case)

a = earth's radius

h = reflecting height of ionosphere

h' = mean height of energy flow in the guide

f = frequency

v_0 = free velocity in the medium

ϕ_g = ground reflection coefficient

ϕ_i = ionospheric reflection coefficient

Thus the ratio of two phase measurements can be written as

$$\frac{\phi_2}{\phi_1} = \frac{f_2}{f_1}\frac{T_2}{T_1} = \frac{f_2}{f_1}\frac{v_{p1}}{v_{p2}}$$

$$= \frac{f_2}{f_1}\frac{\{1 - h_1'/a + (1 - h/a)^2[2\pi + (\phi_g + \phi_i)_1 v_0/4\pi f_1 h]^2/2\}}{\{1 - h_2'/a + (1 - h/a)^2[2\pi + (\phi_g + \phi_i)_2 v_0/4\pi f_2 h]^2/2\}} \qquad (18)$$

Over the OMEGA frequency range, ϕ_i and ϕ_g are essentially independent of frequency (5), so Equation 18 can be written as

$$\frac{\phi_2}{\phi_1} = g(h, h_1', h_2', (\phi_g + \phi_i)) \qquad (19)$$

It also turns out that h' can be viewed as a function of h and $(\phi_i + \phi_g)$ so that Equation 19 can be rewritten as

$$\frac{\phi_2}{\phi_1} = g'(h, \phi_g + \phi_i) \tag{20}$$

Equation 20 is similar to Equation 14 except that we now have an additional variable $\phi_g + \phi_i$. With the OMEGA transmissions, however, we also have at our disposal another independent phase ratio, ϕ_3/ϕ_1. A similar kind of development for this ratio leads finally to the expressions

$$\frac{\phi_3}{\phi_1} \triangleq R_1 = g''(h, \phi_i + \phi_g)$$

$$\frac{\phi_2}{\phi_1} \triangleq R_2 = g'(h, \phi_i + \phi_g)$$

For the OMEGA range of frequencies, we assume g'' and g' are invertible functions and we thus postulate a model for estimating velocity as

$$v = f(R_1, R_2) \tag{21}$$

where, in our case, R_1 and R_2 are measured phase ratios and the model is empirically determined. Note that in the development above $(\phi_i + \phi_g)$ is viewed as some generalized reflection coefficient which is influenced by many separate propagation factors.

C. Empirical Determination of v_g as a Function of R_1 and R_2

An implementation of the above concepts was applied using three-frequency difference OMEGA (reference frequency=12.0 kHz), although it should be noted that the results are very general and may be applied to any of the algorithms discussed in Chapters II and III.

To obtain the empirical model needed to estimate the true group velocity as a function of R_1 and R_2, the phase measurements from paths B-D, D-C, and C-D were used as raw data. The phase ratios R_1 and R_2 were formed from each measurement and since the distance was known for each path, a measure of the true group velocity was also available. Thus every phase measurement was represented by a point in three dimensional space, (v_g, R_1, R_2) and the total collection of these three-tuples formed the data base for the model.

Once the data base was defined, a fifth-order polynomial surface was fit to the points using standard linear regression techniques (20). Group velocity was designated the dependent variable and an expression was generated which in effect estimated v_g given the measured values of R_1 and R_2, i.e.,

$$\hat{v}_g = \alpha_0 + \alpha_1 R_1 + \alpha_2 R_2 + \alpha_3 R_1 R_2 + \ldots + \alpha_{20} R_2^5 \qquad (22)$$

Values for α_i coefficients are listed with their respective variables in Table II. Those variables which were not significant at level .001 were not included in the basic model (Equation 22) and are identified as those with α_i coefficients equal to zero.

Table II. Fifth-order polynomial fit to B-D, C-D, and D-C data.

Variable	Coefficient	Variable	Coefficient
R_1	-66.88	$R_1^2R_2^2$	0.0
R_2	-200.45	R_1^4	-113.79
R_1R_2	0.0	R_2^4	-3156.29
R_1^2	0.0	$R_1R_2^4$	6365.45
R_2^2	1360.59	$R_1^4R_2$	-90.61
$R_1R_2^2$	-2619.55	$R_1^2R_2^3$	0.0
$R_1^2R_2$	767.14	$R_1^3R_2^2$	0.0
R_1^3	84.36	R_1^5	0.0
R_2^3	0.0	R_2^5	0.0
$R_1R_2^3$	0.0	Mean	31.41
$R_1^3R_2$	0.0		

The surface generated by the regression analysis is shown in Figure 20. Increasing ionospheric height and nominal day and night conditions are indicated. Interpreted in terms of the group velocity versus frequency curves in Figure 10, we see that as one moves along the surface from nominal day (70 km) through transition to night (90 km), the group velocity starts at a fixed level, fluctuates during transition, and then returns to the fixed level at night. We note that as height decreases below 70 km (SID disturbances) the surface decreases approxi-

mately linearly as a function of the ratios. The areas which in general reflect the ratio values for the various paths are also shown in Figure 20. For a fixed value of h, R_1 and R_2 increase from area D-C to C-D.

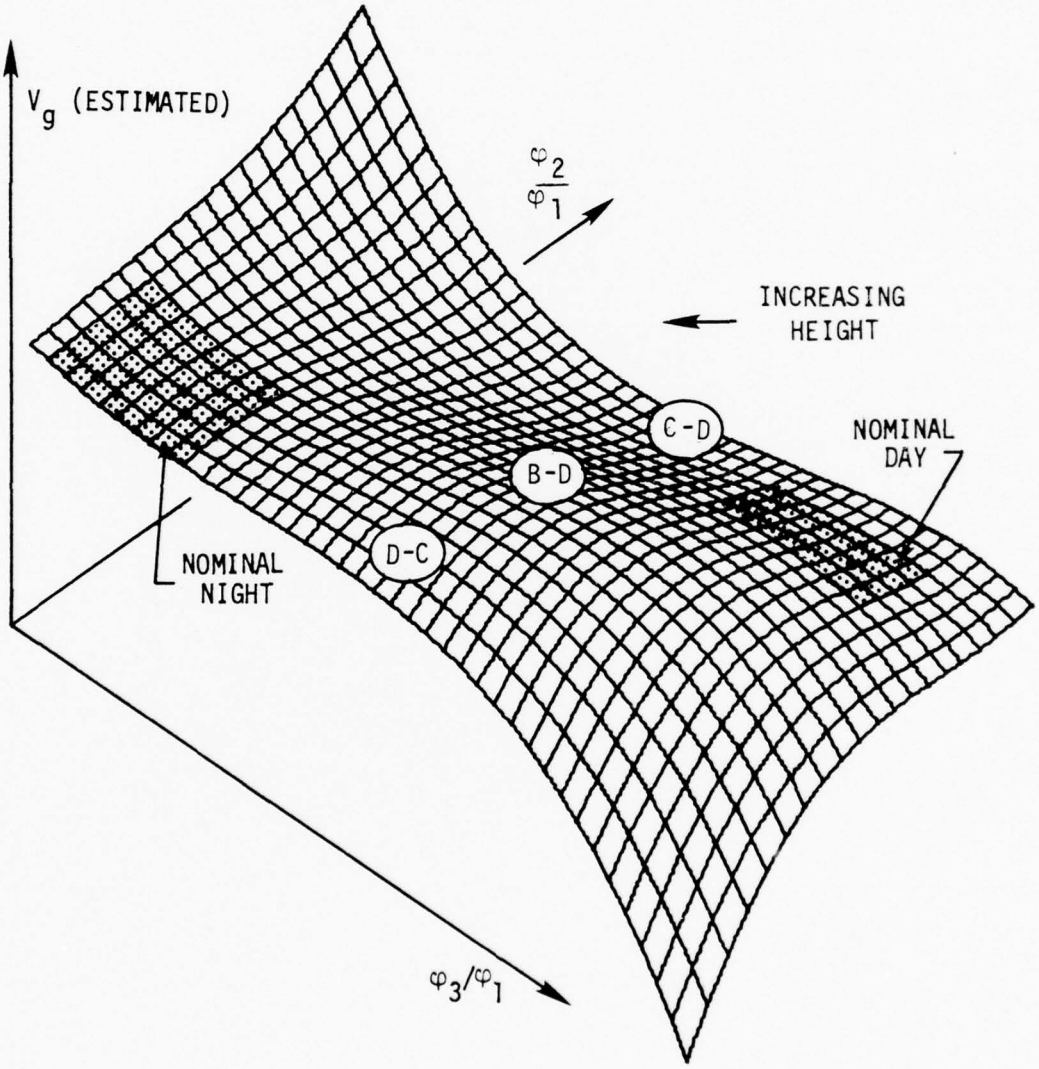

Figure 20. Estimate of group delay versus R_1 and R_2.

This is because, as frequency increases, paths "to the east" (C-D) have increasingly lower phase velocities than paths "to the west" (D-C); thus the C-D phase ratios are higher than the corresponding D-C ratios (1). Note that the estimated v_g increases as we move from D-C to C-D. This is also due to the lower phase velocity since v_g is inversely proportional to v_p and therefore increases as v_p decreases.

The surface can also be interpreted in terms of variations in the earth reflection coefficient ϕ_g. For good conducting ground, ϕ_g is essentially zero, but it takes on negative values for poorly conducting ground (5). A decrease in ϕ_g results in higher v_g (equation 17) and can lead to group velocities which occur in the higher region "to the left" of the nominal night area. Experimentally this is confirmed by observing ratios from the Norway - North Dakota (A-D) path over which ground conductivity is extremely low. At 10 kHz, in fact, ground conductivity which takes on values from 3-5 mhos/meter for seawater decreases to something on the order of 2×10^{-5} mho/meter for Greenland ice (1).

D. Experimental Results

In this section the effects of phase ratio compensation are discussed as they concern (i) overall system accuracy under "nominal" propagation conditions, (ii) transition periods, (iii) polar conductivity paths, and (iv) composite applications. With the exception of (iv), the three-frequency difference algorithm was selected for comparison and the following procedure was used. For each set of phase measurements, the phase ratios were first formed and an estimate of group velocity,

$v_{g_{est}}$, was obtained from the fifth-order model. A propagation delay, $T_{g_{cal}}$, was then calculated and compensated by $v_{g_{est}}/v_{g_{nom}}$, i.e.,

$$T_{g_{est}} = T_{g_{cal}}\left(\frac{v_{g_{est}}}{v_{g_{nom}}}\right)$$

where $v_{g_{nom}}$ is some nominal reference velocity and $T_{g_{est}}$ is our new estimate of propagation delay referred to $v_{g_{nom}}$. For this study $v_{g_{nom}}$ was chosen to be .9915 c (where c is the velocity of light) and it appears to be typical of day/night velocities for the B-D path.

(i) Nominal propagation conditions. The results of applying the compensation to the three-frequency difference algorithm (f=12.0 kHz) are shown in Figure 21 for path B-D. Uncompensated group delays are plotted versus time of day (GMT) in the first figure while the second contains the delays compensated as discussed above. Random variations during the day and night periods have clearly been reduced. The severe dips characteristic of the transition period have been attenuated but not eliminated. Such "before" and "after" pictures for all the paths investigated (B-D, C-D, D-C) are included in Appendix B and show similar results. Table III gives the overall rms accuracies associated with both uncompensated and compensated three-frequency difference OMEGA and we see that there is an improvement in overall accuracy of 0.34-0.41 nautical miles depending upon the particular path. Comparing Tables I and III, we note that with phase ratio compensation, three-frequency difference OMEGA achieves a lower rms error than any of the navigation algorithms which do not use

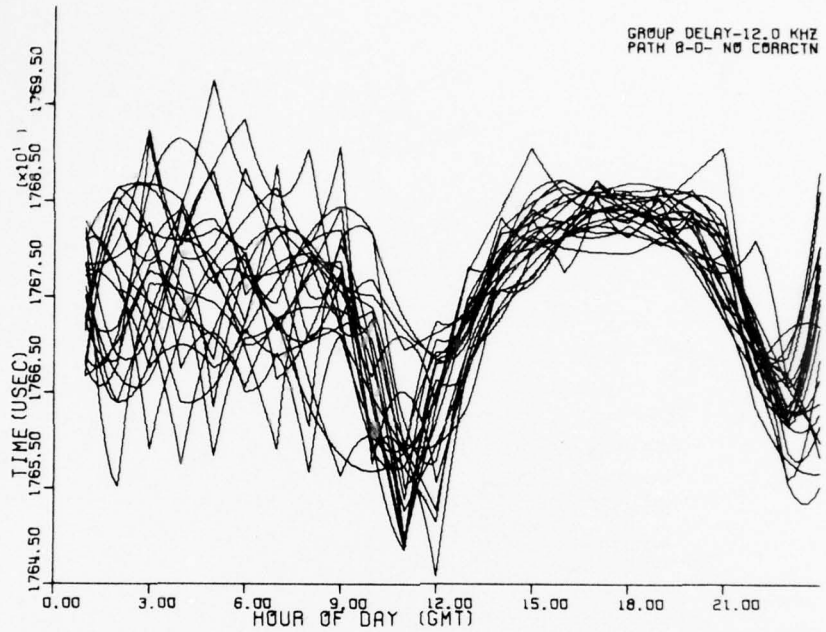

(a) Uncompensated group delay

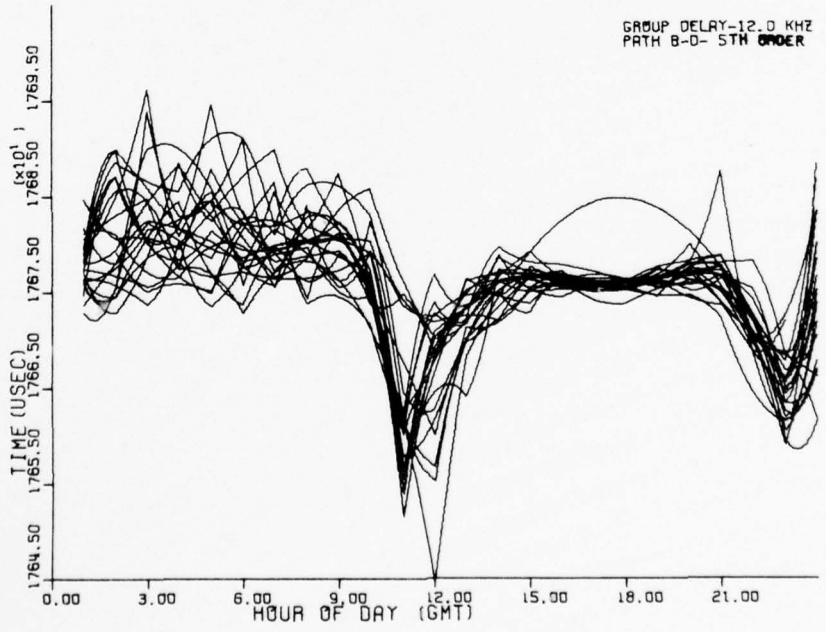

(b) Compensated group delay

Figure 21. Uncompensated and compensated group delay versus time of day (GMT). Trinidad - North Dakota. 10-31 March 1975.

Table III. RMS Errors for Three-frequency Difference OMEGA. 10-31 March 1975.

Three-frequency Difference OMEGA (f=12.0 kHz)	RMS Error B-D	D-C	C-D	Average RMS Error for All Three Paths
Uncompensated	1.56 n.m.	1.93 n.m.	1.74 n.m.	1.74 n.m.
With Phase Ratio Compensation	1.15 n.m.	1.54 n.m.	1.40 n.m.	1.36 n.m.

PPC tables. Also note that the uncompensated rms errors in Table III differ slightly from those in Table I because of different reference velocities used.

(ii) Transition periods. We mentioned earlier that the transition times, those times between day and night, appear to be improved very little by the phase ratio correction scheme. In fact, by deleting a successively larger number of transition hours from the data base, we can obtain polynomial fits which do correspondingly better in estimating the group velocity from R_1 and R_2. This can be seen by examining the square of the multiple correlation coefficient associated with the fit analysis. This number essentially indicates the amount of random variation in the data which is accounted for by the regression model (21), and we note from Table IV that this percentage ranges from 47% in the case where all of the transition times are considered as part of the data base, to 72% when the transition times are deleted. This indicates that transition effects are not modeled very well by our approach and suggests that other phenomena (such as mode energy conversion) are at work during this period. We should note in passing that researchers have been investigating transition phenomena for some time (22) - (24), and transitional effects are still not well understood to date. Also from Table IV we see that the day and night delays are compensated very well by phase ratio compensation. In fact, with the compensation, rms error for path B-D is reduced to 0.6 n.m. during day and night.

(iii) Polar propagation paths. Another interesting possibility for phase ratio compensation is the application to propagation paths which

Table IV. Compensation performance for varying amounts of transition times - Path B-D.

	Number of data pts.	$\left(\text{Correlation Coefficient}\right)^2$	RMS Errors	
			Without Compensation	With Compensation
All transition times <u>included</u> in data base	1396	.47	1.56 n.m.	1.15 n.m.
Two hours at beginning of sunrise transition <u>deleted</u>	1278	.56	*	*
All transition times <u>deleted</u> from data base	971	.72	1.20 n.m.	0.60 n.m.

exhibit very low surface conductivity. To investigate this, a fifth-order polynomial was generated using the procedure described above with path A-D (Norway - North Dakota) included in the data base. The results for the low conductivity path A-D are summarized in Table V and are quite dramatic in that, normally, information from this path is essentially

Table V. Effect of phase ratio compensation on Norway - North Dakota (A-D) rms errors. 1-31 March 1975.

	RMS Error
Three-frequency difference OMEGA (f=12.0 kHz)	
without compensation	15.50 n.m.
with phase ratio compensation	2.65 n.m.
Composite OMEGA (m=3.0)	11.44 n.m.
Modified Composite OMEGA	19.47 n.m.
Single frequency OMEGA (Using PPC tables)	2.30 n.m.
Difference OMEGA (Using PPC tables)	12.61 n.m.

unusable with the algorithms which do not use PPC tables. Figure 22 shows the results of using this particular polynomial to compensate for propagation conditions on all four paths (A-D, B-D, D-C, and C-D respectively). Although performance on non-polar paths is somewhat degraded because of the diurnal shift induced, accuracies on all four paths are within 2.7 nautical miles rms which is quite reasonable. Note that the diurnal error occurs totally in the night portion of the guide where the phase ratios for the polar and the "normal" paths tend to overlap. This shift in the night values occurs because the estimated Norway - North

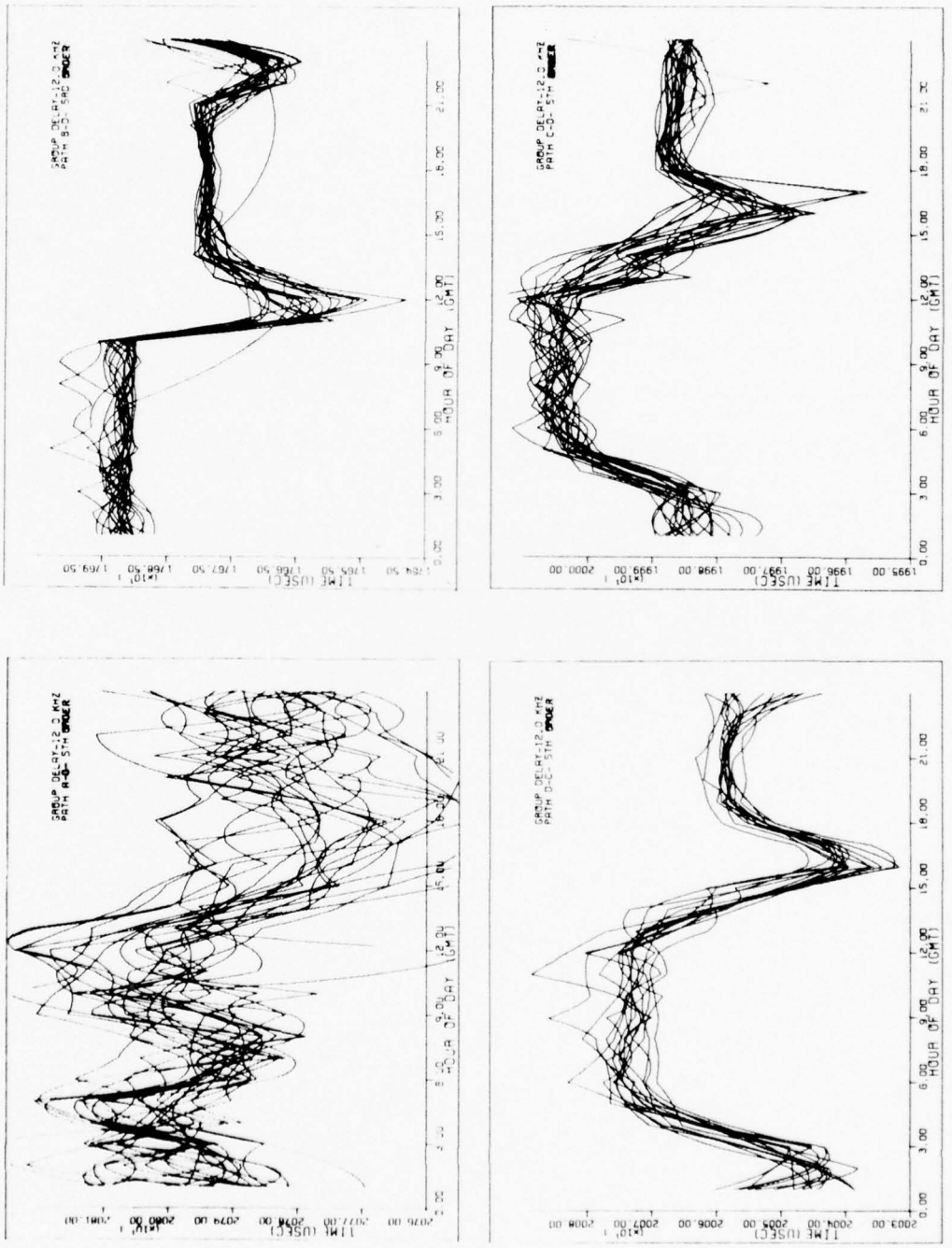

Figure 22. Group delay with phase ratio compensation versus time of day (GMT) for various propagation paths. 10-31 March 1975.

Dakota group velocities are slightly higher than for the other paths, which may be due to auroral effects (1), or mode conversion at ice/seawater boundaries (5).

(iv) Composite applications. Phase ratio compensation can also be applied to other navigation algorithms. The results of using a fifth-order polynomial function to correct composite delays (m=2.25) are shown in Figure 23 (a) and (b). Although transition effects are still pronounced, overall rms error has been improved from 1.89 n.m. for (a) to 1.03 n.m. in (b).

E. Application to SID Events

Sudden Ionospheric Disturbances (SID's) occur in conjunction with high solar activity and are characterized by sudden phase advances in received VLF signals. The phase advances are caused by an increase in signal phase velocity due to a drop in the effective reflecting height of the ionosphere and, since they are not predictable, can result in severe navigation problems. Since SID's can be thought of as resulting from ionospheric height changes, the phase ratio compensation scheme presented above should be applicable to these phenomena also. Unfortunately so few SID's occurred during March 1975 that utilization of the "usual" data base was not possible.

In order to establish some sort of data base with which to investigate this application, the U. S. Coast Guard was requested to furnish reduced OMEGA phase measurements from the Hawaii and North Dakota monitoring sites. This data (at frequencies of 10.2 and 13.6 kHz) was re-

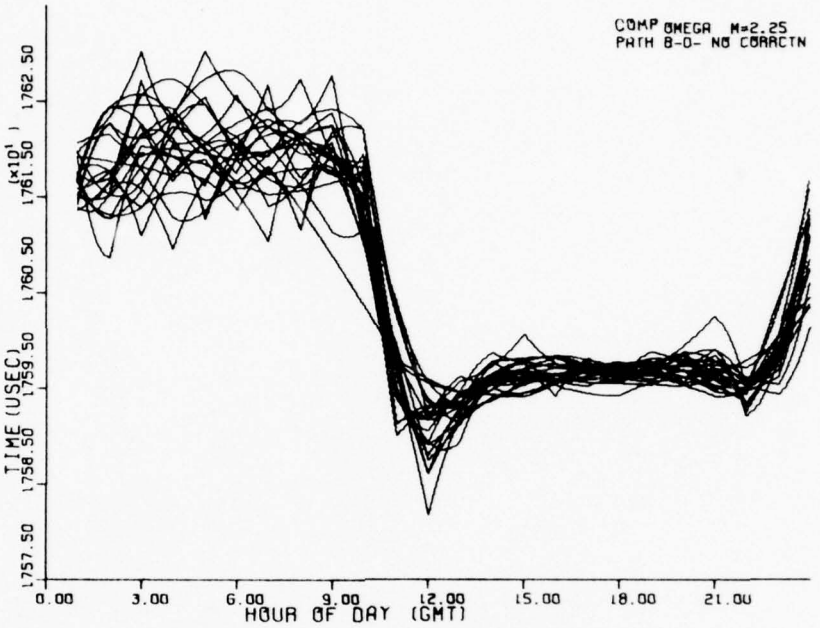

(a) Without compensation

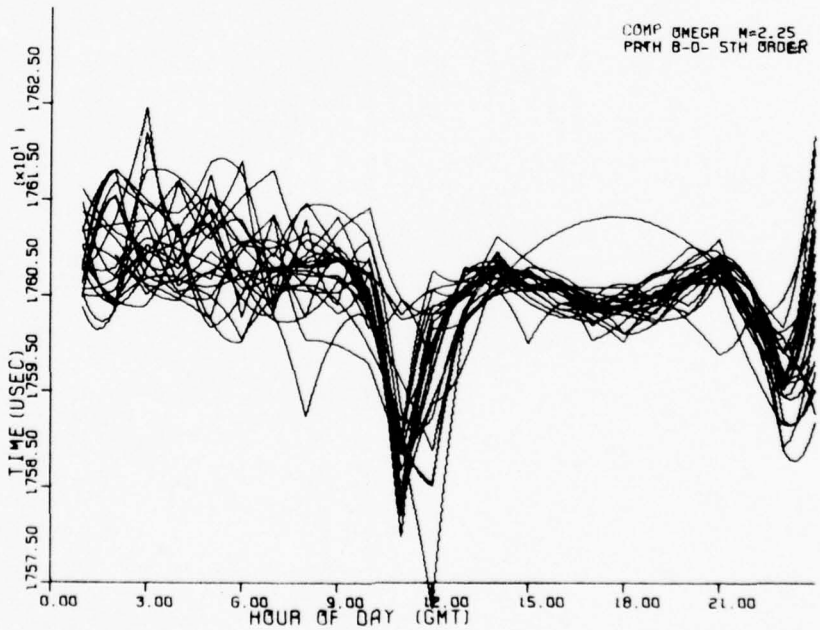

(b) With phase ratio compensation

Figure 23. Composite delays (m=2.25) versus time of day (GMT). Trinidad - North Dakota (B-D). 10-31 March 1975.

ceived and appropriate SID events identified during the time period 1 January 1974 to 30 June 1975. The lack of $11\frac{1}{3}$ kHz phase data, which was not furnished because of certain atmospheric modeling problems which the Coast Guard has experienced, required a number of modifications to be instituted for the analysis:

(1) It was decided to refer the group delay algorithm to 11.9 kHz thereby requiring only phase measurements at <u>two</u> frequencies.

(2) A linear compensation as a function of one ratio was assumed in the region $R_1 \geq 1.3368$.

(3) Each of the three paths involved (B-D, C-D, D-C) were examined individually and assigned a different value for the slope of the linear compensation.

(4) Only SID's which occurred during "day" periods were considered. This restriction essentially forced us to consider only those values of R_1 which were greater than about 1.3368, i.e., in the region where we assumed a linear compensation.

A complete listing of the days and paths considered for the analysis is included in Appendix C. Appropriate slopes for the linear compensation functions were determined from an examination of the raw phase ratios and are also tabulated.

The SID's used in the analysis range in severity from very minor to potentially catastrophic. Results are summarized in Table VI and we see that the application of phase ratio compensation does improve system

Table VI. SID- induced daytime rms errors for various OMEGA configurations - January 1974 to June 1975.

	RMS Errors		
	B-D	D-C	C-D
Three-frequency difference OMEGA (f=11.9 kHz)			
without compensation	2.2 n.m.	4.7 n.m.	2.8 n.m.
with phase ratio compensation	0.6 n.m.	1.0 n.m.	0.5 n.m.
Composite OMEGA (m=3.0)	1.3 n.m.	2.7 n.m.	1.0 n.m.
Modified composite OMEGA	1.0 n.m.	2.9 n.m.	1.7 n.m.
Single-frequency OMEGA (Using PPC tables)	2.8 n.m.	1.1 n.m.	0.8 n.m.
Number of data points	73	12	38

performance even with the rather simple algorithm postulated here. What's more, rms figures aside, the maximum peak errors associated with SID's are the most critical insofar as navigation is concerned. As an example, consider the effect of a particular SID as shown in Figure 24.

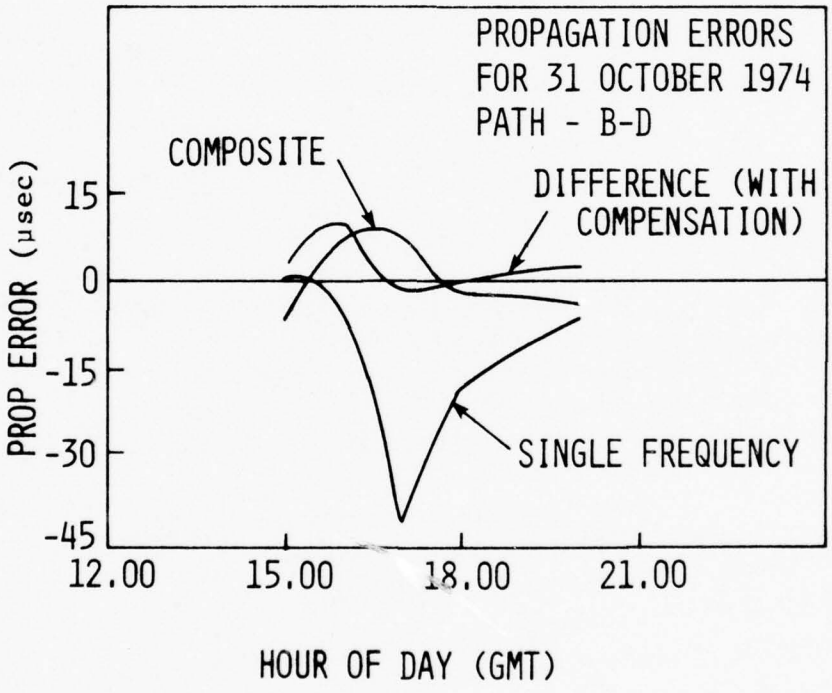

Figure 24. Propagation error versus time of day (GMT) for SID event. Trinidad - North Dakota (B-D). 31 October 1974.

The SID occurred on 31 October 1974 along the propagation path B-D and the peak error incurred by the single frequency OMEGA algorithm using PPC tables is approximately 40 μsec or about 7 nautical miles. Furthermore, such an error can be insiduous in the sense that SID's cannot be

predicted and the user may not be aware that such an event is occurring. Also from Figure 24, we see that both composite OMEGA and the compensated three-frequency algorithm do creditable jobs in mitigating the SID effects.

Another possible SID application of the phase ratio compensation technique concerns the detection of the SID's as they occur. In Figure 25, smoothed curves of propagation errors are drawn versus the ratio R_1, and we see that the phase ratio can be viewed as an indicator of whether or not a SID is in progress. That is, if during normal operation the ratio crosses a certain threshold, the navigator can be reasonably sure that a SID is occurring. This detection capability can be of considerable value in many applications particularly if one is using one of the PPC table algorithms for primary navigation (18).

F. Observations

1. Based on the limited amount of data analyzed, it appears that phase measurement ratios can be used to sense propagation conditions and correct for propagation-induced errors. System performance with this form of compensation is comparable to that of single-frequency OMEGA compensated with PPC tables.

2. Results appear to be very general in the sense that the compensation algorithm can be made independent of the transmission path.

3. Inherent to the phase ratio technique is a capability to detect as well as compensate for SID events, the detection aspect of which is not available in other OMEGA algorithms.

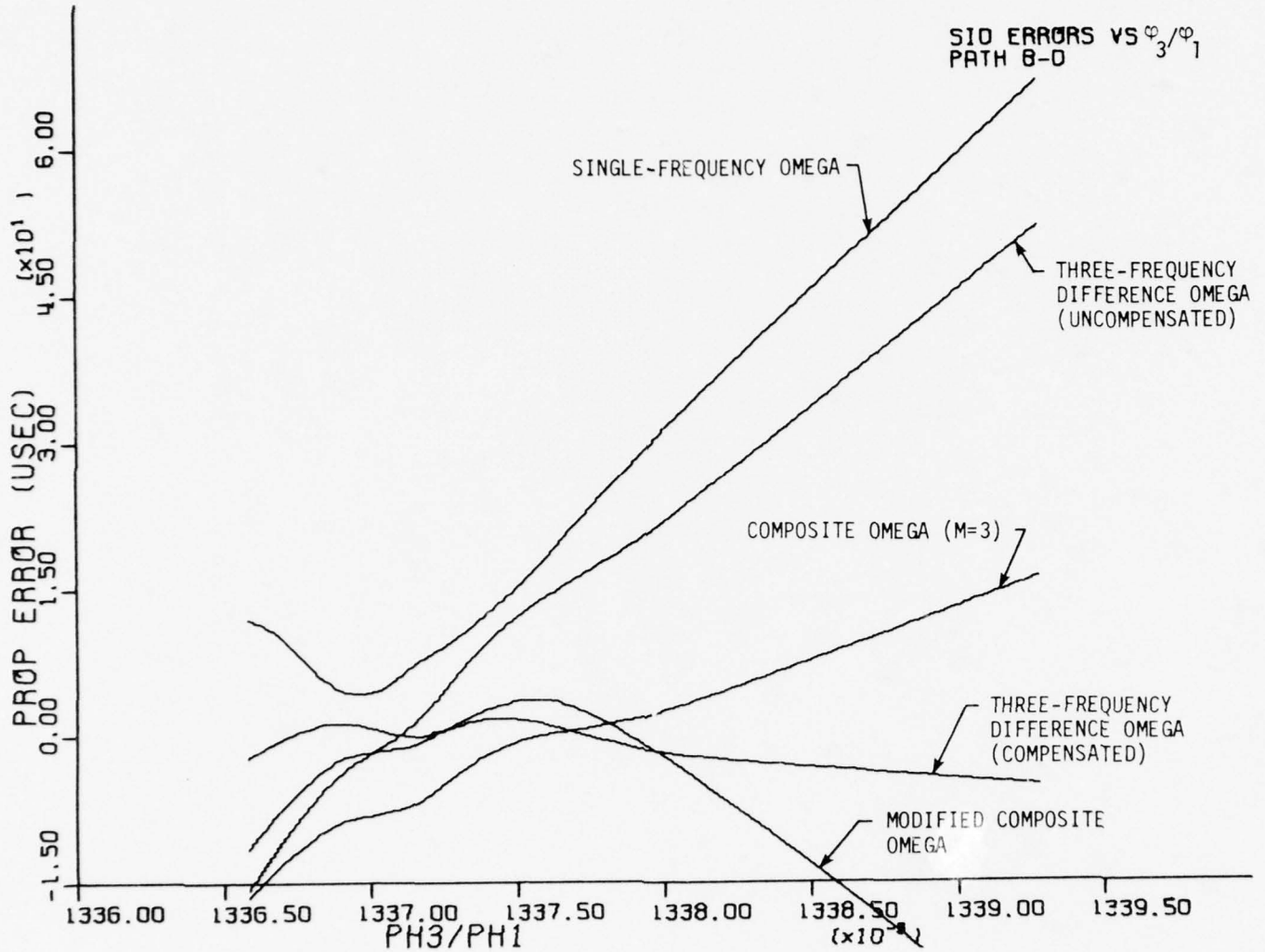

Figure 25. SID induced propagation time errors versus R_1 for various OMEGA algorithms. January 1974 - June 1975.

V. SUMMARY

The two analytical techniques presented in this dissertation offer new methods for compensating for propagation-induced errors in the OMEGA navigation system. Both techniques were derived primarily from consideration of the physical phenomena involved with VLF propagation and are theoretically satisfying in this respect.

The three-frequency difference OMEGA approach illustrated that errors due to the diurnal phase shift of the OMEGA signals could be compensated for by a judicious selection of the frequency to which the group time delay was referred. Overall navigation accuracies using this scheme were comparable to those of composite OMEGA.

Another technique, phase ratio compensation, was used to sense propagation conditions along the transmission path and to correct for propagation-induced errors. It was demonstrated that this form of compensation significantly improved the three-frequency difference OMEGA performance and in the case of anomalous propagation conditions (i.e., SID's, polar transmission paths) allowed navigation when one or more of the other algorithms was, for all practical purposes, inoperative.

VI. LITERATURE CITED

1. Morris, Peter B.; and Cha, Milton Y. "OMEGA Propagation Corrections: Background and Computational Algorithm." ONSOD-01-74 (U. S. Department of Transportation), December, 1974.

2. Swanson, E. R.; and Adrian, D. J. "OMEGA Envelope Capability for Lane Resolution and Timing." NELC/Report 1901 (U. S. Navy), November 20, 1973.

3. Stout, C. C. "The OMEGA System of Navigation." In Advanced Navigational Techniques, pp. 47-62. Edited by W. T. Blackband. Slough, England: Technivision Services, January, 1970.

4. Swanson, E. R. "VLF Radio Navigation Systems." In Modern Navigation Systems-Fundamentals and Applications. Vol. 2. An Intensive Short Course. University of Michigan Engineering Summer Conference, August 4-15, 1965.

5. Watt, Arthur O. VLF Radio Engineering. London: Pergamon Press, 1967.

6. Davies, Kenneth. Ionospheric Radio Propagation. Washington, D. C.: Government Printing Office, 1965.

7. Beavers, A. N., Jr.; Gentry, D. E.; and Kasper, J. F. "Evaluation of Real-Time Algorithms for OMEGA Propagation Prediction." Navigation 22 (Fall, 1975): 252-58.

8. Papousek, W.; and Reder, F. H. "A Modified Composite Wave Technique for OMEGA." Navigation 20 (Summer, 1973): 171-77.

9. Pierce, J. A. "The Use of Composite Signals at Very Low Radio Frequencies." Technical Report No. 552 (Division of Engineering and Applied Physics, Harvard University), February, 1968.

10. Brown, R. G.; Sharpe, R. A.; Hughes, W. L.; and Post, R. E. Lines, Waves, and Antennas. 2nd ed. New York: Ronald Press, 1973.

11. Jordan, E. C.; and Balmain, K. G. Electromagnetic Waves and Radiating Systems. Englewood Cliffs, N.J.: Prentice-Hall, 1968.

12. Wait, J. R.; and Spies, K. P. "Characteristics of the Earth-Ionosphere Wave Guide for VLF Radio Waves." Technical Note No. 300 (National Bureau of Standards), December, 1964.

13. Hampton, D. E. "Group Velocity Variations of VLF Signals." Technical Report No. 65282 (Royal Aircraft Establishment), December, 1965.

14. Mactaggart, Don. "An Empirical Computed Evaluation of Composite OMEGA." Proceedings of the Second OMEGA Symposium. Washington, D. C.: Institute of Navigation, November, 1974.

15. Brown, R. G.; and VanAllen, R. L. "Three-Frequency Difference OMEGA." Paper presented at the National Aerospace Symposium of the Institute of Navigation, Warminster, Pa., April 27-28, 1976. Engineering Research Institute (Iowa State University) ERI-76273 Preprint, March, 1976.

16. Kasper, J. F.; and Creekmore, E. E. "OMEGA Utilization by Non-military Subscribers." Navigation 19 (Fall, 1972): 215-25.

17. Swanson, E. R. "Blunders Caused by OMEGA Propagation: SPA's and PCA's." Proceedings of the Second OMEGA Symposium. Washington, D. C.: Institute of Navigation, November, 1974.

18. Luken, Konrad. "OMEGA Phase Shifts in the Auroral Region Due to Solar Phenomena." Proceedings of the First OMEGA Symposium. Washington, D. C.: Institute of Navigation, November, 1971.

19. Sakran, Frank C., Jr. "Accuracy Specifications for Automatic OMEGA Navigators." Proceedings of the Second OMEGA Symposium. Washington, D. C.: Institute of Navigation, November, 1971.

20. Service, Jolayne. A User's Guide to the Statistical Analysis System. Raleigh, N.C.: Student Supply Stores, August, 1972.

21. Bevington, Philip R. Data Reduction and Error Analysis for the Physical Sciences. New York: McGraw-Hill, 1969.

22. Chilton, Charles J.; Crombie, Douglas D.; and Jean, A. Glenn. "Phase Variations in V.L.F. Propagation." In Propagation of Radio Waves at Frequencies Below 300 Kc/s, pp. 257-90. Edited by W. T. Blackband. New York: Macmillan Co., 1964.

23. Reder, F. H. "VLF Propagation Phenomena Observed During Low and High Solar Activity." In Progress in Radio Science 1966-1969, pp. 113-40. Edited by J. A. Lane, J. W. Findley, and C. E. White. Vol. 2. Brussels, Belgium: International Scientific Radio Union, 1971.

24. Crombie, D. D. "Further Observations of Sunrise and Sunset Fading of VLF Signals." Radio Science 1 (January, 1966): 47-51.

VII. ACKNOWLEDGEMENTS

The author was supported in this research with assistance from the Electrical Engineering Department and assistantship support from the Engineering Research Institute. The author is also grateful to many individuals for their assistance throughout this project. Dr. R. Grover Brown served as major professor and provided the inspiration and technical guidance for this study, Messrs. Robert Willems and Howard Santamore (ONSOD) furnished all the OMEGA phase data and considerable technical information about OMEGA system operation, Dr. Richard W. Mensing (Statistics Department, Iowa State University) provided invaluable assistance during the regression analysis, and Mr. Kim Strohbehn assisted in transcribing the phase data for the polar path study. Finally, this work is dedicated to my wife Janet.

VIII. APPENDIX A: PROPAGATION TIMES FOR VARIOUS OMEGA CONFIGURATIONS

A. Propagation Path Trinidad - North Dakota (B-D)

Figure 26. Group delay versus time of day (GMT). f=11.7 kHz. Trinidad - North Dakota (B-D). 10-31 March 1975.

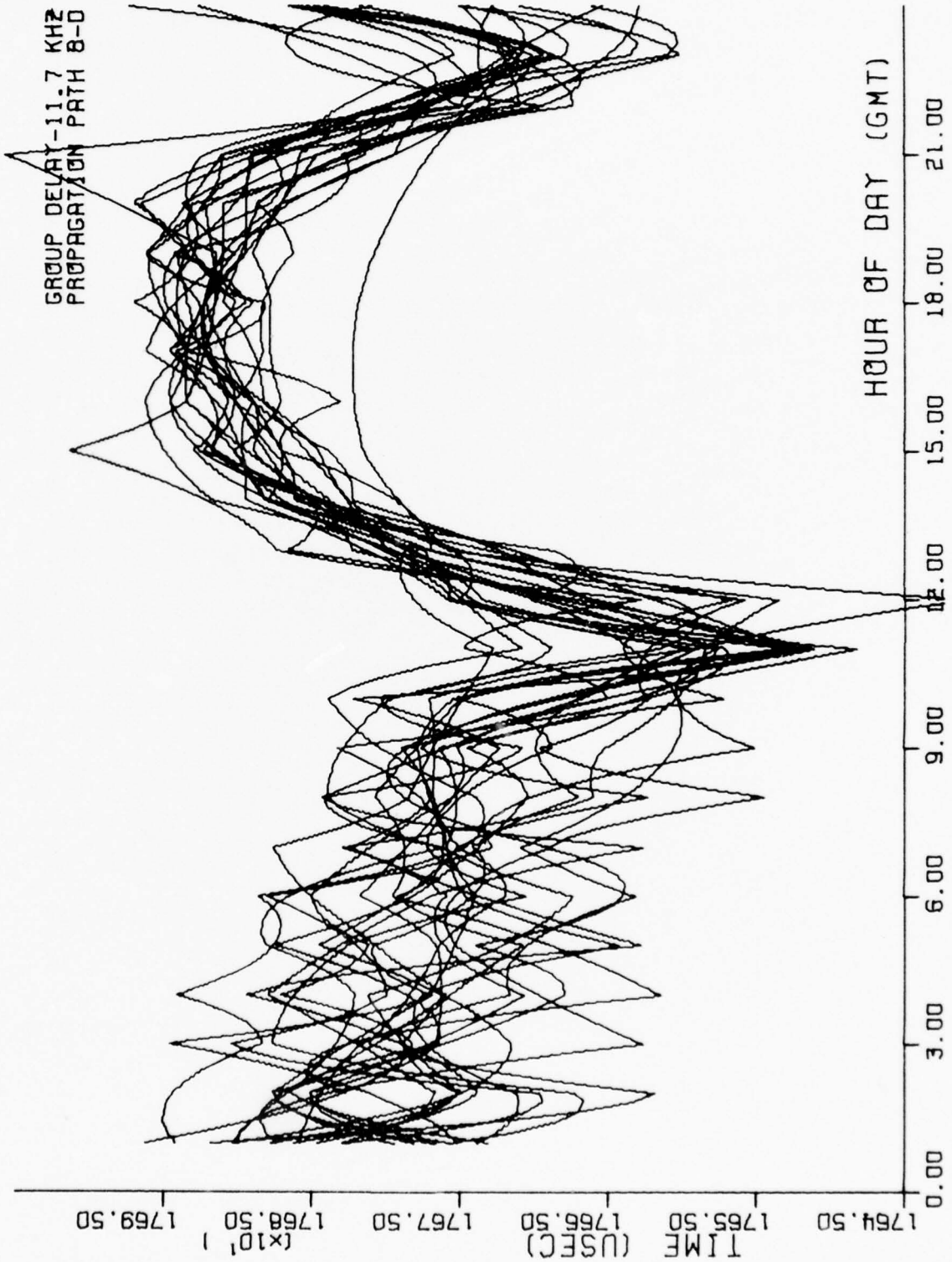
GROUP DELAY-11.7 KHZ
PROPAGATION PATH B-D
HOUR OF DAY (GMT)
0.00
3.00
6.00
9.00
12.00
15.00
18.00
21.00
TIME (USEC)
(x10')
1764.50
1765.50
1766.50
1767.50
1768.50
1769.50

Figure 27. Group delay versus time of day (GMT). f=11.9 kHz. Trinidad - North Dakota (B-D). 10-31 March 1975.

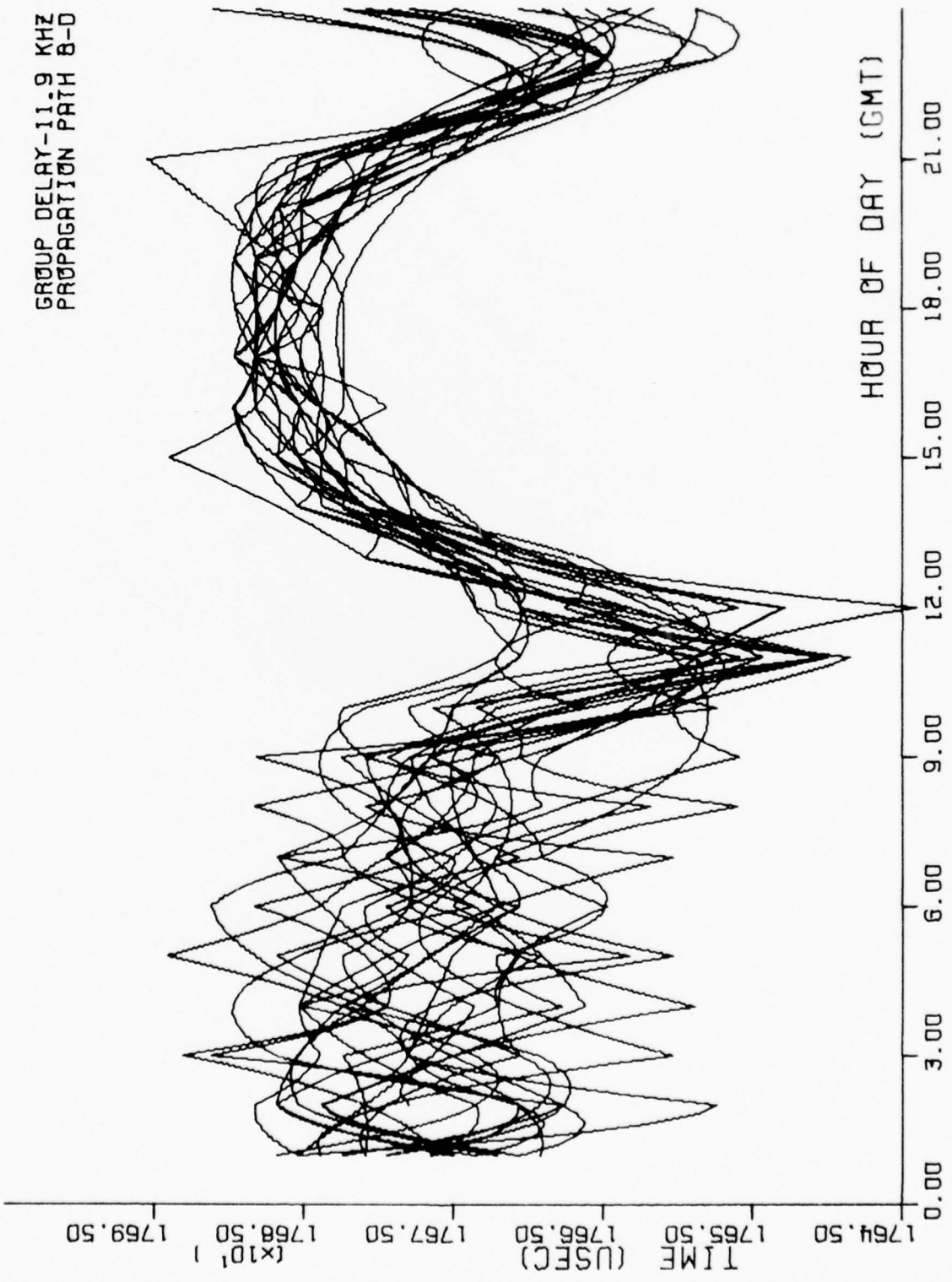
GROUP DELAY-11.9 KHZ
PROPAGATION PATH B-D
HOUR OF DAY (GMT)
0.00
3.00
6.00
9.00
12.00
15.00
18.00
21.00
TIME (USEC)
(x10')
1764.50
1765.50
1766.50
1767.50
1768.50
1769.50

Figure 28. Group delay versus time of day (GMT). f=12.0 kHz. Trinidad - North Dakota (B-D). 10-31 March 1975.

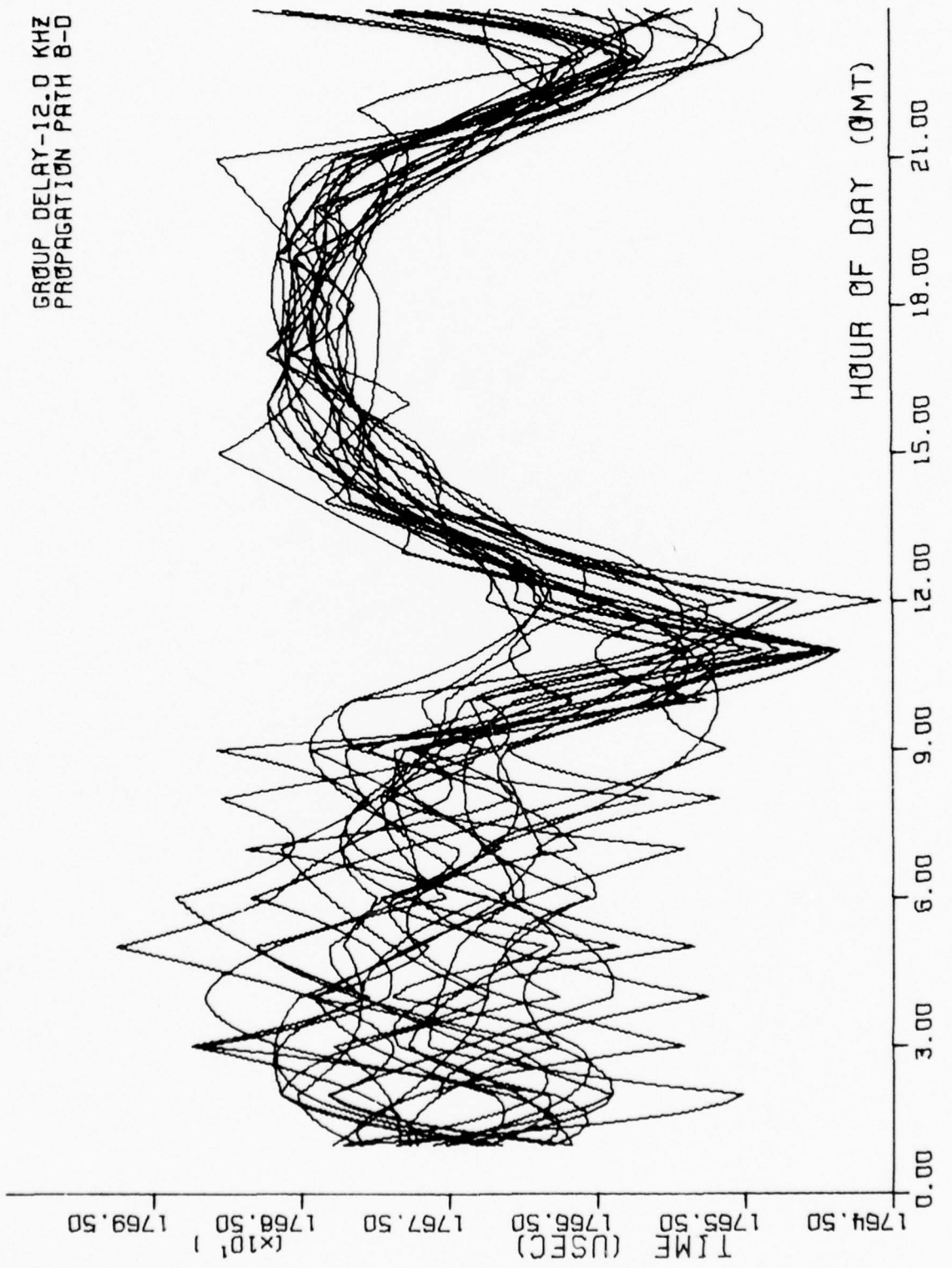
GROUP DELAY-12.0 KHZ
PROPAGATION PATH B-D
HOUR OF DAY (GMT)
0.00
3.00
6.00
9.00
12.00
15.00
18.00
21.00
TIME (USEC)
(x10¹)
1764.50
1765.50
1766.50
1767.50
1768.50
1769.50

Figure 29. Group delay versus time of day (GMT). f=12.2 kHz. Trinidad - North Dakota (B-D). 10-31 March 1975.

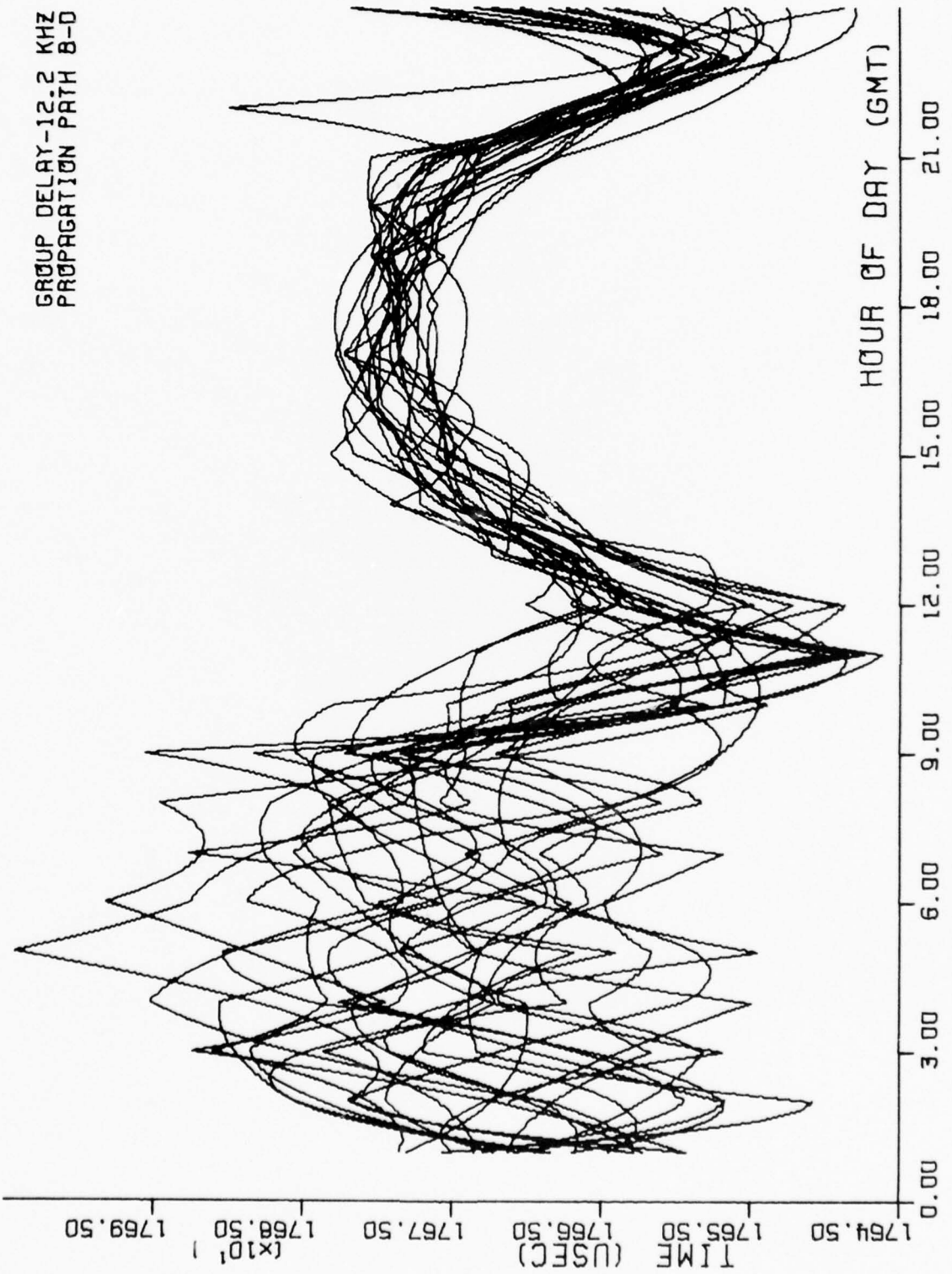
GROUP DELAY-12.2 KHZ
PROPAGATION PATH 8-D
TIME (USEC)
(x10¹)
1764.50
1765.50
1766.50
1767.50
1768.50
1769.50
HOUR OF DAY (GMT)
0.00
3.00
6.00
9.00
12.00
15.00
18.00
21.00

Figure 30. Group delay versus time of day (GMT). f=12.4 kHz. Trinidad - North Dakota (B-D). 10-31 March 1975.

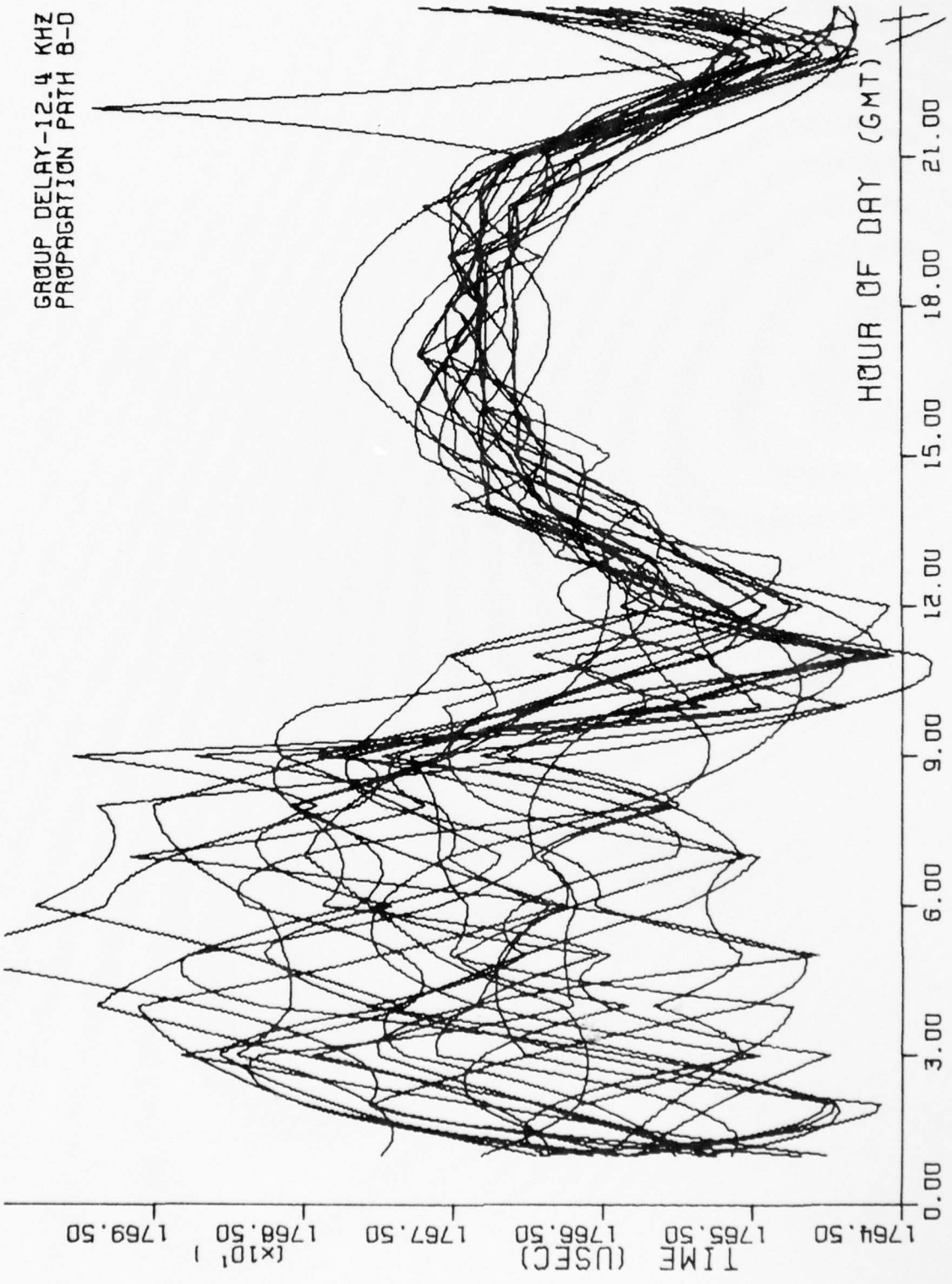
GROUP DELAY-12.4 KHZ
PROPAGATION PATH 8-D
HOUR OF DAY (GMT)
0.00
3.00
6.00
9.00
12.00
15.00
18.00
21.00
TIME (USEC)
(x10¹)
1764.50
1765.50
1766.50
1767.50
1768.50
1769.50

Figure 31. Composite OMEGA propagation time versus time of day (GMT). m=2.25. Trinidad - North Dakota (B-D). 10-31 March 1975.

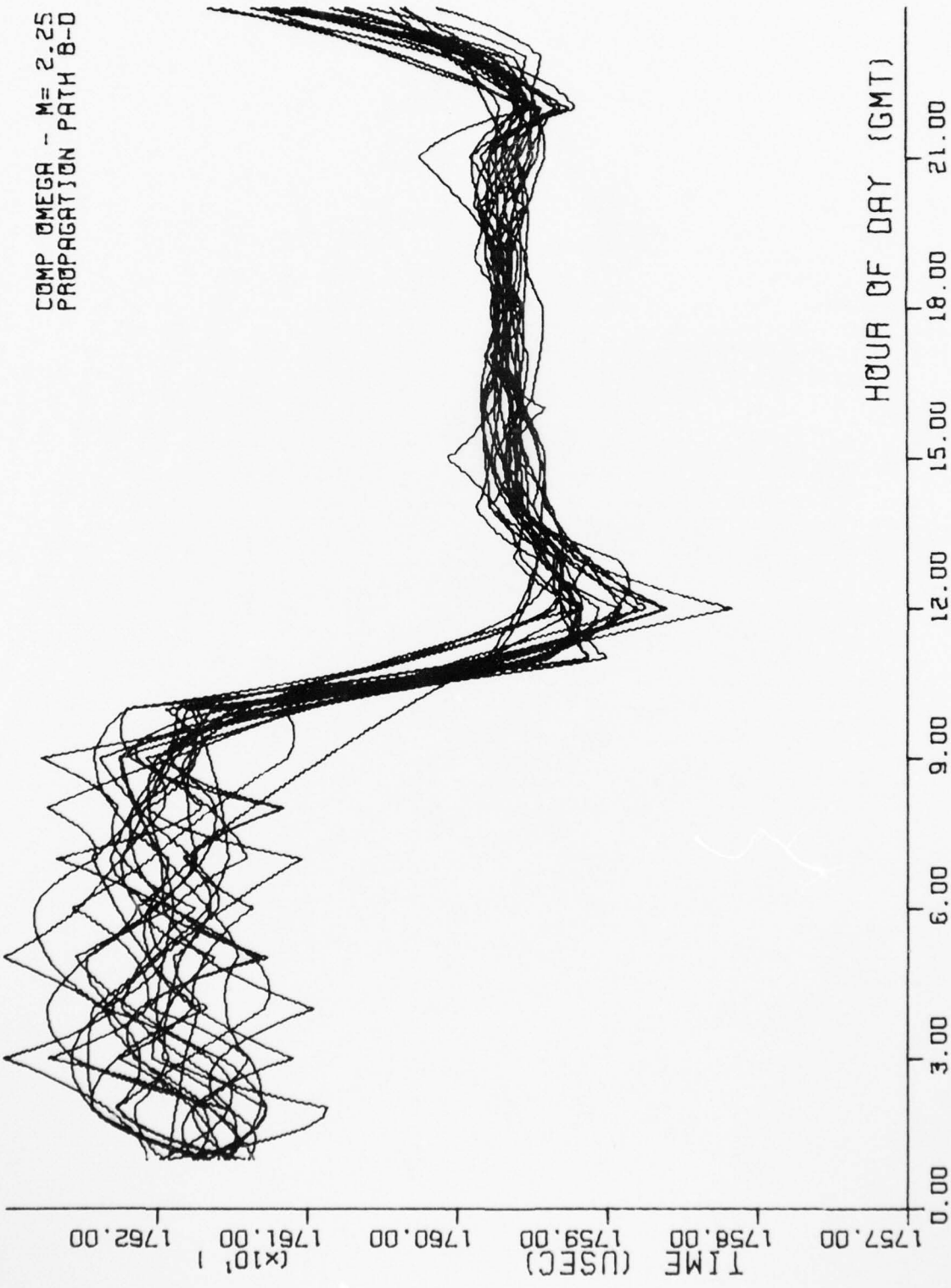
COMP OMEGA - M= 2.25
PROPAGATION PATH B-D
HOUR OF DAY (GMT)
0.00
3.00
6.00
9.00
12.00
15.00
18.00
21.00
TIME (USEC)
1757.00
1758.00
1759.00
1760.00
1761.00
1762.00
(x10¹)

Figure 32. Composite OMEGA propagation time versus time of day (GMT). m=3.0. Trinidad - North Dakota (B-D). 10-31 March 1975.

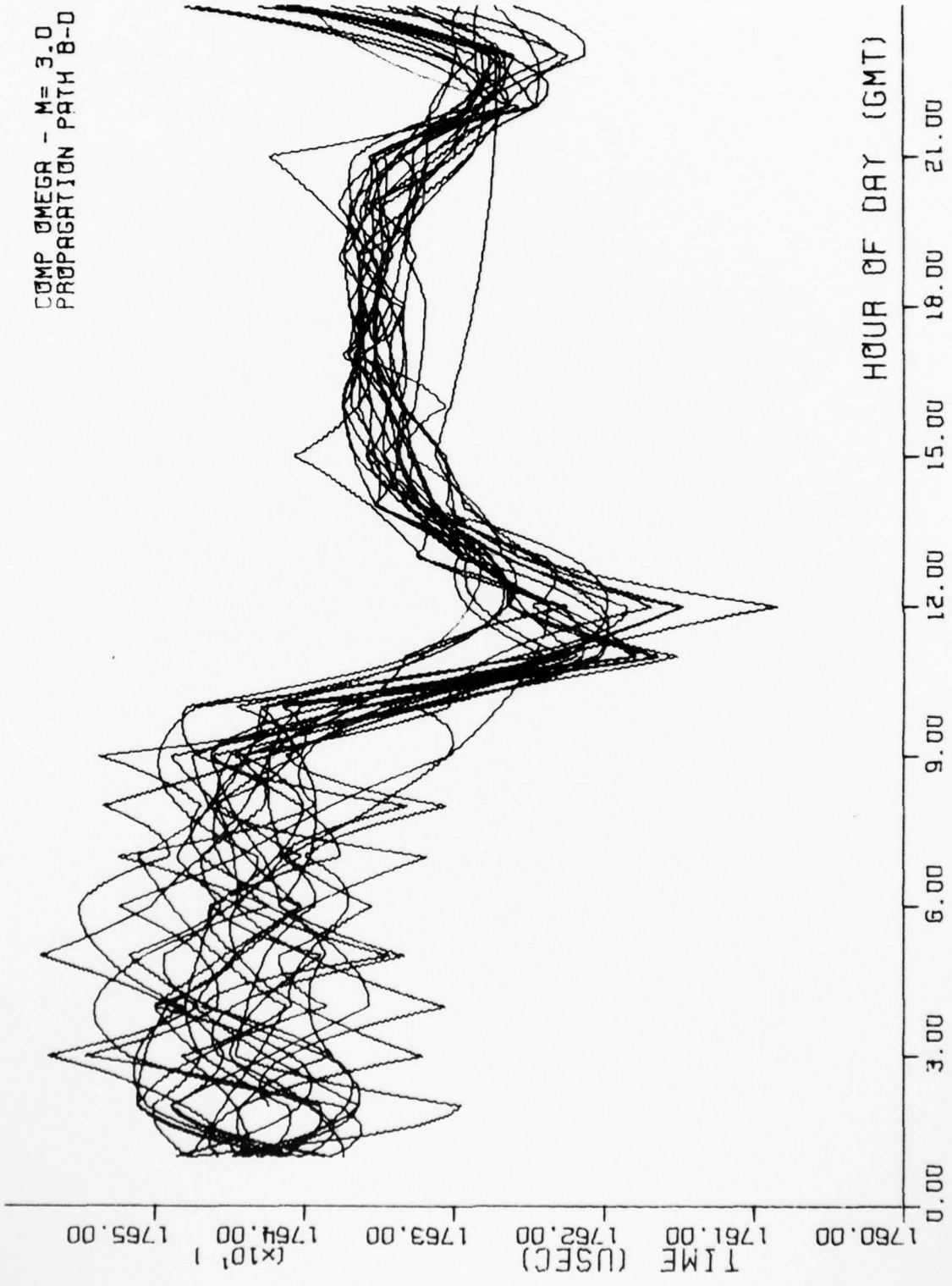
COMP OMEGA - M= 3.0
PROPAGATION PATH B-D
HOUR OF DAY (GMT)
0.00
3.00
6.00
9.00
12.00
15.00
18.00
21.00
TIME (USEC)
(x10')
1760.00
1761.00
1762.00
1763.00
1764.00
1765.00

Figure 33. Composite OMEGA propagation time versus time of day (GMT). m=3.3. Trinidad - North Dakota (B-D). 10-31 March 1975.

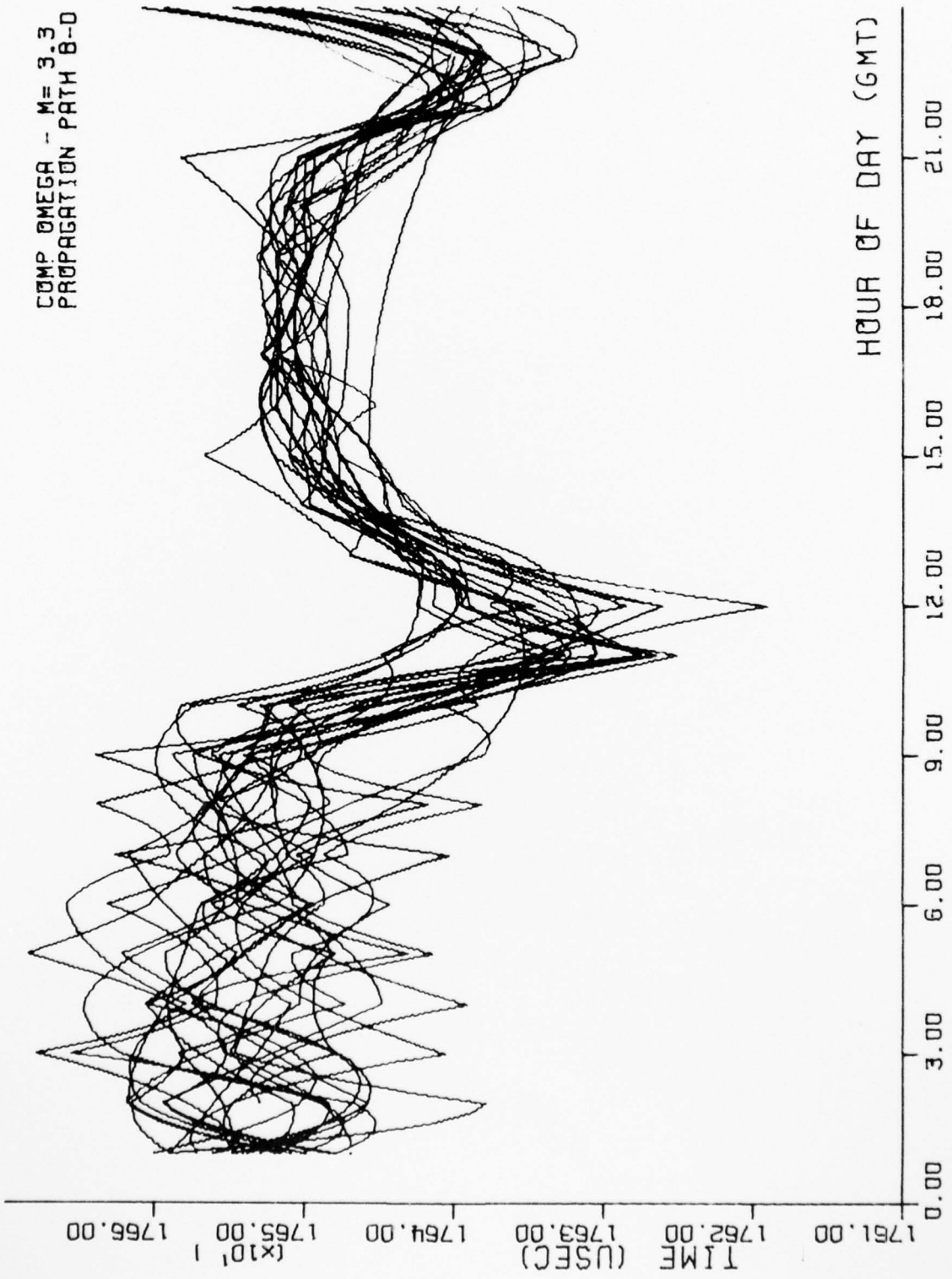
COMP OMEGA - M= 3.3
PROPAGATION PATH B-D
HOUR OF DAY (GMT)
0.00
3.00
6.00
9.00
12.00
15.00
18.00
21.00
TIME (USEC)
(x10')
1761.00
1762.00
1763.00
1764.00
1765.00
1766.00

Figure 34. Modified composite OMEGA propagation time versus time of day (GMT). Trinidad - North Dakota (B-D). 10-31 March 1975.

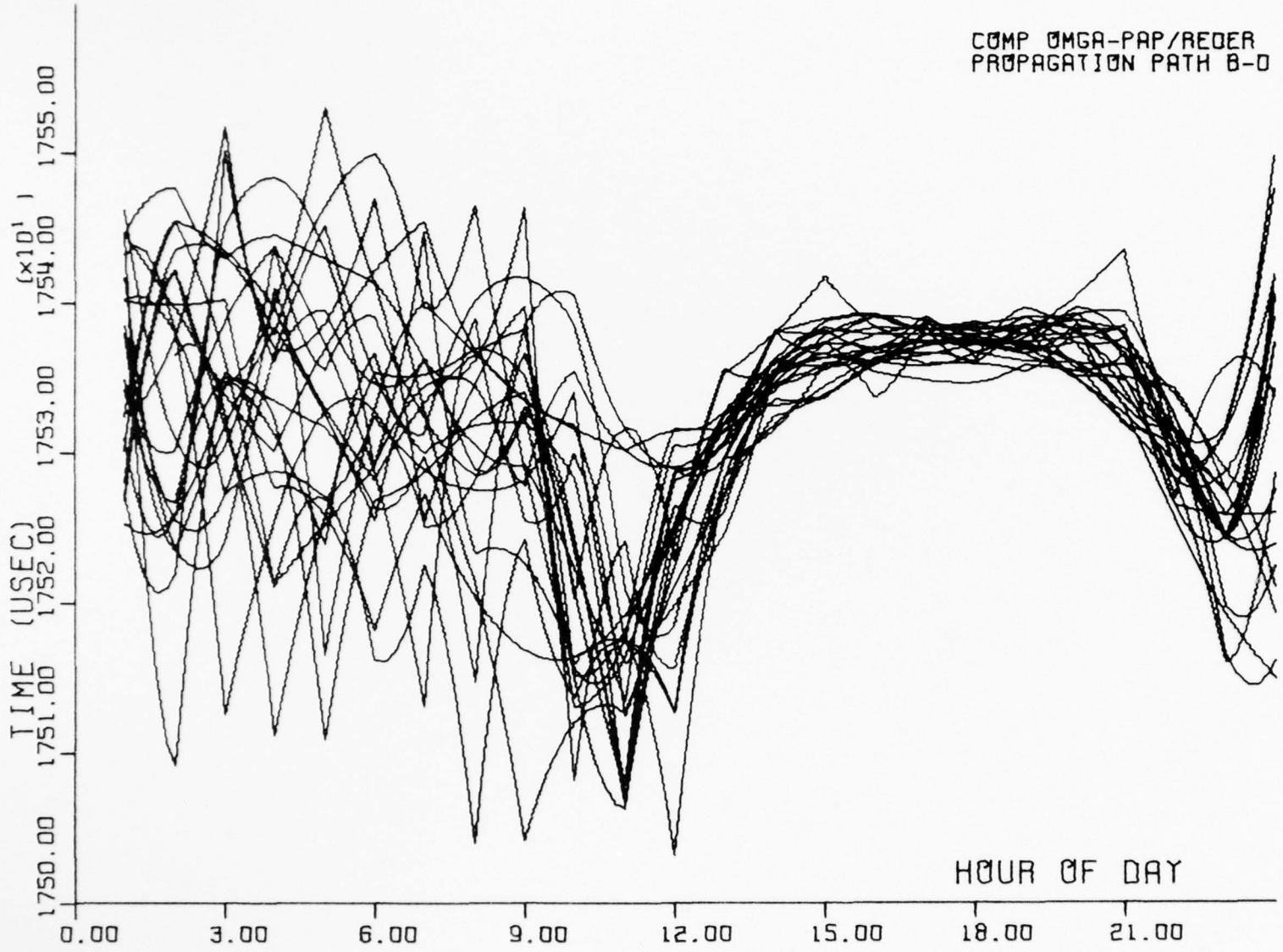
COMP OMGA-PAP/REDER
PROPAGATION PATH B-D
TIME (USEC) (x10¹)
1750.00
1751.00
1752.00
1753.00
1754.00
1755.00
HOUR OF DAY
0.00
3.00
6.00
9.00
12.00
15.00
18.00
21.00

Figure 35. Single-frequency OMEGA propagation time (Using PPC tables) versus time of day (GMT). Trinidad - North Dakota (B-D). 10-31 March 1975.

SNGL FREQ-SWC
PROPAGATION PATH B-O
TIME (USEC)
(x10¹)
1745.00
1746.00
1747.00
1748.00
1749.00
1750.00
0.00
3.00
6.00
9.00
12.00
15.00
18.00
21.00
HOUR OF DAY

Figure 36. Difference OMEGA propagation time (Using PPC tables) versus time of day (GMT).

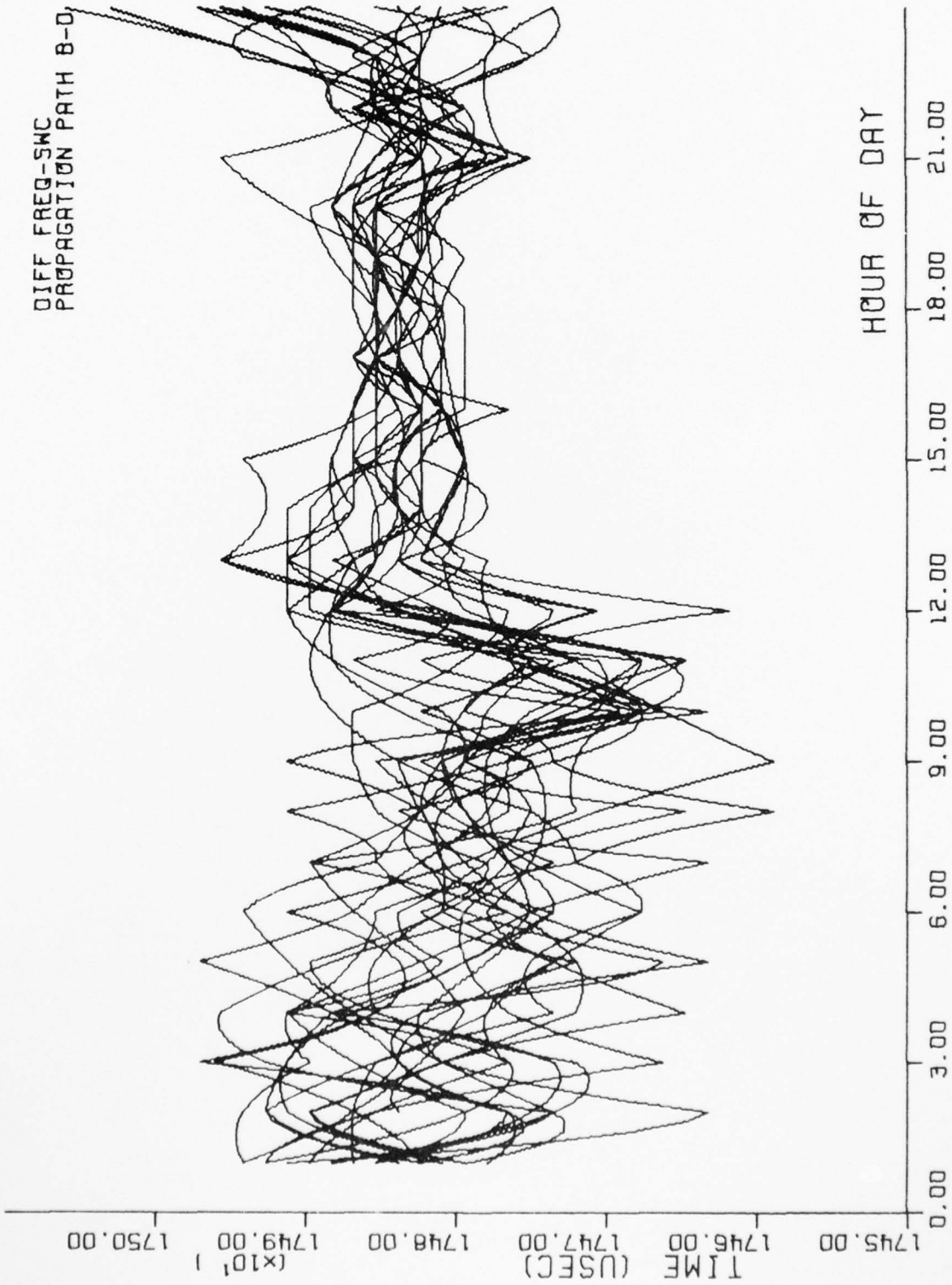
DIFF FREQ-SWC
PROPAGATION PATH B-D
HOUR OF DAY
0.00
3.00
6.00
9.00
12.00
15.00
18.00
21.00
TIME (USEC)
(x10')
1745.00
1746.00
1747.00
1748.00
1749.00
1750.00

B. Propagation Path North Dakota - Hawaii (D-C)

Figure 37. Group delay versus time of day (GMT). f=11.7 kHz. North Dakota - Hawaii (D-C). 10-22 March 1975.

AD-A047 124 AIR FORCE INST OF TECH WRIGHT-PATTERSON AFB OHIO F/G 17/7
COMPENSATION FOR PROPAGATION UNCERTAINTIES IN THE OMEGA NAVIGAT--ETC(U)
1976 R L VANALLEN
UNCLASSIFIED AFIT-CI-77-13 NL

2 OF 2
ADA047 124

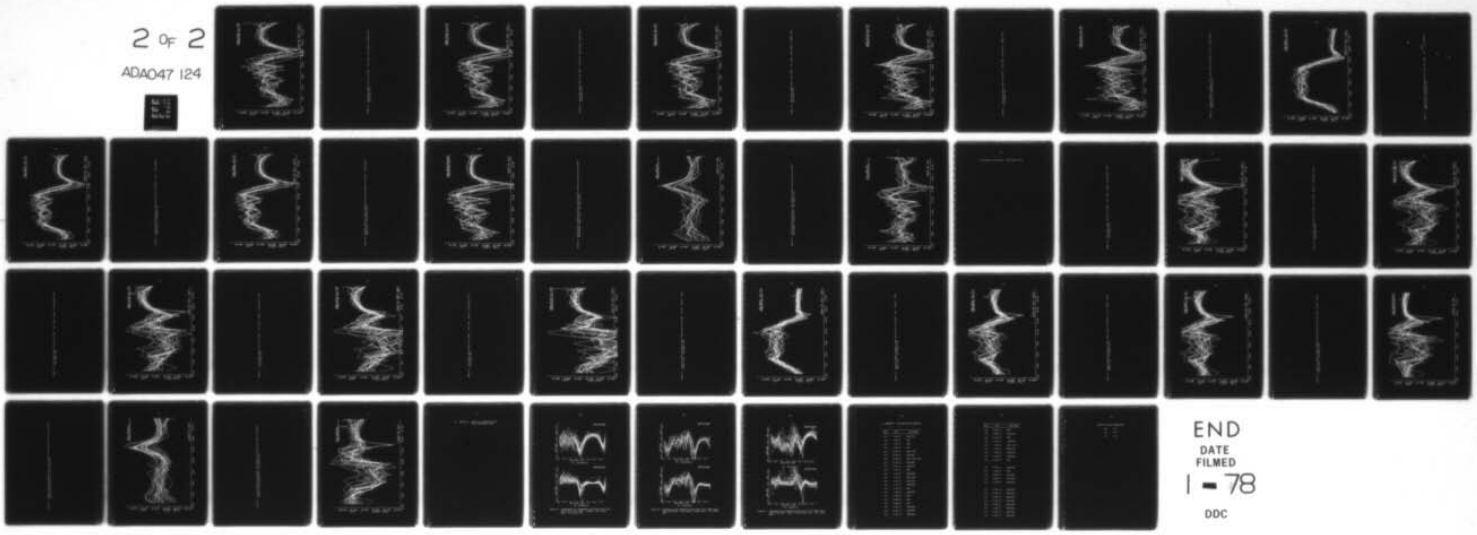

END
DATE FILMED
1 - 78
DDC

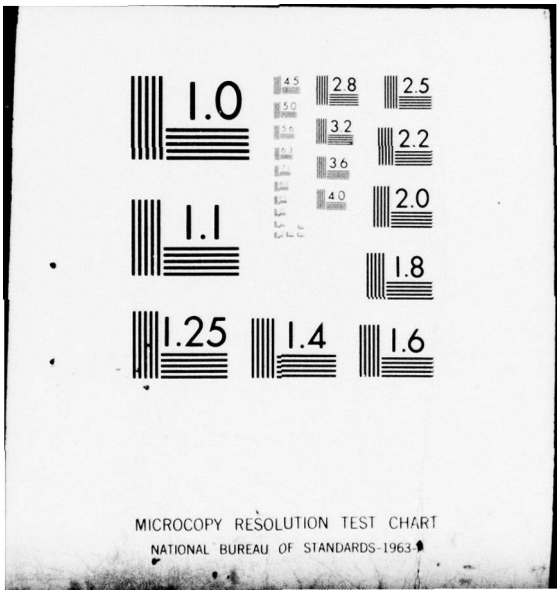
1.0
1.1
1.25
1.4
1.6
1.8
2.0
2.2
2.5
2.8
3.2
3.6
4.0
4.5
5.0
MICROCOPY RESOLUTION TEST CHART
NATIONAL BUREAU OF STANDARDS-1963-A

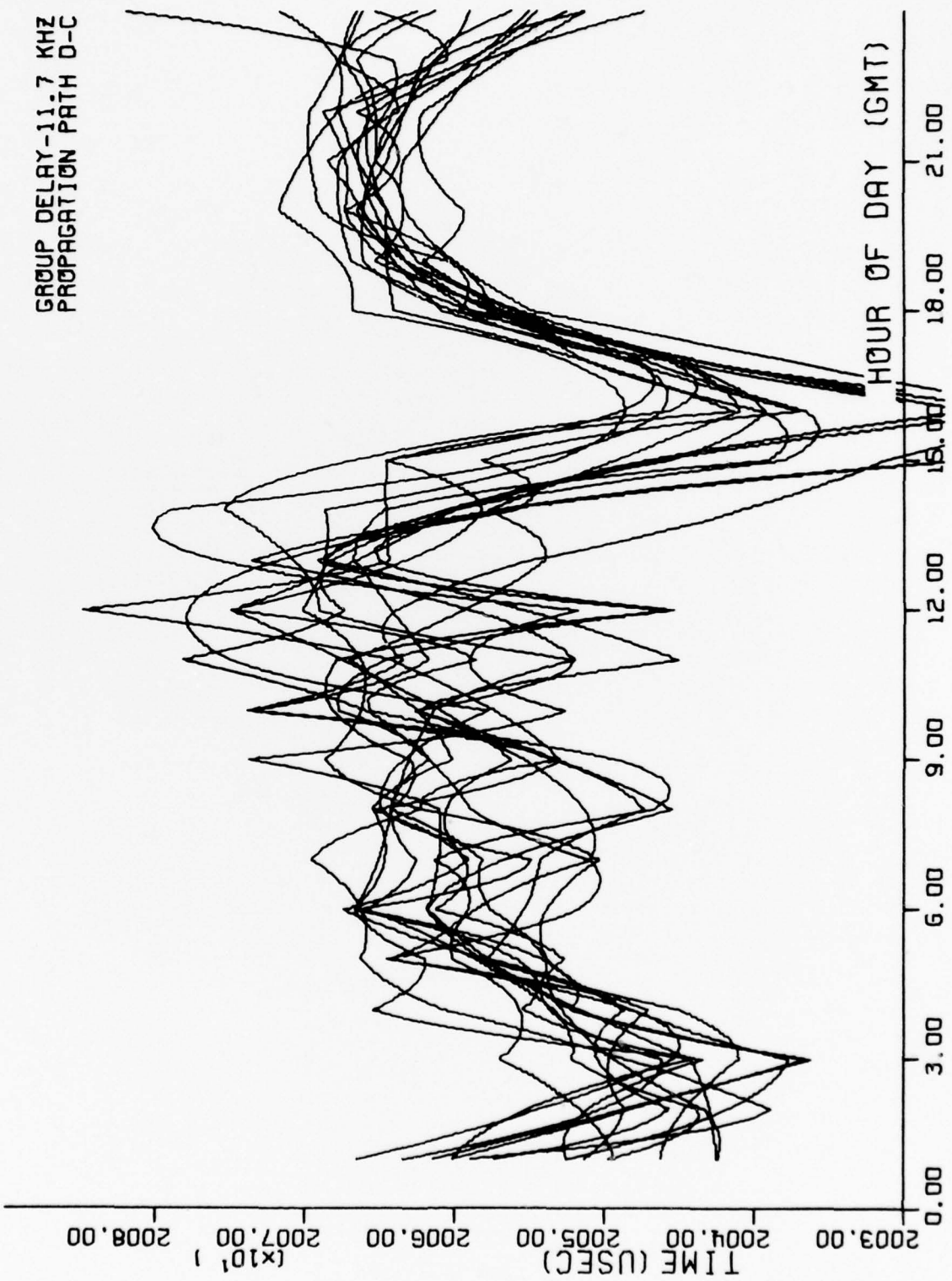
GROUP DELAY-11.7 KHZ
PROPAGATION PATH D-C
TIME (USEC)
(x10¹)
2003.00
2004.00
2005.00
2006.00
2007.00
2008.00
0.00
3.00
6.00
9.00
12.00
15.00
18.00
21.00
HOUR OF DAY (GMT)

Figure 38. Group delay versus time of day (GMT). f=11.9 kHz. North Dakota - Hawaii (D-C). 10-22 March 1975.

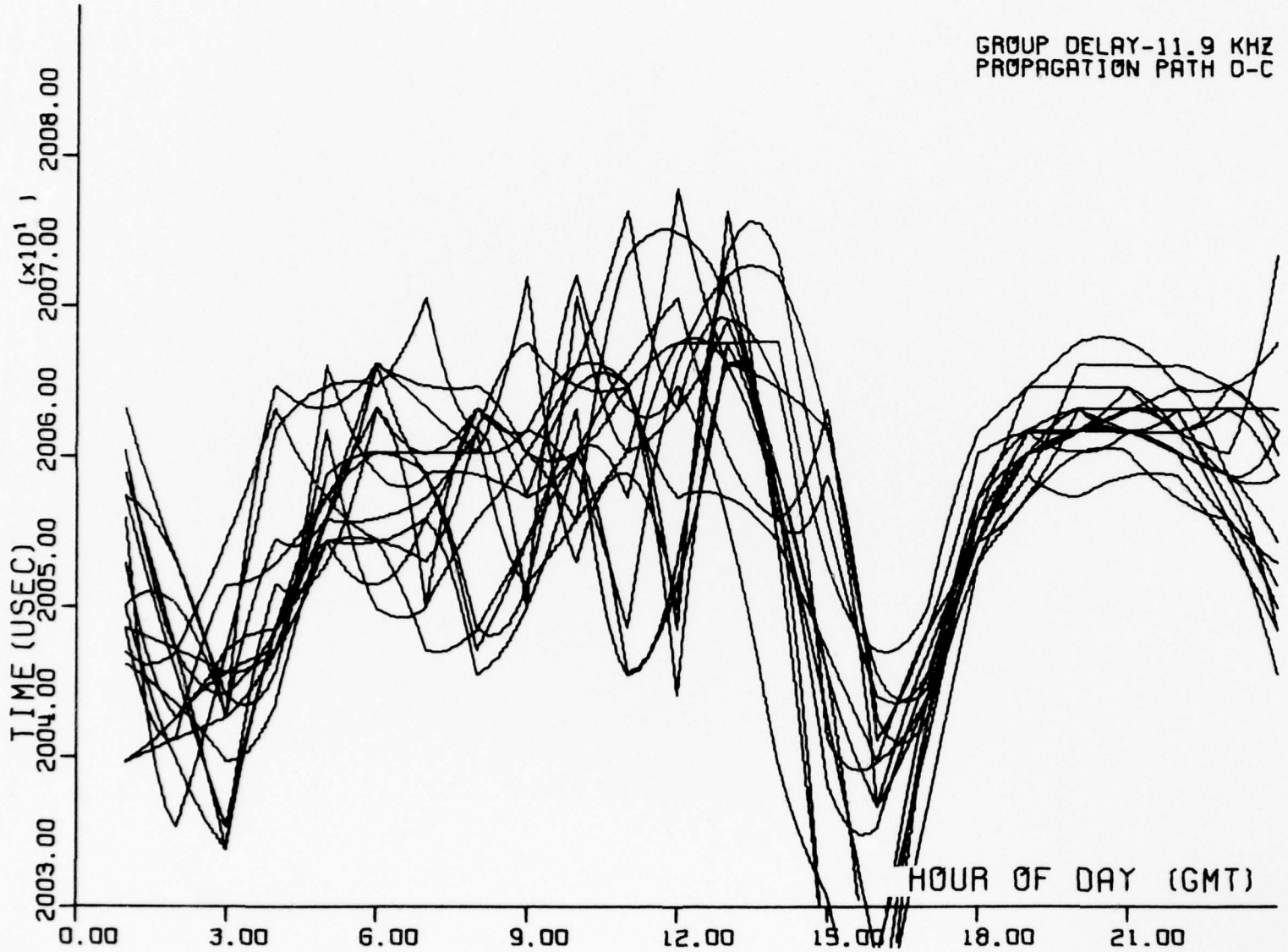
GROUP DELAY-11.9 KHZ
PROPAGATION PATH O-C
TIME (USEC) (x10¹)
2003.00
2004.00
2005.00
2006.00
2007.00
2008.00
0.00
3.00
6.00
9.00
12.00
15.00
18.00
21.00
HOUR OF DAY (GMT)

Figure 39. Group delay versus time of day (GMT). f=12.0 kHz. North Dakota - Hawaii (D-C). 10-22 March 1975.

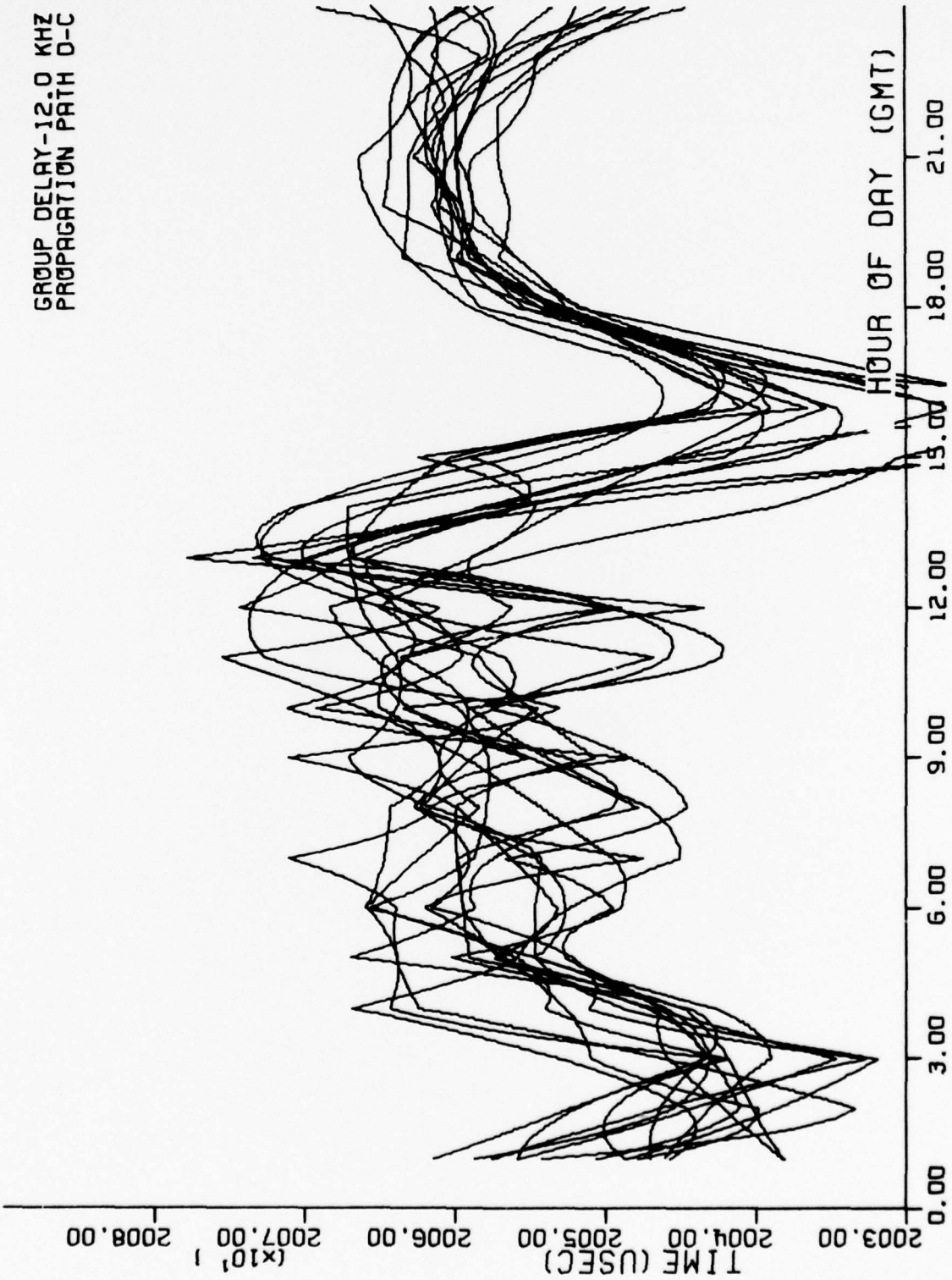
GROUP DELAY-12.0 KHZ
PROPAGATION PATH O-C
HOUR OF DAY (GMT)
0.00
3.00
6.00
9.00
12.00
15.00
18.00
21.00
TIME (USEC)
2003.00
2004.00
2005.00
2006.00
2007.00
2008.00
(x10¹)

Figure 40. Group delay versus time of day (GMT). f=12.2 kHz. North Dakota - Hawaii (D-C). 10-22 March 1975.

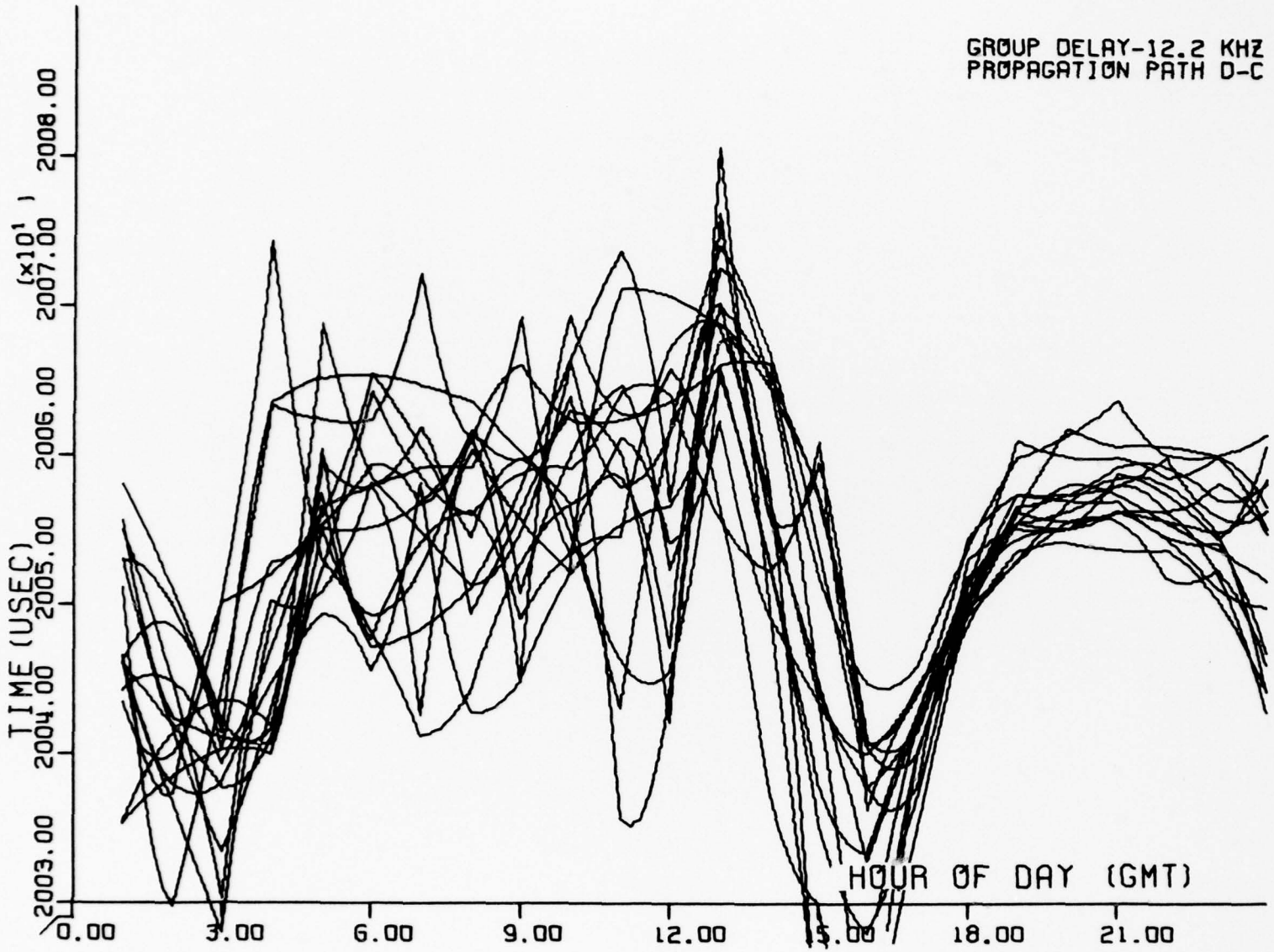
GROUP DELAY-12.2 KHZ
PROPAGATION PATH D-C
TIME (USEC) (x10¹)
2003.00
2004.00
2005.00
2006.00
2007.00
2008.00
0.00
3.00
6.00
9.00
12.00
15.00
18.00
21.00
HOUR OF DAY (GMT)

Figure 41. Group delay versus time of day (GMT). f=12.4 kHz. North Dakota - Hawaii (D-C). 10-22 March 1975.

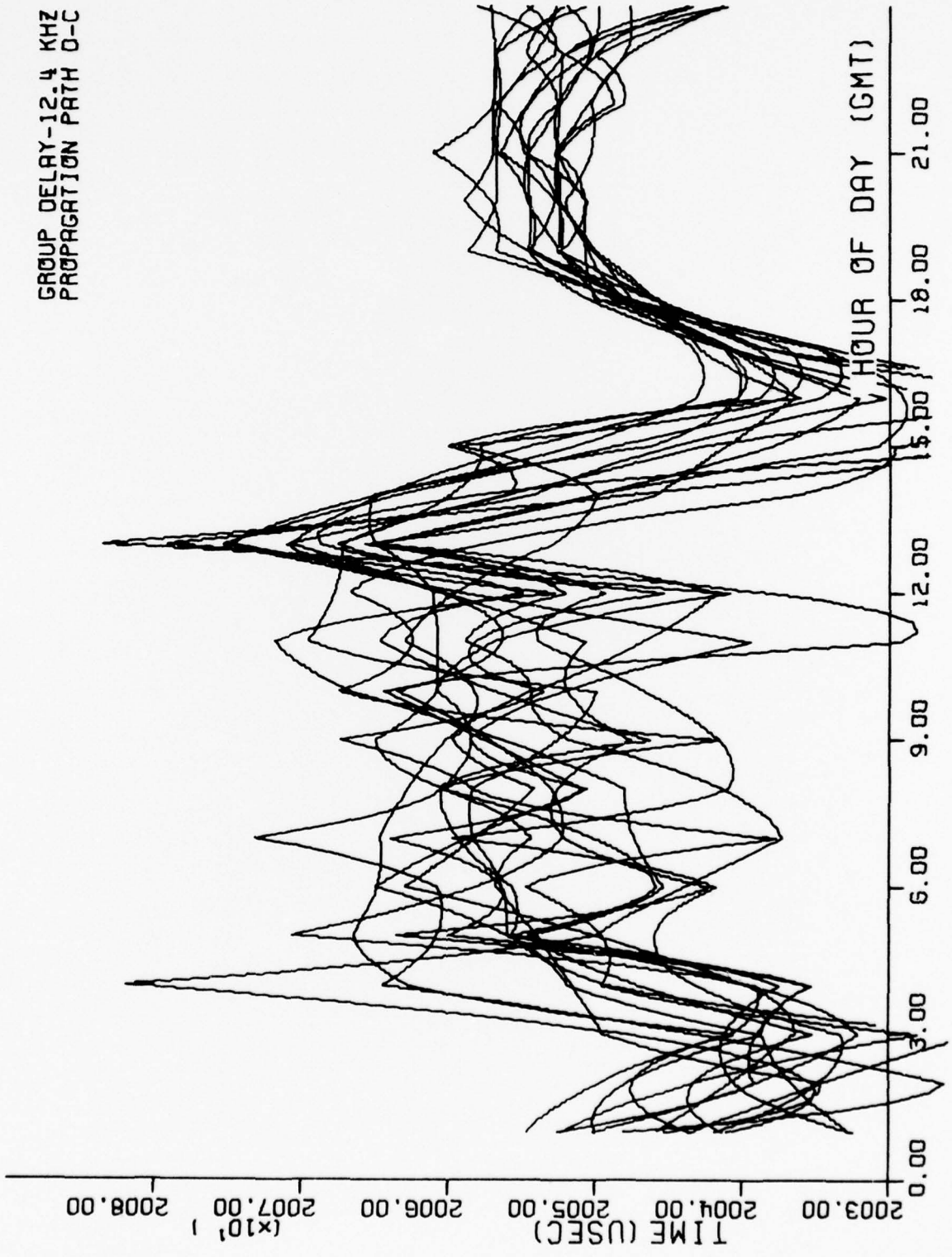
GROUP DELAY-12.4 KHZ
PROPAGATION PATH O-C
TIME (USEC)
(x10')
2003.00
2004.00
2005.00
2006.00
2007.00
2008.00
0.00
3.00
6.00
9.00
12.00
15.00
18.00
21.00
HOUR OF DAY (GMT)

Figure 42. Composite OMEGA propagation time versus time of day (GMT). m=2.25. North Dakota - Hawaii (D-C). 10-22 March 1975.

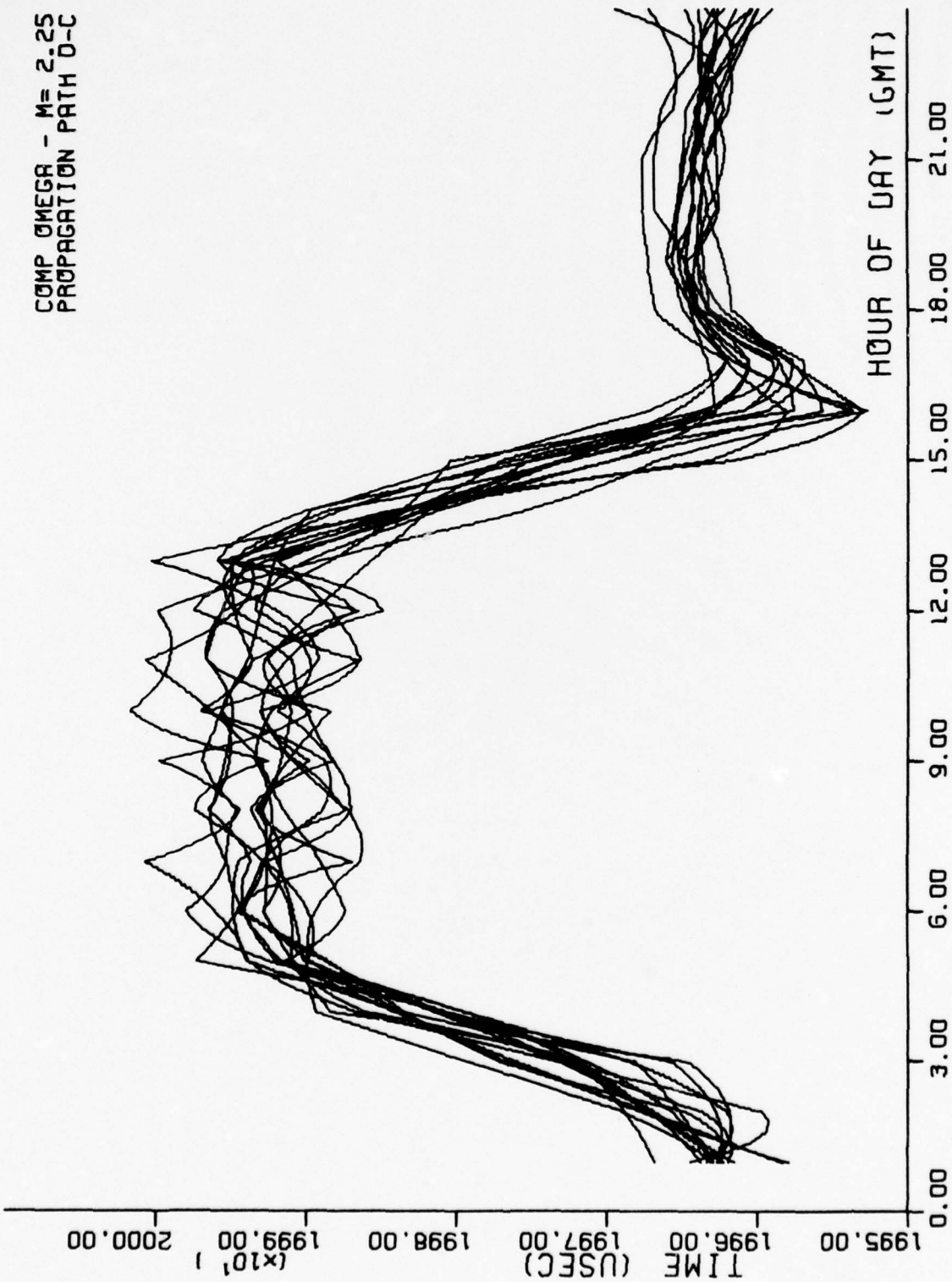
COMP OMEGA - M= 2.25
PROPAGATION PATH D-C
HOUR OF DAY (GMT)
0.00
3.00
6.00
9.00
12.00
15.00
18.00
21.00
TIME (USEC)
1995.00
1996.00
1997.00
1998.00
1999.00
2000.00
(x10')

Figure 43. Composite OMEGA propagation time versus time of day (GMT). m=3.0. North Dakota - Hawaii (D-C). 10-22 March 1975.

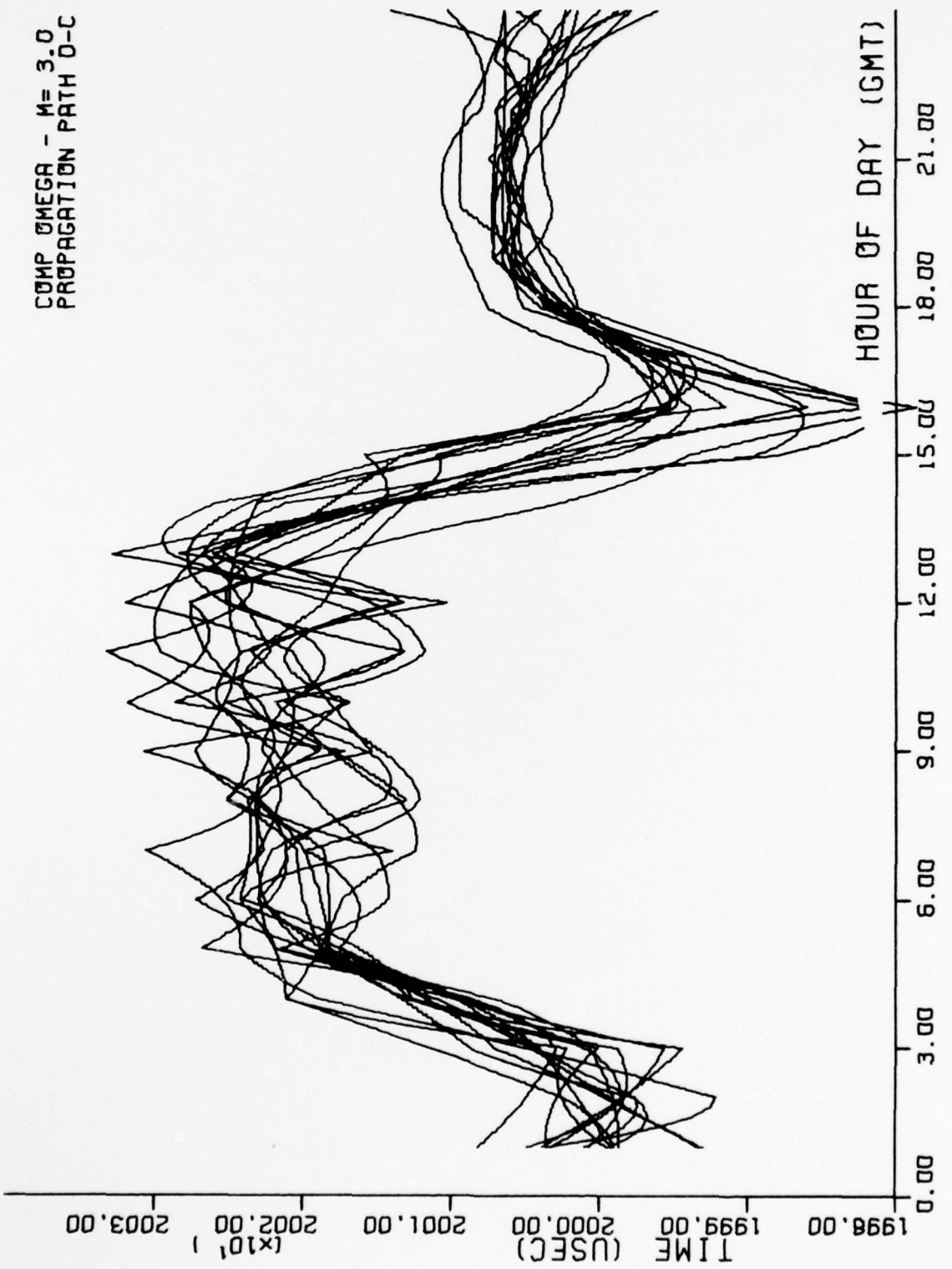
COMP OMEGA - M= 3.0
PROPAGATION PATH O-C
HOUR OF DAY (GMT)
0.00
3.00
6.00
9.00
12.00
15.00
18.00
21.00
TIME (USEC)
1998.00
1999.00
2000.00
2001.00
2002.00
2003.00
(x10¹)

Figure 44. Composite OMEGA propagation time versus time of day (GMT). m=3.3. North Dakota - Hawaii (D-C). 10-22 March 1975.

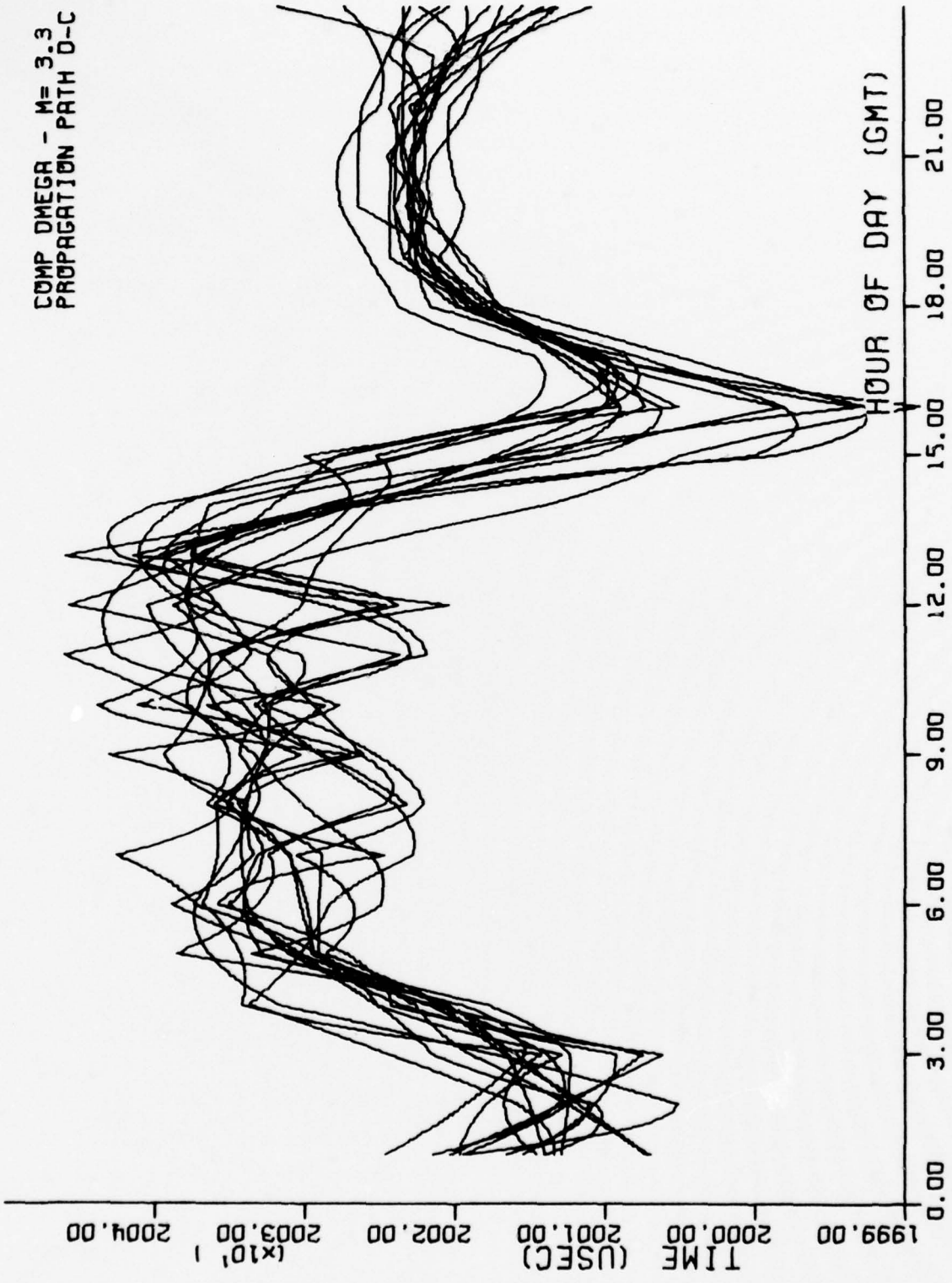
COMP OMEGA - M= 3.3
PROPAGATION PATH D-C
HOUR OF DAY (GMT)
0.00
3.00
6.00
9.00
12.00
15.00
18.00
21.00
TIME (USEC)
(x10')
1999.00
2000.00
2001.00
2002.00
2003.00
2004.00

Figure 45. Modified composite OMEGA propagation time versus time of day (GMT). North Dakota - Hawaii (D-C). 10-22 March 1975.

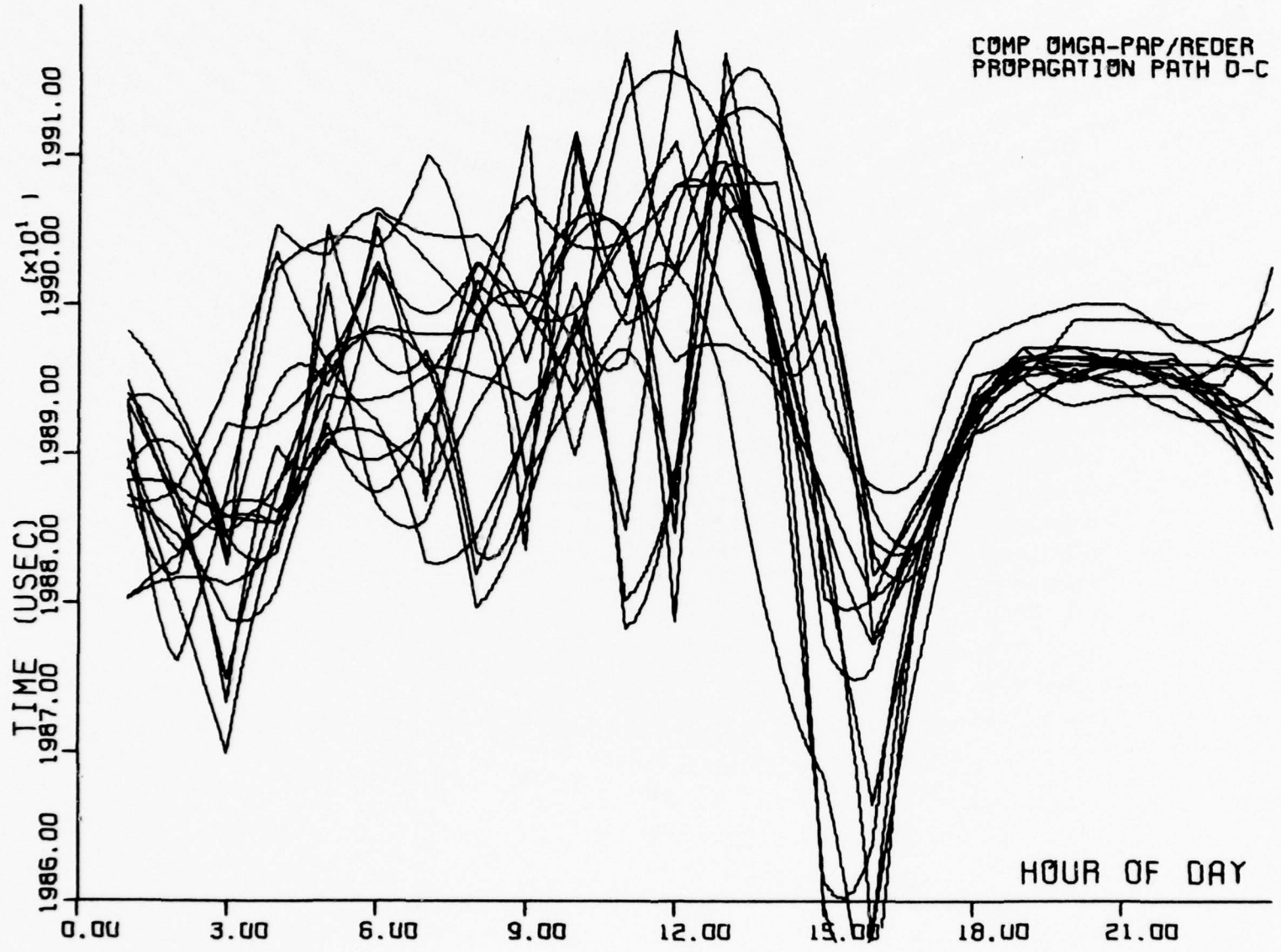
COMP OMGA-PAP/REDER
PROPAGATION PATH O-C
TIME (USEC) (x10¹)
1986.00
1987.00
1988.00
1989.00
1990.00
1991.00
0.00
3.00
6.00
9.00
12.00
15.00
18.00
21.00
HOUR OF DAY

Figure 46. Single-frequency OMEGA propagation time (Using PPC tables) versus time of day (GMT). North Dakota - Hawaii (D-C). 10-22 March 1975.

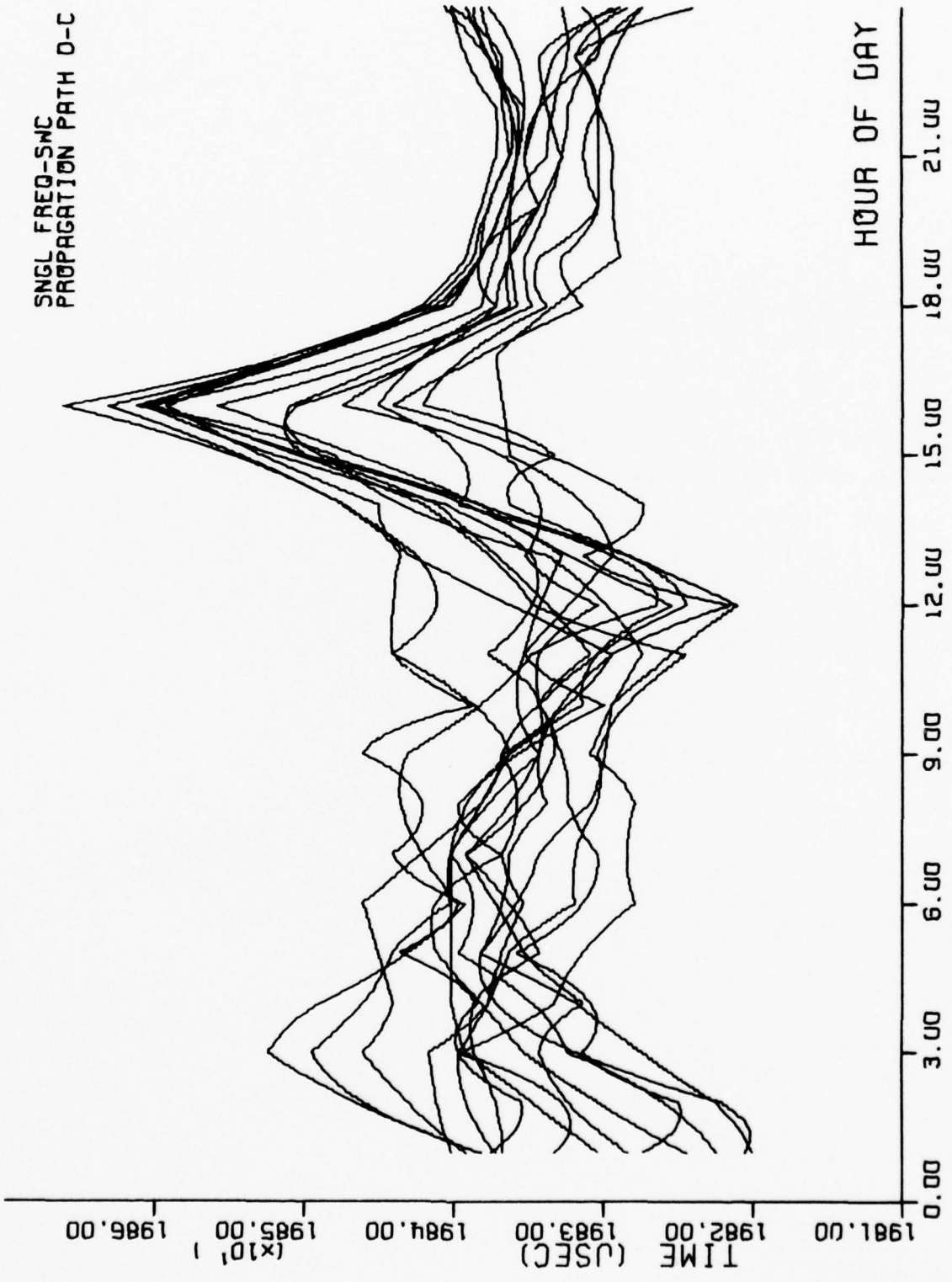
SNGL FREQ-SWC
PROPAGATION PATH O-C
HOUR OF DAY
0.00
3.00
6.00
9.00
12.00
15.00
18.00
21.00
TIME (USEC)
(x10')
1981.00
1982.00
1983.00
1984.00
1985.00
1986.00

Figure 47. Difference OMEGA propagation time (Using PPC tables) versus time of day (GMT). North Dakota - Hawaii (D-C). 10-22 March 1975.

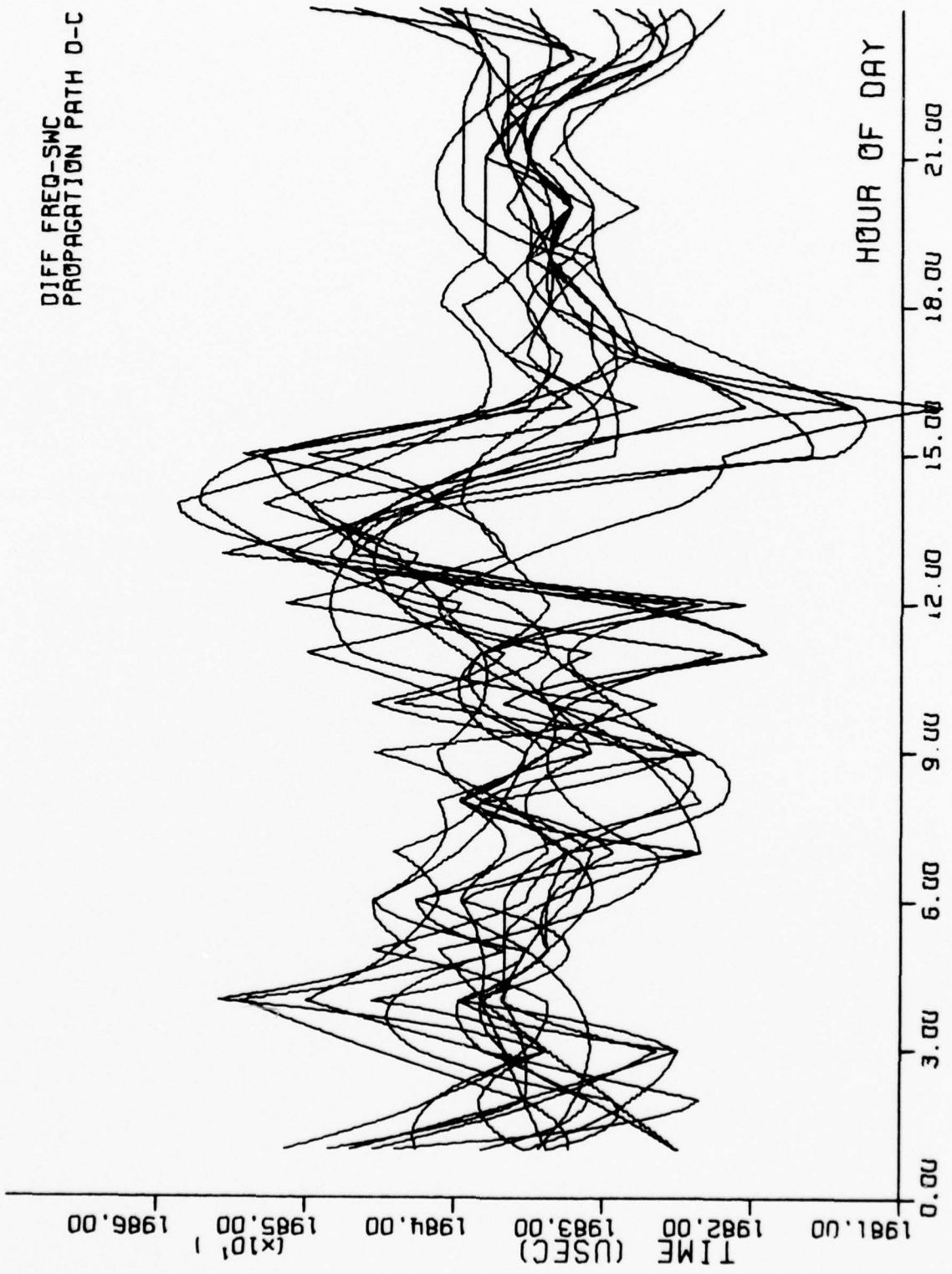
DIFF FREQ-SWC
PROPAGATION PATH O-C
HOUR OF DAY
0.00
3.00
6.00
9.00
12.00
15.00
18.00
21.00
TIME (USEC)
1981.00
1982.00
1983.00
1984.00
1985.00
1986.00
(x10')

C. Propagation Path Hawaii - North Dakota (C-D)

Figure 48. Group delay versus time of day (GMT). f=11.7 kHz. Hawaii - North Dakota (C-D). 10-31 March 1975.

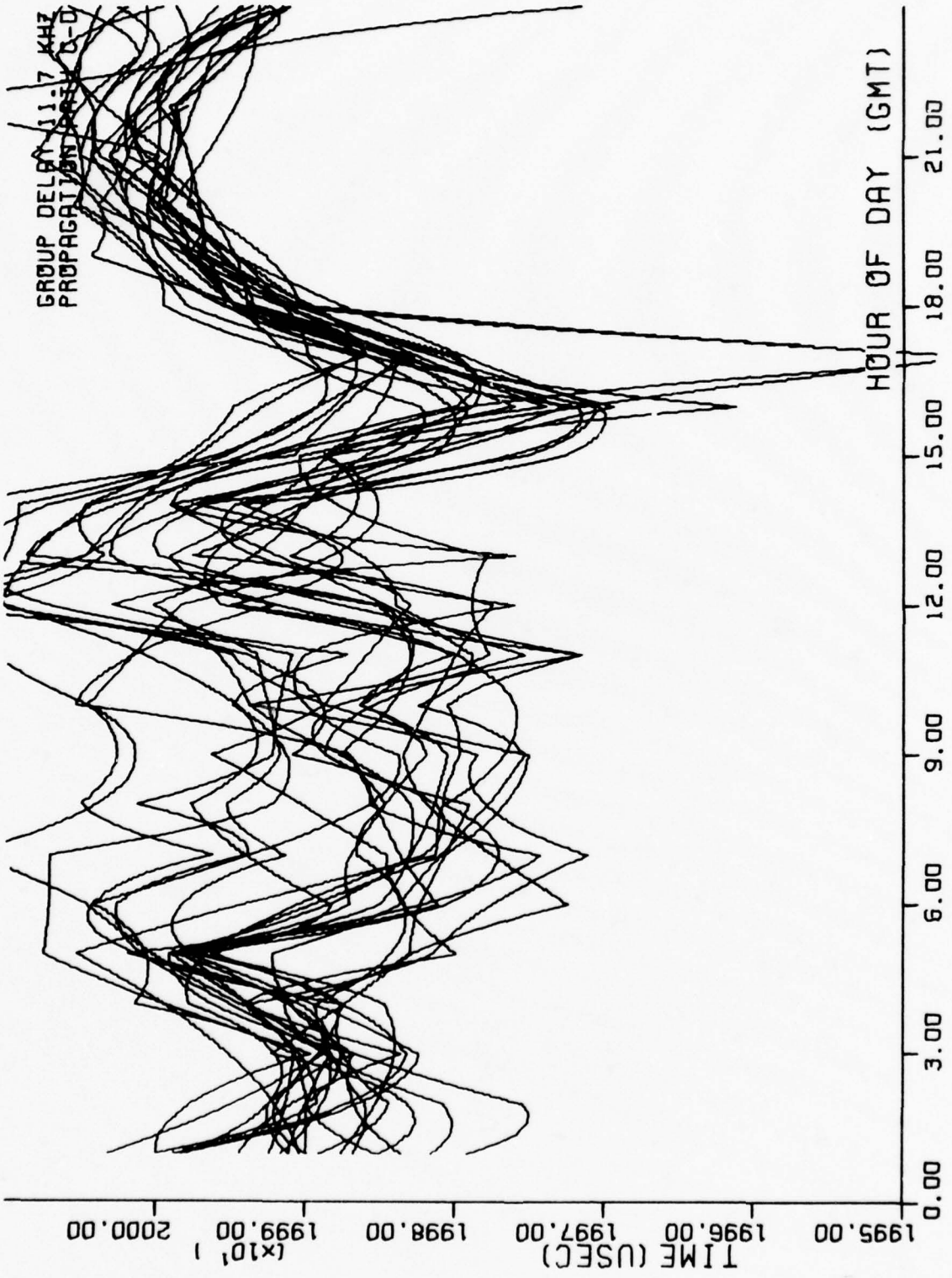
GROUP DELAY 11.7 KHZ
PROPAGATION PATH Q-D
HOUR OF DAY (GMT)
0.00
3.00
6.00
9.00
12.00
15.00
18.00
21.00
TIME (USEC)
1995.00
1996.00
1997.00
1998.00
1999.00
2000.00
(x10¹)

Figure 49. Group delay versus time of day (GMT). f=11.9 kHz. Hawaii - North Dakota (C-D). 10-31 March 1975.

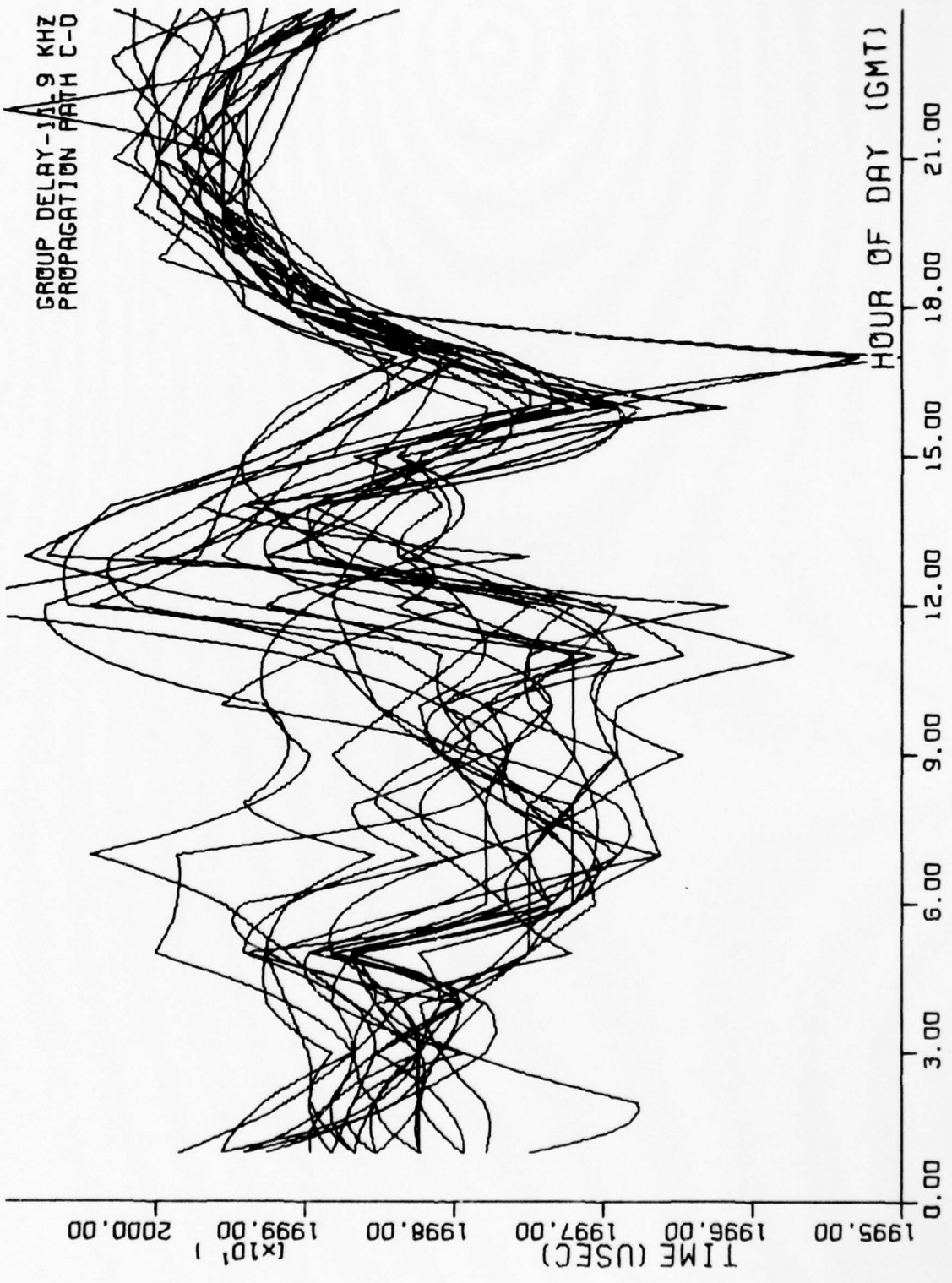
GROUP DELAY-JA 9 KHZ
PROPAGATION PATH C-D
HOUR OF DAY (GMT)
0.00
3.00
6.00
9.00
12.00
15.00
18.00
21.00
TIME (USEC)
1995.00
1996.00
1997.00
1998.00
1999.00
2000.00
(x10')

Figure 50. Group delay versus time of day (GMT). f=12.0 kHz. Hawaii - North Dakota (C-D). 10-31 March 1975.

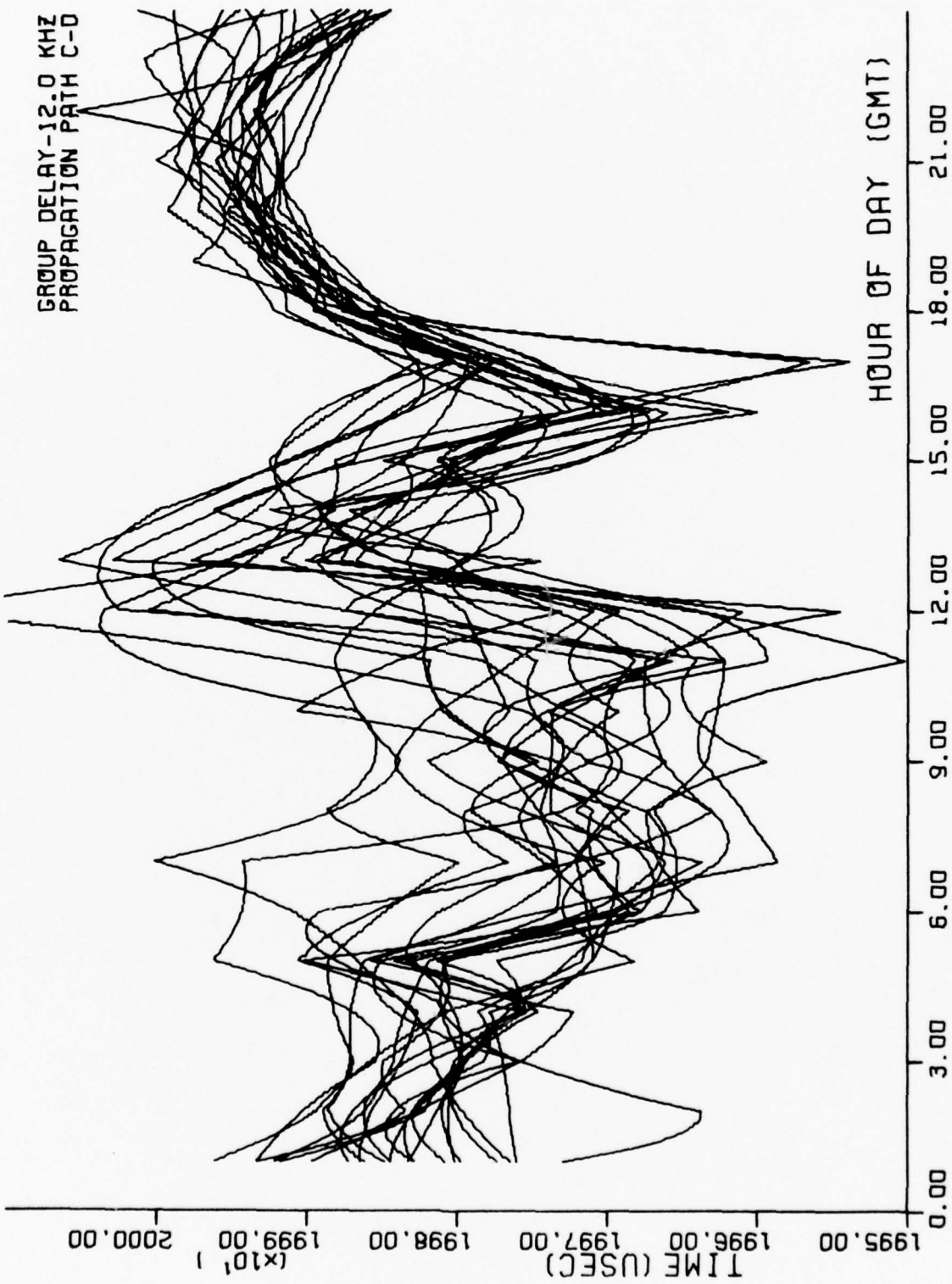
GROUP DELAY-12.0 KHZ
PROPAGATION PATH C-D
HOUR OF DAY (GMT)
0.00
3.00
6.00
9.00
12.00
15.00
18.00
21.00
TIME (USEC)
(x10¹)
1995.00
1996.00
1997.00
1998.00
1999.00
2000.00

Figure 51. Group delay versus time of day (GMT). f=12.2 kHz. Hawaii - North Dakota (C-D). 10-31 March 1975.

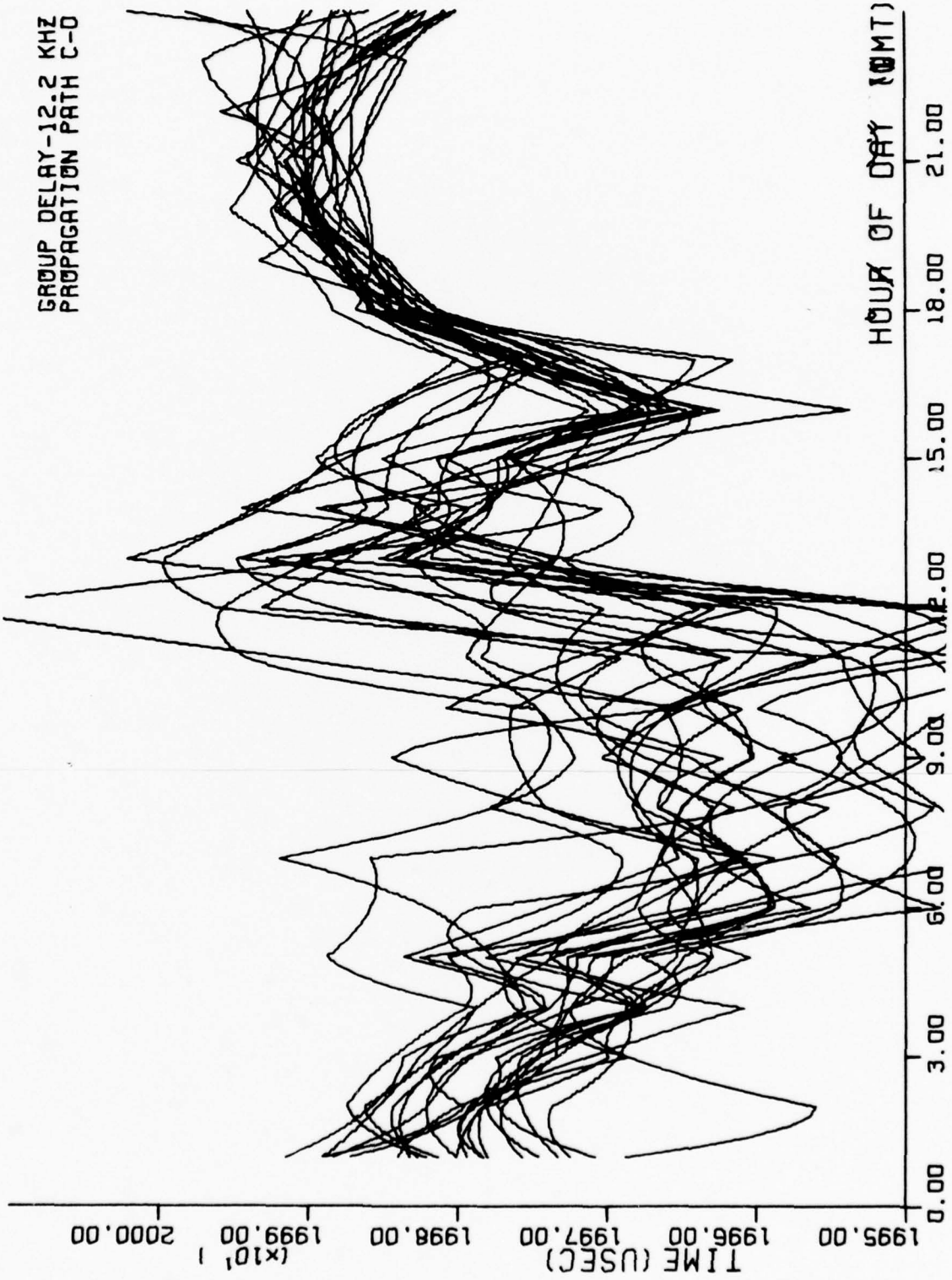
GROUP DELAY-12.2 KHZ
PROPAGATION PATH C-O
HOUR OF DAY (GMT)
0.00
3.00
6.00
9.00
12.00
15.00
18.00
21.00
TIME (USEC)
1995.00
1996.00
1997.00
1998.00
1999.00
2000.00
(x10¹)

Figure 52. Group delay versus time of day (GMT). f=12.4 kHz. Hawaii - North Dakota (C-D). 10-31 March 1975.

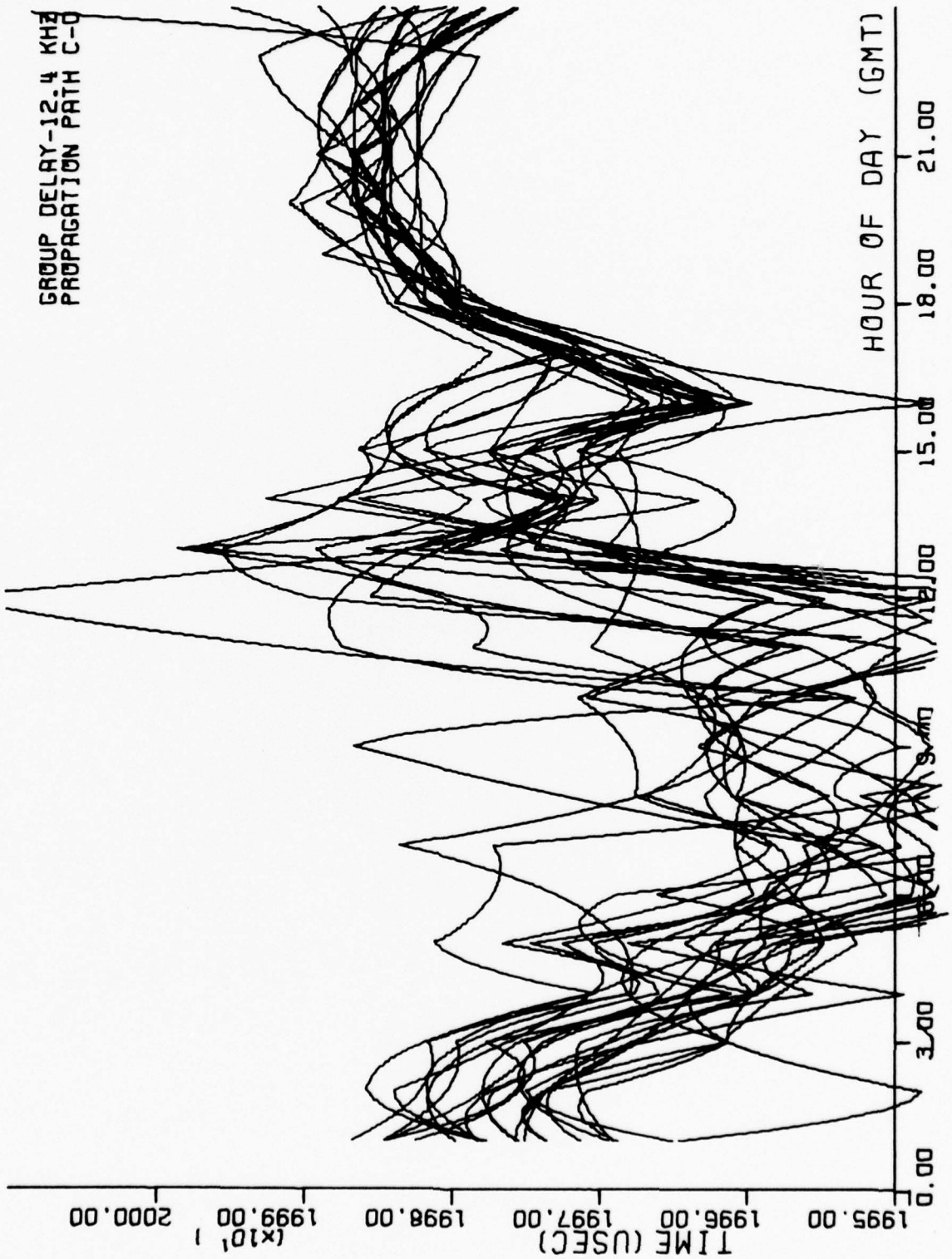
GROUP DELAY-12.4 KHZ
PROPAGATION PATH C-O
HOUR OF DAY (GMT)
0.00
3.00
6.00
9.00
12.00
15.00
18.00
21.00
TIME (USEC)
1995.00
1996.00
1997.00
1998.00
1999.00
2000.00
(x10')

Figure 53. Composite OMEGA propagation time versus time of day (GMT). m=2.25. Hawaii - North Dakota (C-D). 10-31 March 1975.

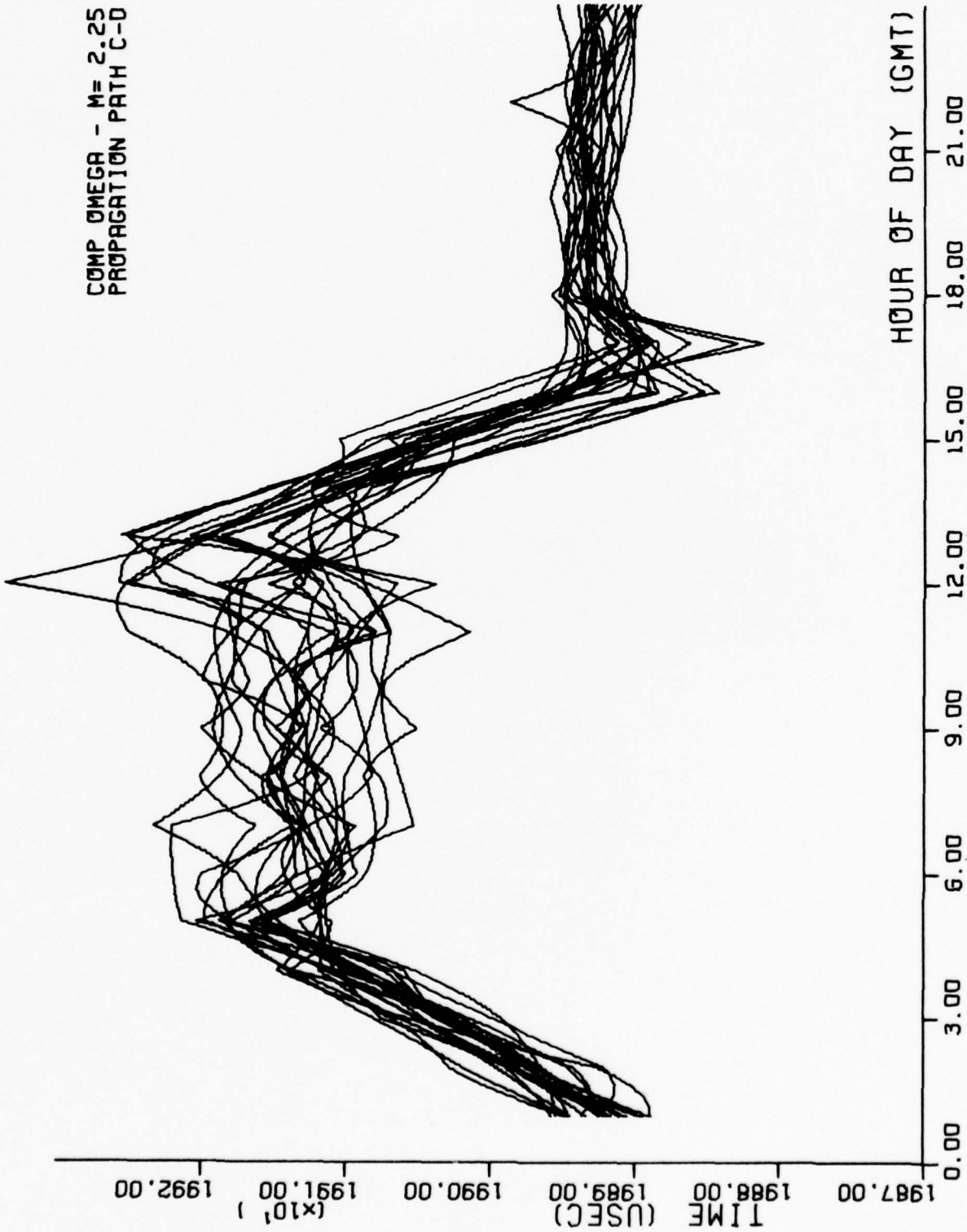
COMP OMEGA - M= 2.25
PROPAGATION PATH C-D
HOUR OF DAY (GMT)
0.00
3.00
6.00
9.00
12.00
15.00
18.00
21.00
TIME (USEC)
(x10¹)
1987.00
1988.00
1989.00
1990.00
1991.00
1992.00

Figure 54. Composite OMEGA propagation time versus time of day (GMT). m=3.0. Hawaii - North Dakota (C-D). 10-31 March 1975.

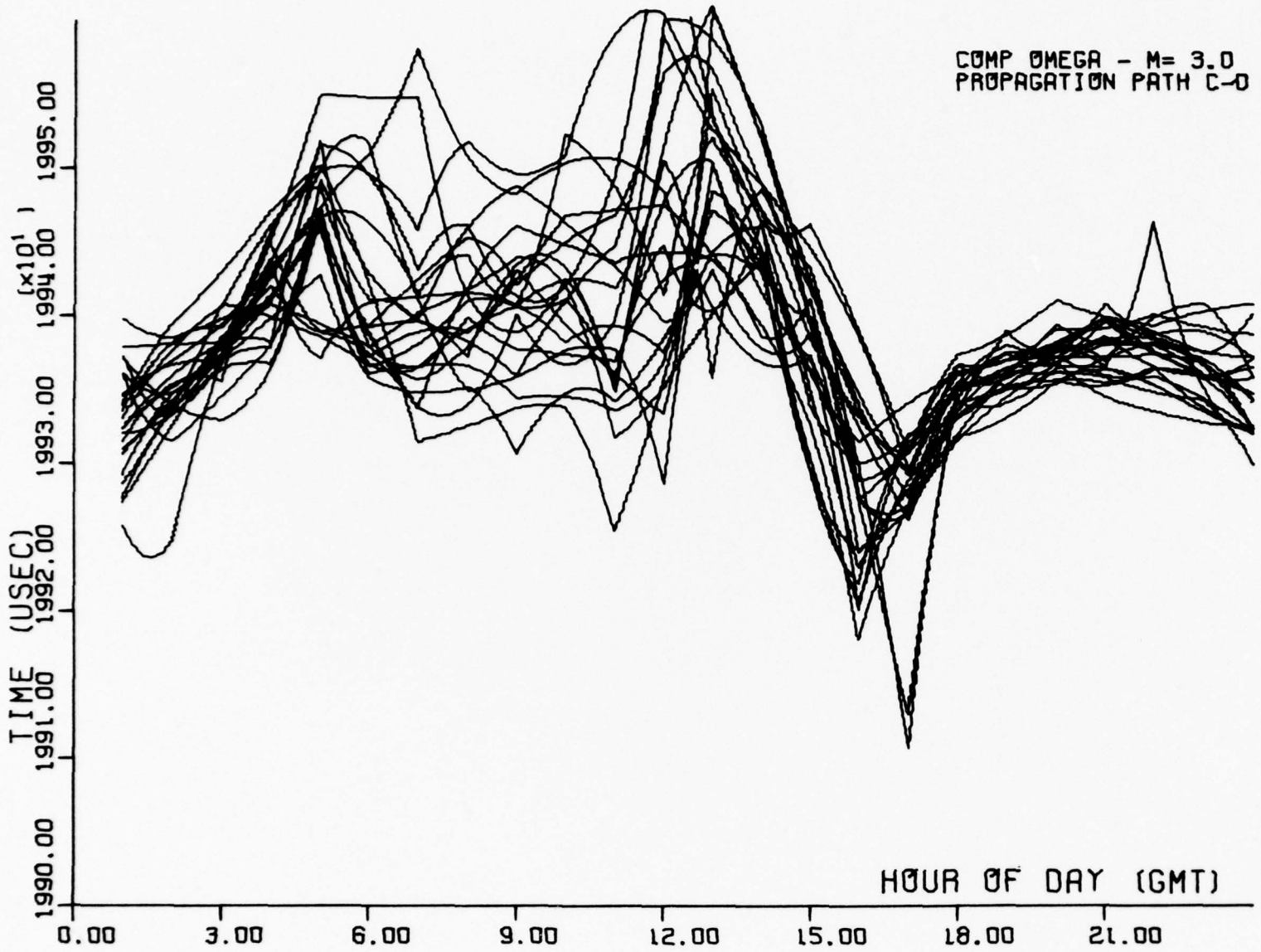
COMP OMEGA - M= 3.0
PROPAGATION PATH C-D
TIME (USEC) (x10^1)
1990.00
1991.00
1992.00
1993.00
1994.00
1995.00
0.00
3.00
6.00
9.00
12.00
15.00
18.00
21.00
HOUR OF DAY (GMT)

Figure 55. Composite OMEGA propagation time versus time of day (GMT). m=3.3. Hawaii - North Dakota (C-D). 10-31 March 1975.

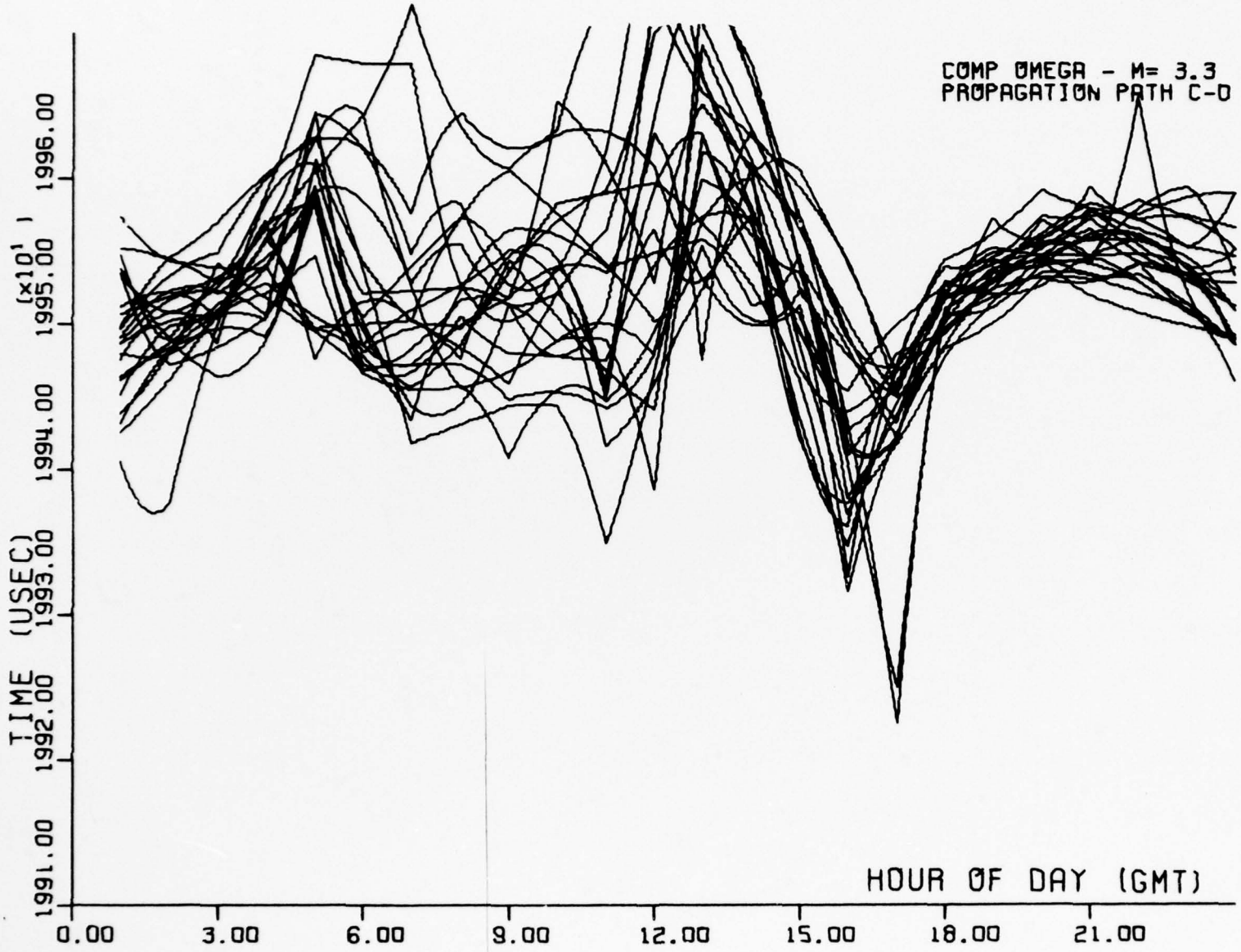
COMP OMEGA - M= 3.3
PROPAGATION PATH C-D
TIME (USEC) (x10¹)
1991.00
1992.00
1993.00
1994.00
1995.00
1996.00
HOUR OF DAY (GMT)
0.00
3.00
6.00
9.00
12.00
15.00
18.00
21.00

Figure 56. Modified composite OMEGA propagation time versus time of day (GMT). Hawaii - North Dakota (C-D). 10-31 March 1975.

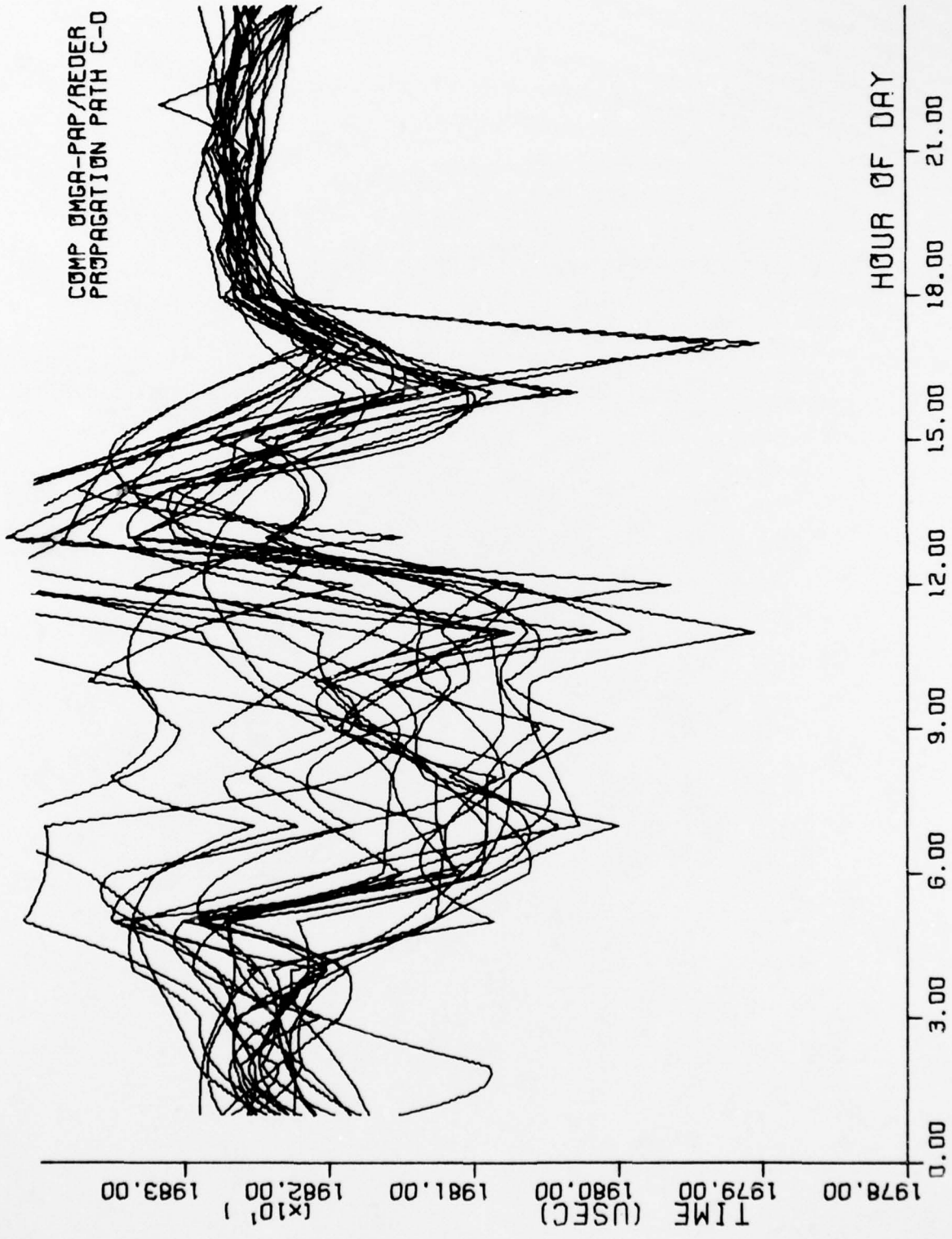
COMP OMGA-PAP/REDER
PROPAGATION PATH C-D
TIME (USEC)
(x10')
1978.00
1979.00
1980.00
1981.00
1982.00
1983.00
0.00
3.00
6.00
9.00
12.00
15.00
18.00
21.00
HOUR OF DAY

Figure 57. Single-frequency OMEGA propagation time (Using PPC tables) versus time of day (GMT). Hawaii-North Dakota (C-D). 10-31 March 1975.

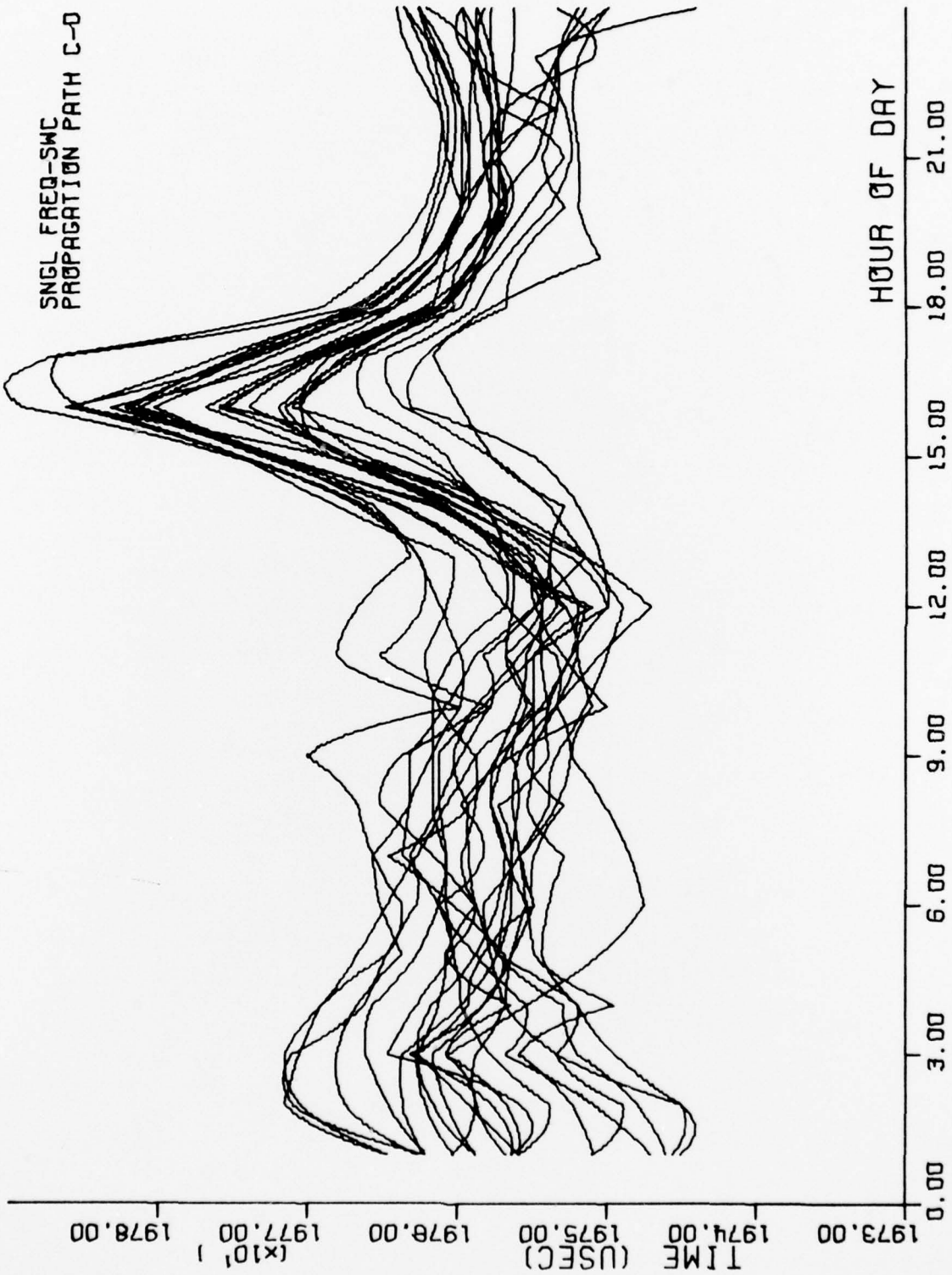
SNGL FREQ-SWC
PROPAGATION PATH C-D
HOUR OF DAY
0.00
3.00
6.00
9.00
12.00
15.00
18.00
21.00
TIME (USEC)
(x10')
1973.00
1974.00
1975.00
1976.00
1977.00
1978.00

Figure 58. Difference OMEGA propagation time (Using PPC tables) versus time of day (GMT). Hawaii - North Dakota (C-D). 10-31 March 1975.

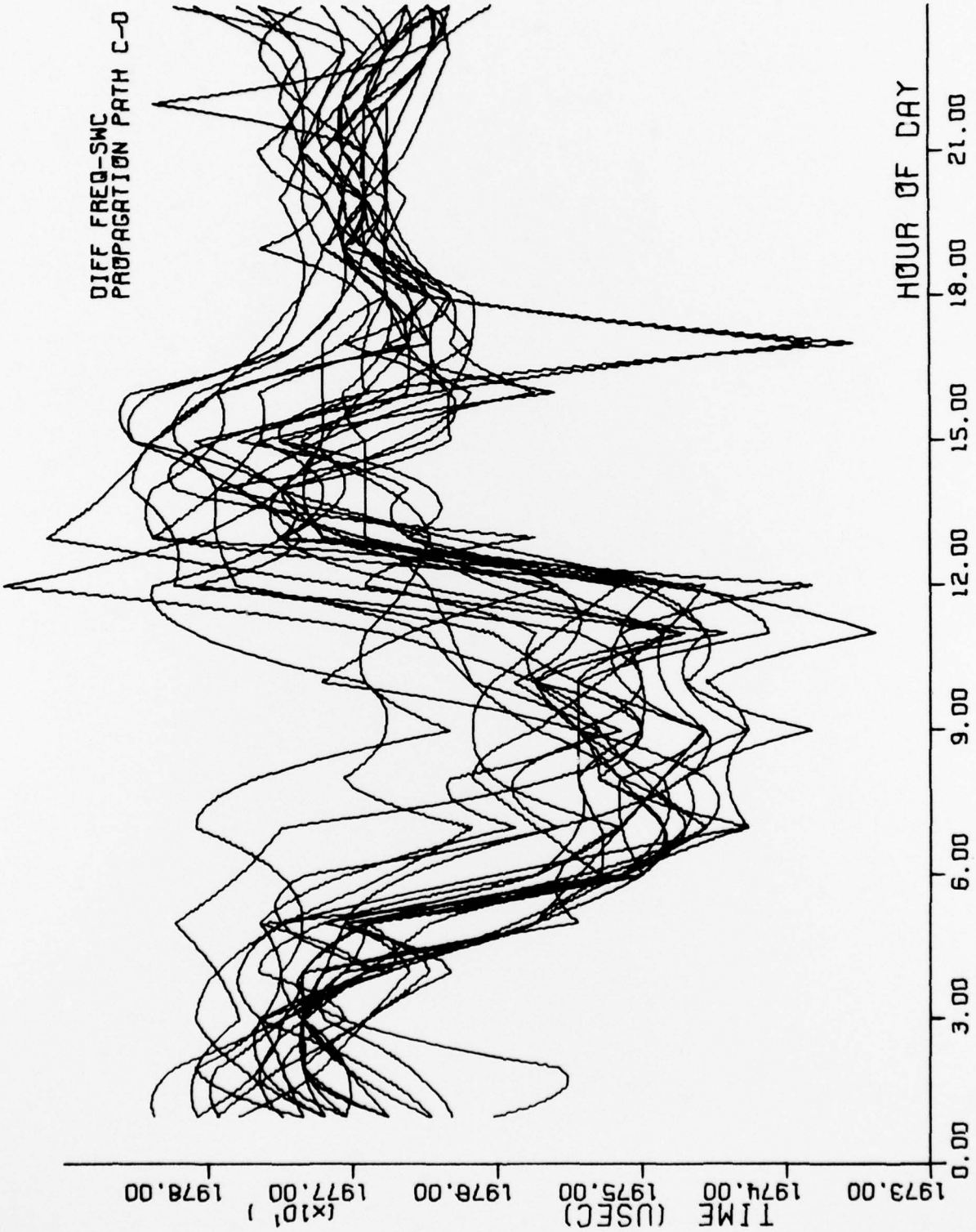
DIFF FREQ-SWC
PROPAGATION PATH C-D
HOUR OF DAY
0.00
3.00
6.00
9.00
12.00
15.00
18.00
21.00
TIME (USEC)
1973.00
1974.00
1975.00
1976.00
1977.00
1978.00
(x10')

IX. APPENDIX B: PHASE RATIO COMPENSATION FOR VARIOUS PROPAGATION PATHS

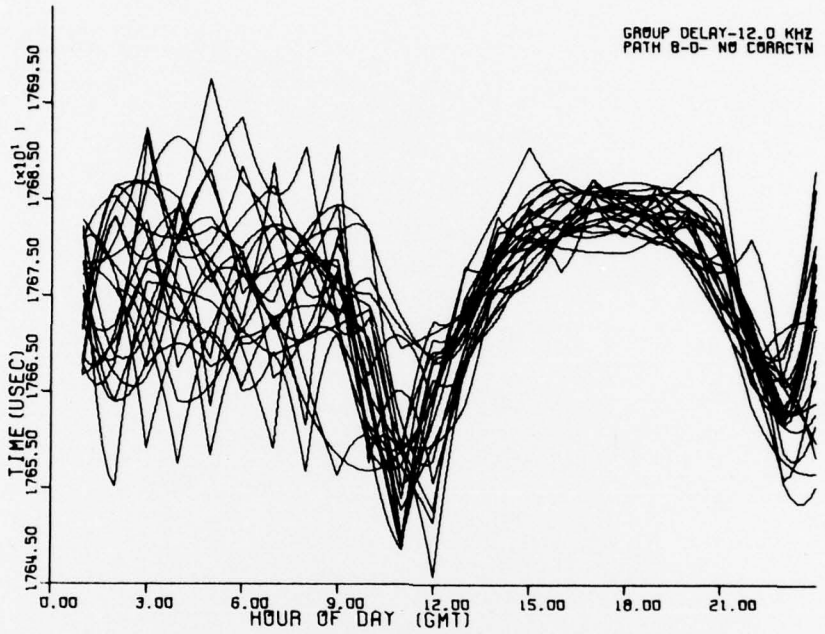

(a) Uncompensated

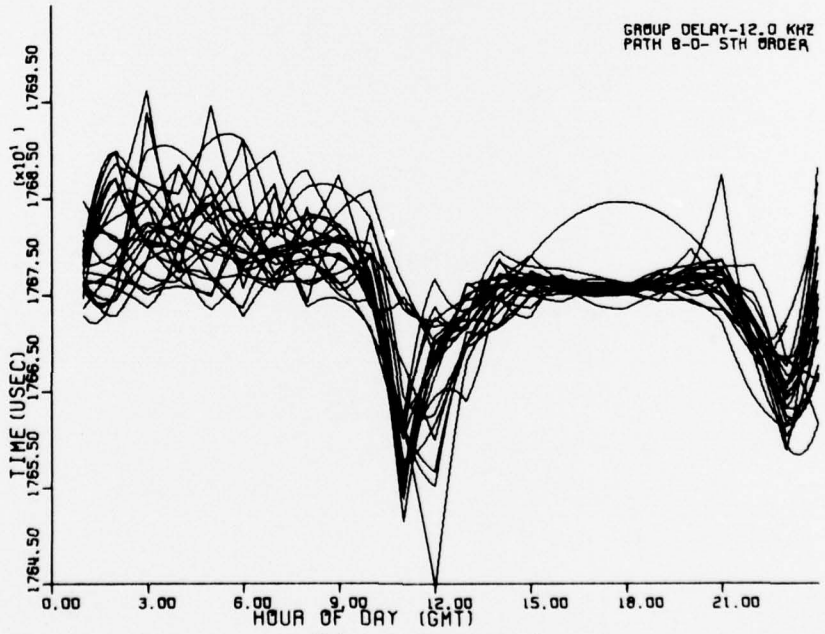

(b) Compensated

Figure 59. Uncompensated and compensated group delay (f=12.0 kHz) versus time of day (GMT). Trinidad - North Dakota (B-D). 10-31 March 1975.

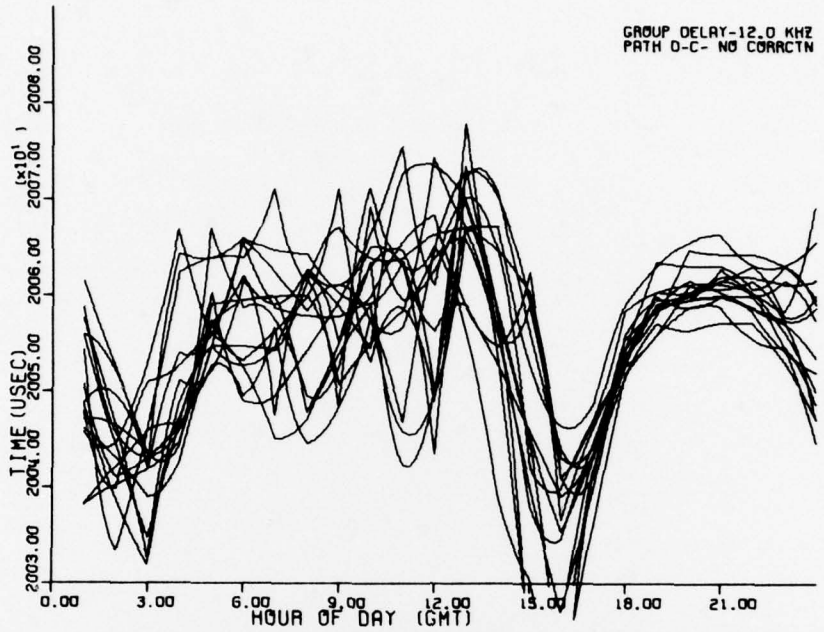

(a) Uncompensated

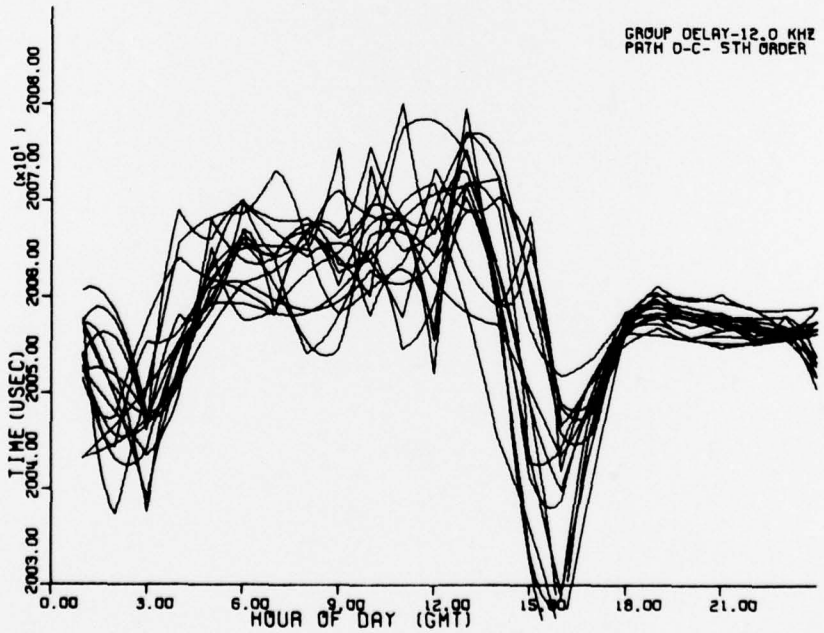

(b) Compensated

Figure 60. Uncompensated and compensated group delay (f=12.0 kHz) versus time of day (GMT). North Dakota - Hawaii (D-C). 10-22 March 1975.

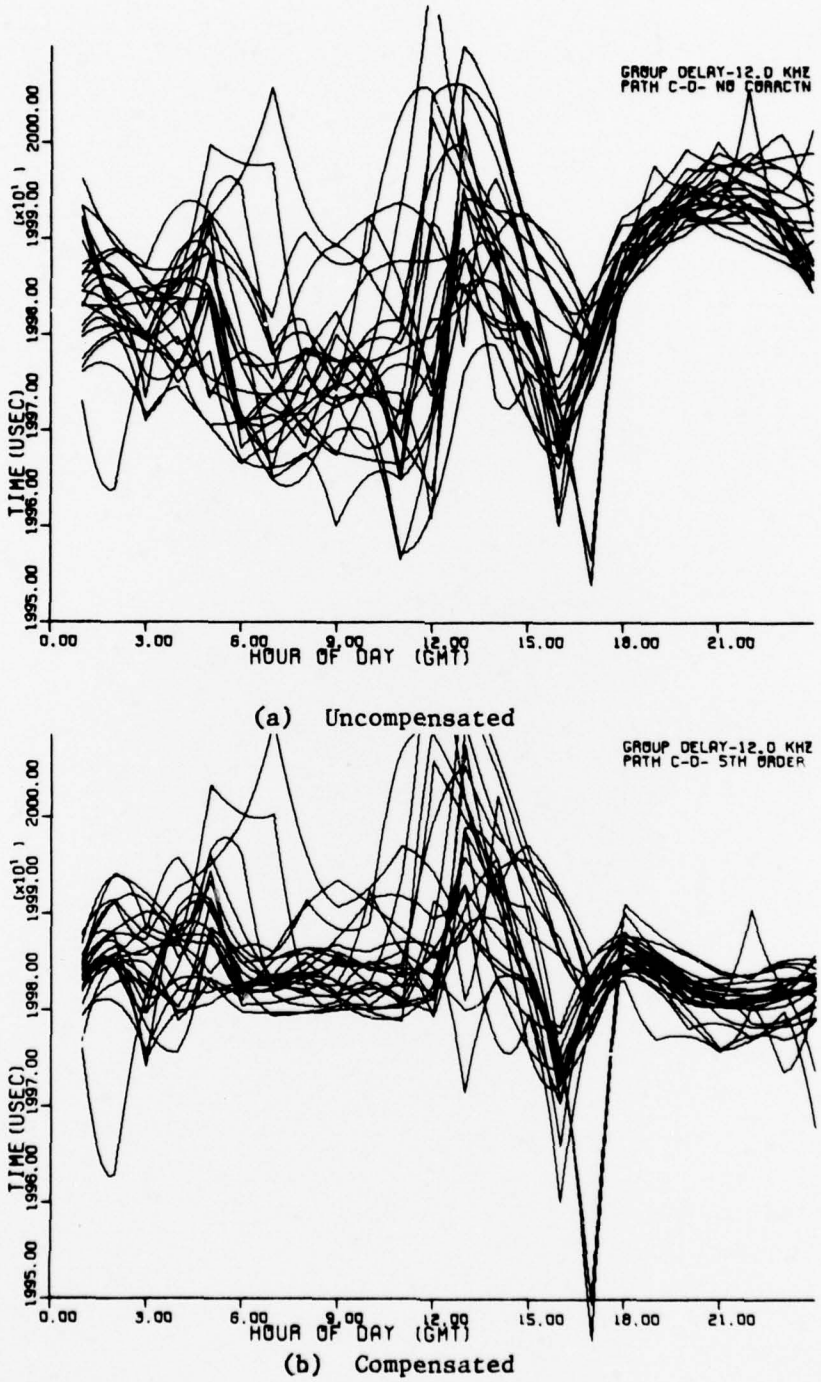

Figure 61. Uncompensated and compensated group delay (f=12.0 kHz) versus time of day (GMT). Hawaii - North Dakota (C-D). 10-31 March 1975.

X. APPENDIX C: DATA BASE FOR SID ANALYSIS

Path	Day	Hour (GMT)
B-D	1 Feb 74	1900-2200
B-D	3 Feb 74	1900
B-D	4 Feb 74	2200
B-D	5 Feb 74	2100
B-D	15 Feb 74	1600, 1900
B-D	16 Feb 74	1900-2200
B-D	21 Feb 74	1600, 1700, 2200
B-D	22 Feb 74	2100-2200
B-D	13 Apr 74	1600-1900
B-D	1 Jul 74	1900
B-D	4 Jul 74	1500-2000
B-D	5 Jul 74	1700, 2300
B-D	6 Jul 74	1300-1500
B-D	6 Jul 74	2000-2200
B-D	8 Jul 74	1800
B-D	2 Aug 74	1600-1900
B-D	6 Aug 74	1800
B-D	28 Aug 74	1200
B-D	31 Aug 74	2000
B-D	8 Oct 74	1500-2000
B-D	10 Oct 74	1600-1900
B-D	11 Oct 74	1800-1900

Path	Day	Hour (GMT)
B-D	12 Oct 74	1900
B-D	18 Oct 74	1300-1500
B-D	30 Oct 74	1700
B-D	31 Oct 74	1600-1900
B-D	3 Nov 74	1800, 2200
B-D	5 Nov 74	1600-1700
B-D	8 Nov 74	1500-2100
B-D	11 Feb 75	2000-2100
B-D	24 Feb 75	1800
D-C	25 Dec 74	2100-2200
D-C	5 May 75	2200
D-C	19 May 75	2100-2200
D-C	26 May 75	2100-2400
D-C	27 May 75	0100-0300
C-D	10 Mar 75	2200-2400
C-D	13 Mar 75	2000-2400
C-D	14 Mar 75	2000-2400
C-D	15 Mar 75	1900-2400
C-D	27 Mar 75	2000-2100
C-D	9 Apr 75	2000-2400
C-D	21 Apr 75	1900-2400
C-D	22 Apr 75	1900-2400

Slopes for linear compensation

B-D	-1.47
D-C	-3.12
C-D	-3.12